1969

Application of selected finite difference techniques to the solution of conical flow problems

Paul Kutler
Iowa State University

70-7713

KUTLER, Paul, 1943-

APPLICATION OF SELECTED FINITE DIFFERENCE TECHNIQUES TO THE SOLUTION OF CONICAL FLOW PROBLEMS.

Iowa State University, Ph.D., 1969
Engineering, aeronautical

University Microfilms, Inc., Ann Arbor, Michigan

APPLICATION OF SELECTED FINITE DIFFERENCE TECHNIQUES TO THE SOLUTION OF CONICAL FLOW PROBLEMS

by

Paul Kutler

A Dissertation Submitted to the

Graduate Faculty in Partial Fulfillment of

The Requirements for the Degree of

DOCTOR OF PHILOSOPHY

Major Subjects: Aerospace Engineering
Mechanical Engineering

Approved:

Signature was redacted for privacy.

In Charge of Major Work

Signature was redacted for privacy.

Heads of Major Departments

Signature was redacted for privacy.

Dean of Graduate College

Iowa State University
Of Science and Technology
Ames, Iowa

1969

TABLE OF CONTENTS

NOMENCLATURE

A,B,C	Coefficient matrices of gasdynamic equations
$a_{l,m}$	Matrix of constants which describe finite difference methods
c	Speed of sound
c_j	Constants
$C1,C2,C3,C4$	Correction factors
E	Energy per unit volume
E_l	X-dependent conservative variables
E_0	Constant
E_1	Constant
F_l	Y-dependent conservative variables
G	Amplification matrix
G_l	Φ-dependent conservative variables
g	Amplification factor
$\bar{g}$	Complex conjugate of g
H_l	Conservative variables
H_t	Total enthalpy
h	Static enthalpy
I	Unit matrix
i	Imaginary constant ($\sqrt{-1}$)
$\hat{i},\hat{j},\hat{k}$	Unit vectors for cartesian coordinate system
$\hat{i}_x,\hat{i}_y,\hat{i}_\phi$	Unit vectors for spherical coordinate system

$\hat{i}_r, \hat{i}_\theta, \hat{i}_\phi$	Unit vectors for spherical coordinate system
k_x, k_y	Constants
k	$\gamma-1/2\gamma$
M	Mach number
M_u, M_v	Mach number components in x and y coordinate directions
M_x, M_y	Lax-Wendroff difference operators
P	Pressure
q	Total velocity
r	Cylindrical radius
r, θ, ϕ	Independent variables for spherical coordinate system
S	Entropy
T	Temperature
t	Time
U	Column matrix of dependent variables
u,v,w	Velocity components in the three coordinate directions
x,y,ϕ	Independent variables for body oriented coordinate system
α	Angle of attack
Γ	Defined by Equation 10
γ	Ratio of specific heats
Δ	$\Delta x = \Delta y$
Δx	Forward difference operator in x
Δy	Forward difference operator in y
λ	Wing angle

λ_j	Eigenvalues of G
μ	$v\ \Delta t/\Delta x$
υ	$u\ \Delta t/\Delta x$
ξ, η, ζ	Independent variables for generalized coordinate system
ρ	Density
σ	Cone half angle
σ_{max}	Maximum eigenvalue
∇	Vector operator
∇x	Backward difference operator in x
∇y	Backward difference operator in y

Subscripts:

b	Conditions on the body
j	Mesh point location in y or θ direction
k	Mesh point location in ϕ direction
max	Maximum
o	Stagnation conditions
q	Fraction of spacial mesh interval
w	Conditions on the wedge
∞	Free stream conditions

Superscripts:

n	Time step location
ζ	Fraction of time increment

INTRODUCTION

Multidimensional inviscid flows containing discontinuities such as shock waves present a formidable task for computation. One approach in solving problems of this sort is to integrate the governing equations which describe gas-dynamic flows in regions which contain no discontinuities and apply the integral form of the differential equations at the discontinuities. These techniques although conceptually simple become cumbersome and somewhat lengthy in their actual application.

A logically simple approach to the solution of these complex problems is to introduce time as a new independent variable in the steady flow equations and difference the resulting hyperbolic equations in conservation-law form according to some appropriate numerical algorithm. The time dependent approach allows one to observe the evolution of the flow field with time and also the converged solution after a steady state is reached.

The finite difference techniques which are used in the solution of time dependent flows allow for the formation of shocks where and when they might occur. The shocks, when they appear, are no longer sharp discontinuities, but are spread over a rather narrow region across which pressure, density, etc.,vary rapidly but continuously. The Rankine-Hugoniot equations, which are based on the conservation laws, hold across this transition layer. Thus, problems which possess complicated shock patterns can be easily handled by utilizing the above approach.

The same finite difference techniques that are used to solve the unsteady gas-dynamic equations can also be employed to solve conical flow problems in conjunction with the steady flow equations. In conical flow

problems there exists no characteristic length in one of the coordinate directions, and therefore, this coordinate can be chosen as the independent variable of integration and this variable is thus considered analogous to time.

The material presented in this paper is separated into five sections. The first section is a survey and analysis of selected finite difference techniques used in the solution of partial differential equations. A theoretical stability criterion is presented which is based on amplification matrix theory. In the second section these finite difference techniques are applied to a simple time dependent, one dimensional partial differential equation which is representative of the gas-dynamic equations. In the third section a technique is developed which is capable of determining the self-similar flow fields about conically shaped bodies. This technique is demonstrated for the case of supersonic flow over a wedge. The fourth section is concerned with the determination of the flow field about a cone at small and large incidences using the finite difference technique which proved most successful in solving the wedge problem. In the final section the flow field about a flat-top or conical wing-body combination at angle of attack is calculated.

NUMERICAL DIFFERENCE SCHEMES

Introduction

The development of high-speed electronic computers has brought about an increasing interest in the use of finite difference techniques for the solution of the partial differential equations which describe gas-dynamic flows. With the advent of larger and faster computers, the solutions to more complex problems using numerical differencing schemes are evolving.

The basis for the solution of the partial differential equations describing fluid flow problems is quite simple. The flow field that is of interest is divided into a discrete number of points which is termed the grid or mesh. The governing equations are then differenced according to some scheme at these points with appropriate boundary conditions being applied at the extremities of the mesh. This results in a system of difference equations which are solved to obtain discrete solutions throughout the mesh provided certain convergence and stability criteria are met.

The accuracy of the solutions obtained depend on the mesh size which in turn is limited by the storage capacity of the computer. Insofar as accuracy is concerned, the use of a lower order differencing scheme in conjunction with a fine mesh can sometimes be comparable to a high-order technique used with a coarse mesh. The required computation time, however, increases with a corresponding increase in the number of mesh points and one usually strives to obtain the best solution while using a minimum of computer time.

One of the main advantages of the finite difference approach is its ability to solve complicated nonlinear problems without the use of restrictive assumptions. Some of the problems solved in this study involve complicated shock patterns which would pose a difficult task for solution by classical techniques which use the Rankine-Hugoniot jump conditions. The numerical algorithms presented here are inherently capable of allowing for the formation of shocks when and where they occur. In general, however, these schemes tend to smooth shocks, hence the flow variables change rapidly but not discontinuously across them.

In the first section a discussion on the stability of difference schemes based on the amplification matrix is presented. In the succeeding sections the difference schemes are presented and discussed. The difference schemes presented are variants of Lax (27) or Lax-Wendroff (28) type schemes which difference the gas-dynamic equations in their conservative form. Recently derived versions by Gourlay and Morris (21) and by MacCormack (31) are described. In certain instances explicit artificial viscosity terms associated with a particular scheme are discussed, but in general only schemes resulting in an implicit artificial viscosity are mentioned.

Amplification Matrix Theory

The explanation presented by Richtmyer (42) for predicting stability by use of the amplification matrix, is quite straightforward and is summarized below.

When partial differential equations are solved using numerical dif-

ferencing schemes, instabilities which sometimes occur appear as small amplitude, short wave length oscillations superimposed in a narrow region on a smooth solution. The prediction of the growth and decay of these instabilities can, therefore, be made using the linearized equations. The assumptions made are that the coefficients of the differential equations are constant, the solution is assumed to be smooth, and the boundary conditions are not taken into account. Under these assumptions, the results of an amplification matrix stability analysis are applicable only in regions which are separated from the boundaries and which contain no discontinuities such as shock waves. The stability relations which are predicted using this theory result in a local stability condition which places a bound on the ratio $\Delta t/\Delta x$ which appears in the differenced equations. The ability of this theory to predict the experimentally determined stability bound for complicated, coupled sets of nonlinear equations is sometimes doubtful. Examples of this are discussed in later sections.

A discrete, harmonic analysis is performed to study the growth and decay of instabilities which sometimes occur in the differenced equations. Consider the following partial differential equation in divergent or conservation-law form:

$$E_t + F_x = 0 \tag{1}$$

where E and F are termed conservative variables. Equation 1 can be written as

$$E_t + AE_x = 0 \tag{2}$$

where A is the Jacobian of F with respect to E($A = \partial F/\partial E$).

The exact solution of Equation 2 is:

$$E = e^{ik_x tA} e^{ik_x x} E_0 \tag{3}$$

where k_x is an arbitrary constant, A is a constant matrix, and E_0 is a constant vector.

As an example in this section for demonstrating the use of amplification matrix theory, consider the following differencing scheme as applied to Equation 2:

$$E_j^{n+1} = E_j^n - \frac{\Delta t}{2\Delta x} A(E^n_{j+1} - E^n_{j-1}) \tag{4}$$

where E is the vector of dependent variables, A is a constant matrix, whose eigenvalues are real, j is the mesh index and n the time index such that $E_j^n = E(j\Delta x, n\Delta t)$.

Since the matrix A can be considered constant in Equation 2, this equation is a local approximation of Equation 1, and numerical algorithms which are unstable for Equation 2 can be expected to be unstable for Equation 1.

Substitution of the typical Fourier term

$$E = E_1 e^{ik_x x} \tag{5}$$

where for each n E_1 is a constant vector and k_x an arbitrary constant, into Equation 4 for E_j^n with $x = j\Delta x$ results in the following equation:

$$E_j^{n+1} = E_1^n e^{i\alpha j} \left[I - \frac{\Delta t}{2\Delta x} A(e^{i\alpha} - e^{-i\alpha})\right] \tag{6}$$

where $\alpha = k\Delta x$ and I is the identity matrix.

Equation 6 can be written as:

$$E_j^{n+1} = GE_j^n \tag{7}$$

The right hand sides of Equations 5 and 6 differ only by the constant matrix G. This matrix is called the amplification matrix and for the example given it reduces to:

$$G = I - i \frac{\Delta t}{\Delta x} A \sin \alpha \tag{8}$$

Equation 7 is representative of a linear difference equation whose solution, according to Lomax (30), is:

$$E_j^n = \sum_j C_j(\lambda_j)^n \tag{9}$$

where C_j are constants, λ_j are the eigenvalues of G, and where n in the right hand side represents an exponent.

From Equation 9 it can be seen that in order for the solution to converge the eigenvalues of G must be less than or equal to one.

Substitution of the exact solution, Equation 3, into Equation 4 yields the same form at $t + \Delta t$ except it is multiplied by the factor

$$\Gamma = e^{ik\Delta tA} \tag{10}$$

Under the assumption that the eigenvalues of A are real, the eigenvalues of Γ lie on the unit circle in the complex plane indicating neither a growth nor a decay of waves. It is desirous therefore, that the eigenvalues of the amplification matrix, G, should also lie close to the unit

circle in order for the solution to remain stable. More specifically, for stability the eigenvalues of G must fall on or within the unit circle for all real values of $\alpha = k\Delta x$. In order for this to occur a bound is always required on the value of $\Delta t/\Delta x$ for explicit difference schemes.

For the above example, if a partial differential equation with time and one space dimension as the independent variables is considered, the amplification matrix in Equation 8 reduces to the amplification factor

$$g = 1 - i \frac{\Delta t}{\Delta x} a \sin \alpha \tag{11}$$

where a is the eigenvalue of the partial differential equation.

In order for the example difference scheme to be stable it is necessary that

$$g\bar{g} \leq 1 \tag{12}$$

for all α and real $a \neq 0$, where $\bar{g}$ is the complex conjugate of g.

Substitution of Equation 11 into Equation 12 yields the following relation:

$$g\bar{g} = 1 + \left(\frac{\Delta t}{\Delta x} a \sin \alpha\right)^2 \tag{13}$$

This is always greater than one. Hence, Equation 13 shows that the difference scheme is unconditionally unstable for any value of the ratio $\Delta t/\Delta x$.

It should be pointed out that the two-dimensional counterpart of the above stability analysis is more complicated but does follow the same development scheme. In the succeeding sections various difference schemes

will be presented along with their associated amplification matrices and corresponding stability criteria based on the theory presented in this section.

Lax's Method

Lax (27) proposed an explicit, first order, finite difference scheme for the calculation of time dependent, one-dimensional, compressible fluid flows containing strong shocks. The main feature of Lax's method is his differencing of the gas-dynamic equations in conservative form. He uses a central difference approximation for the spatial derivatives and an averaged value approximation in the forward time difference, i.e.,

$$F_x = \left(F^n_{j+1} - F^n_{j-1}\right)/2\,\Delta x \tag{14}$$

and

$$E_t = \left[E_j^{n+1} - \tfrac{1}{2}\left(E^n_{j-1} + E^n_{j-1}\right)\right]\Big/\Delta t \tag{15}$$

This yields for Equation (1)

$$E_j^{n+1} = \tfrac{1}{2}\left(E^n_{j+1} + E_{j-1}\right) - \frac{\Delta t}{2\Delta x}\left(F^n_{j+1} - F^n_{j-1}\right) \tag{16}$$

Lax's method is a simplification of the method of von Neumann and Richtmyer (43) in that it is conditionally stable and includes no <u>explicit</u> artificial viscosity terms. Von Neumann and Richtmyer modified the unconditionally, unstable Euler predictor difference scheme (Equation 4) by including an additional term called the artificial pressure and arrived at a conditionally stable formulation. Godunov (17) and Rusanov in (12) are

others who used explicit artificial viscosity terms in the Euler predictor to generate stable difference schemes.

Although Lax's method has no explicit artificial viscosity terms, it is commonly said to possess implicit artificial viscosity. This may be seen by adding and subtracting E_j^n to the numerator of the right-hand side of Equation 15 and rearranging. It yields:

$$E_t = \frac{E_j^{n+1} - E_j^n}{\Delta t} - \frac{(\Delta x)^2}{2\Delta t}\left[\frac{E^n_{j+1} - 2E_j^n + E^n_{j-1}}{(\Delta x)^2}\right] \tag{17}$$

where the bracketed term represents the differenced form of E_{xx}. Therefore, the artificial viscosity term in Lax's method is $\frac{(\Delta x)^2}{2\Delta t} E_{xx}$, where the artificial viscosity is $\frac{(\Delta x)^2}{2\Delta t}$, clearly a function of the grid size. From this it is seen that in order to reduce the effect of this artificial viscosity term the quantity $\frac{(\Delta x)^2}{2\Delta t}$ should be made as small as possible while not exceeding the stability criteria which is presented later.

Lax's method, as suggested by him, is generalized in two and three dimensions by Bohachevsky and Rubin (3) and Bohachevsky and Mates (2) respectively.

In two dimensions the partial differential equation

$$E_t + F_x + G_y = 0 \tag{18}$$

is differenced as follows:

$$E^{n+1}_{j,k} = \tfrac{1}{4}\left(E^n_{j+1,k} + E^n_{j-1,k} + E^n_{j,k+1} + E^n_{j,k-1}\right) - \frac{\Delta t}{2\Delta x}\left(F^n_{j+1,k} - F^n_{j-1,k}\right) - \frac{\Delta t}{2\Delta y}\left(G^n_{j,k+1} - G^n_{j,k-1}\right) \tag{19}$$

In certain types of flow problems, e.g. an ideal dissociating, diatomic gas and for certain coordinate systems an additional term appears in Equation 1 and results in the following equation:

$$E_t + F_x + G_y + H = 0 \tag{20}$$

This equation is differenced according to Bohachevsky and Rubin (3) by adding the following term to Equation 1 :

$$- \frac{\Delta t}{4} \left(H^n_{j+1,k} + H^n_{j-1,k} + H^n_{j,k+1} + H^n_{j,k-1} \right) \tag{21}$$

However, they demonstrated that the differencing of the nonhomogeneous term is not critical and could be replaced simply by:

$$- \Delta t \; H^n_{j,k} \tag{22}$$

In three dimensions the partial differential equation including the nonhomogeneous term is:

$$E_t + F_x + G_y + I_z + H = 0 \tag{23}$$

and is differenced in a fashion analogous to Equation 20.

The amplification matrix for Lax's method in one-dimension is:

$$G = I \cos \alpha - i \frac{\Delta t}{\Delta x} A \sin \alpha \tag{24}$$

The stability condition for Lax's scheme, therefore, is:

$$\left| \frac{\Delta t}{\Delta x} \right| \left| \sigma_{max} \right| \leq 1 \tag{25}$$

where σ_{max} is the maximum eigenvalue of the matrix A. Programming Lax's method for the computer is a rather simple task and requires a minimum

amount of storage for the conservative and flow variables at each mesh point.

This technique has been utilized for inviscid flow solutions by Bohachevsky and Rubin (3), Bochachevsky and Mates (2), DeJarnette (8), and Emery (12).

Leith's Method

Leith (29) developed a second order numerical method for his study of the earth's atmosphere. He considered the problem of advection in one space dimension described by the following scalar equation:

$$\frac{DE}{Dt} = \frac{\partial E}{\partial t} + u \frac{\partial E}{\partial x} = 0 \tag{26}$$

His difference scheme for the solution of this equation is:

$$E_j^{n+1} = E^n_j - \frac{\upsilon}{2}\left(E^n_{j+1} - E^n_{j-1}\right) + \frac{\upsilon^2}{2}\left(E^n_{j+1} - 2E^n_j + E^n_{j-1}\right) \tag{27}$$

where

$$\upsilon = \frac{u\Delta t}{\Delta x}$$

Equation 27 is merely a second order Taylor series expansion of E with respect to t with the derivatives in time replaced by derivatives in x according to the following approximations:

$$E_t)_j = -u \left.\frac{\partial E}{\partial x}\right)_j \approx - u \frac{E_{j+1}+E_{j-1}}{(\Delta x)^2} \tag{28}$$

and

$$E_{tt})_j = u^2 \left.\frac{\partial^2 E}{\partial x^2}\right)_j \approx u^2 \frac{E_{j+1}-2E_j+E_{j-1}}{(\Delta x)^2} \tag{29}$$

The amplification factor for this difference scheme is:

$$g = 1 - i\upsilon \sin \alpha - \upsilon^2(1 - \cos \alpha) \tag{30}$$

where as before,

$$\alpha = k\Delta x$$

Stability of the difference scheme requires that

$$g\bar{g} \leq 1$$

or

$$g\bar{g} = 1 - \upsilon^2(1 - \upsilon^2)(1 - \cos \alpha)^2 \leq 1 \tag{31}$$

This scheme is stable under the condition that

$$|\upsilon| \leq 1 \tag{32}$$

or

$$\left| u \frac{\Delta t}{\Delta x} \right| \leq 1 \tag{33}$$

For two dimensions Leith developed a fractional time step method which results in the component-wise addition of convection contributions. That is, the results obtained by a one-dimensional calculation are operated upon successively in extending the dimensionality. In effect this predicts in one direction and corrects in the other.

For the partial differential equation

$$\frac{\partial E}{\partial t} + u \frac{\partial E}{\partial x} + v \frac{\partial E}{\partial y} = 0 \tag{34}$$

where E is a single dependent variable Leith's predictor-corrector scheme is:

$$E^{n+\frac{1}{2}}_{j,k} = E^{n}_{j,k} - \frac{\mu}{2}(E^{n}_{j,k+1} - E^{n}_{j,k-1}) + \frac{\mu^2}{2}(E^{n}_{j,k+1} - 2E^{m}_{j,k} + E^{n}_{j,k-1})$$

$$E^{n+1}_{j,k} = E^{n+1}_{j,k} - \frac{\upsilon}{2}(E^{n+\frac{1}{2}}_{j+1,k} - E^{n+\frac{1}{2}}_{j-1,k}) + \frac{\upsilon^2}{2}(E^{n+\frac{1}{2}}_{j+1,k} - 2E^{n+\frac{1}{2}}_{j,k} + E^{n+\frac{1}{2}}_{j-1,k}) \quad (35)$$

where

$$\upsilon = \frac{u\Delta t}{\Delta x}, \quad \mu = \frac{v\Delta t}{\Delta x}$$

and

$$E^{n}_{j,k} = (j\Delta x,\ k\Delta y,\ n\Delta t).$$

The amplification factor for this scheme is:

$$\tilde{g} = \tilde{g}_{j,k} + \frac{\mu}{2}(\tilde{g}_{j,k-1} - \tilde{g}_{j,k+1}) + \frac{\mu^2}{2}(\tilde{g}_{j,k-1} - 2\tilde{g}_{j,k} + \tilde{g}_{j,k+1}) \quad (36)$$

where

$$\tilde{g}_{j,k} = 1 - i\upsilon \sin\alpha + \upsilon^2(\cos\alpha - 1)$$

$$\tilde{g}_{j,k+1} = (\cos\beta + i \sin\beta)\tilde{g}_{j,k}$$

$$\tilde{g}_{j,k-1} = (\cos\beta - i \sin\beta)\tilde{g}_{j,k}$$

with $\alpha = k_x\Delta x$ and $\beta = k_y\Delta y$. Fromm (16) discusses the stability of this scheme by comparing parametric plots of μ versus υ for the parameters $g\bar{g}$ and $\theta(\alpha=\beta=\theta)$. He concludes that for stability μ and υ should be less than or equal to one.

Fromm's Method

Fromm (16) developed a difference scheme which reduces the dispersion or phase shift of a solution obtained by a numerical differencing technique. He calls it "the zero average phase error method" and assumes that a directional difference approximation can be written to effect an advanced time solution in any direction. The direction chosen is backward in time. The following scheme, valid only for a single partial differential equation in which both μ and υ are greater than zero, is averaged with the predictor-corrector scheme (Equation 35) developed by Leith (29):

$$\tilde{E}_{j,k} = E^n_{j-1,k} + \frac{\upsilon^n_{j,k-1}}{2}\left(E^n_{j-2,k} - E^n_{j,k}\right) + \frac{\left(\upsilon^n_{j,k-1}\right)^2}{2}\left(E^n_{j-2,k} - 2E^n_{j-1,k} + E^n_{j,k}\right) \tag{37}$$

$$E^{n+1}_{j,k} = \tilde{E}_{j,k-1} + \frac{\mu^n_{j,k-1}}{2}\left(\tilde{E}_{j,k-2} - \tilde{E}_{j,k}\right) + \frac{\left(\mu^n_{j,k-1}\right)^2}{2}\left(\tilde{E}_{j,k-2} - 2\tilde{E}_{j,k-1} + \tilde{E}_{j,k}\right)$$

$$\tilde{E}_{j,k} = E^n_{j,k} + \frac{\upsilon^n_{j,k}}{4}\left(E^n_{j-1,k} - E^n_{j+1,k} + E^n_{j-2,k} - E^n_{j,k}\right) + \frac{\left(\upsilon^n_{j,k}\right)^2}{4}\left(E^n_{j-1,k} - 2E^n_{j,k} + E^n_{j+1,k}\right) + \frac{\left(\upsilon^n_{j,k}\right)^2 - 2\upsilon^n_{j,k}}{4}\left(E^n_{j-2,k} - 2E^n_{j-1,k} + E^n_{j,k}\right) \tag{38}$$

$$E^{n+1}_{j,k} = \tilde{E}_{j,k} + \frac{\mu^n_{j,k}}{4}\left(\tilde{E}_{j,k-1} - \tilde{E}_{j,k+1} + \tilde{E}_{j,k-2} - \tilde{E}_{j,k}\right)$$

$$+ \frac{\left(\mu^n_{j,k}\right)^2}{4}\left(\tilde{E}_{j,k-1} - 2\tilde{E}_{j,k} + \tilde{E}_{j,k+1}\right)$$

$$+ \frac{\left(\mu^n_{j,k}\right)^2 - 2\mu^n_{j,k}}{4}\left(\tilde{E}_{j,k-2} - 2\tilde{E}_{j,k-1} + \tilde{E}_{j,k}\right)$$

The amplification factor for Equation 38 is:

$$g = \tilde{g}_{j,k} + \frac{\mu}{4}(\tilde{g}_{j,k-1} - \tilde{g}_{j,k+1} + \tilde{g}_{j,k-2} - \tilde{g}_{j,k})$$

$$+ \frac{\mu^2}{4}(\tilde{g}_{j,k-1} - 2\tilde{g}_{j,k} + \tilde{g}_{j,k+1})$$

$$+ \frac{\mu^2-2\mu}{4}(\tilde{g}_{j,k-2} - 2\tilde{g}_{j,k-1} + \tilde{g}_{j,k}) \qquad (39)$$

where

$$\tilde{g}_{j,k} = 1 - \frac{iv}{2}\sin\alpha - \frac{iv}{2}(\cos\alpha - i\sin\alpha)\sin\alpha$$

$$+ \frac{v^2}{2}(\cos\alpha - 1) + \frac{v^2-2v}{2}(\cos\alpha - i\sin\alpha)(\cos\alpha - 1)$$

$$\tilde{g}_{j,k+1} = (\cos\beta + i\sin\beta)\tilde{g}_{j,k}$$

$$\tilde{g}_{j,k-1} = (\cos\beta - i\sin\beta)\tilde{g}_{j,k}$$

and

$$\tilde{g}_{j,k-2} = (\cos 2\beta - i\sin 2\beta)\tilde{g}_{j,k}$$

Fromm concludes that this technique reduces phase errors without extending the order of the method as is done by others, e.g. Roberts and Weiss (44). The stability criteria are the same as that for Leith's

method, namely μ and $\upsilon \leq 1$.

Lax-Wendroff Method

The method presented by Leith (29) is not directly applicable to the differencing of the Eulerian equations in conservative form. Leith's two step method was developed for a scalar partial differential equation only. Lax-Wendroff (28) developed a second order difference scheme based on a second order Taylor series expansion, as was done, by Leith, which differences the conservation-law form of the gas-dynamic equations.

Differencing Equation 18, the Lax-Wendroff scheme is:

$$
\begin{aligned}
E^{n+1}_{j,k} = E^{n}_{j,k} &- \frac{\Delta t}{2\Delta x}\left(F^{n}_{j+1,k} - F^{n}_{j-1,k}\right) - \frac{\Delta t}{2\Delta y}\left(G^{n}_{j,k+1} - G^{n}_{j,k-1}\right) \\
&+ \frac{1}{2}\left(\frac{\Delta t}{\Delta x}\right)^2\left[A^{n}_{j+\frac{1}{2},k}\left(F^{n}_{j+1,k} - F^{n}_{j,k}\right) - A^{n}_{j-\frac{1}{2},k}\left(F^{n}_{j,k} - F^{n}_{j-1,k}\right)\right] \\
&+ \frac{1}{2}\left(\frac{\Delta t}{\Delta y}\right)^2\left[B^{n}_{j,k+\frac{1}{2}}\left(G^{n}_{j,k+1} - G^{n}_{j,k}\right) - B^{n}_{j,k-\frac{1}{2}}\left(G^{n}_{j,k} - G^{n}_{j,k-1}\right)\right] \\
&+ \frac{1}{8}\frac{(\Delta t)^2}{\Delta x \Delta y}\left[A^{n}_{j+1,k}\left(G^{n}_{j+1,k+1} - G^{n}_{j-1,k+1}\right)\right. \\
&- A^{n}_{j-1,k}\left(G^{n}_{j+1,k-1} - G^{n}_{j-1,k-1}\right) \\
&\left. + B^{n}_{j,k+1}\left(F^{n}_{j+1,k+1} - F^{n}_{j+1,k-1}\right) - B^{n}_{j,k-1}\left(F^{n}_{i-1,j+1} - F^{n}_{i-1,j-1}\right)\right] \qquad (40)
\end{aligned}
$$

where A and B are respectively the Jacobians of F and G with respect to E ($A = \partial F/\partial E$, $B = \partial G/\partial E$) and where $A^{n}_{j+\frac{1}{2},k}(E)$ denotes $A\left(\frac{1}{2}E^{n}_{j+1,k} + \frac{1}{2}E^{n}_{j,k}\right)$.

The inclusion of the second order terms produce a conditionally stable formulation of an otherwise unstable scheme.

The amplification matrix for the above scheme is:

$$G = I + i(A \sin \alpha + B \sin \beta) - A^2(1 - \cos \alpha)$$
$$- \tfrac{1}{2}(AB + BA) \sin \alpha \sin \beta - B^2(1 - \cos \beta) \qquad (41)$$

The stability criterion based on Equation 41 is

$$\frac{\Delta t}{\Delta} \leq \frac{1}{\sigma_{max}\sqrt{8}}$$

for two dimensional flows where σ_{max} is the maximum eigenvalue of the matrices A and B and $\Delta = \Delta x = \Delta y$.

One of the disadvantages in using this scheme is the necessity of numerically evaluating the Jacobian A and B and subsequently performing the matrix-vector multiplication. For this reason the programming becomes somewhat involved. Compared to Lax's technique, added storage space is required for the two Jacobian's A and B at each mesh point.

This scheme has been used to solve gas-dynamic problems by Moretti and Abbett (36), Moretti and Bleich (37), Richtmyer (42), Emery (12), Burstein (4), (6), and Moretti (35).

Richtmyer's Method

Richtmyer (43) presents a predictor-corrector variation of Leith's (29) scheme or a "conservation-law form" of the Lax-Wendroff (28) technique. The procedure has second order accuracy and is simpler to use since the Jacobians A and B do not appear which is its main advantage.

For one dimensional, time-dependent flows Equation 1 is differenced according to the following predictor-corrector technique:

$$\tilde{E}_j^{n+\frac{1}{2}} = \tfrac{1}{2}(E^n_{j+\frac{1}{2}}+E^n_{j-\frac{1}{2}}) - \frac{\Delta t}{2\Delta x}(F^n_{j+\frac{1}{2}}-F^n_{j-\frac{1}{2}})$$

$$E_j^{n+1} = E_j^n - \frac{\Delta t}{\Delta x}(\tilde{F}^{n+\frac{1}{2}}_{j+\frac{1}{2}} - \tilde{F}^{n+\frac{1}{2}}_{j-\frac{1}{2}}) \tag{42}$$

The tilde over the dependent variable F in the corrector implies that F is evaluated using the intermediate values of the dependent variables $\tilde{E}$ determined by the predictor.

The amplification matrix for this scheme is:

$$G = I - i\,\frac{\Delta t}{\Delta x} A \sin\alpha - (\frac{\Delta t}{\Delta x} A)^2 (1 - \cos\alpha) \tag{43}$$

where A is again the Jacobian of F with respect tc E and where $\alpha = k\Delta x$.

For stability the following inequality must be satisfied:

$$\frac{\Delta t}{\Delta x} \leq \frac{1}{|\sigma_{max}|} \tag{44}$$

In his paper Richtmyer changed the notation slightly by avoiding fractional indices in generalizing Equation 42 for two-dimensions. This led to a difference scheme which predicted intermediate values at $t + \Delta t$ and corrected them for $t + 2\Delta t$ (Richtmyer double-time step method). In order to be consistent with the format of the other schemes presented in this study, Richtmyer's scheme (single time-step method) is written as follows:

$$\tilde{E}^{n+\frac{1}{2}}_{j,k} = \tfrac{1}{4}(E^n_{j+\frac{1}{2},k} + E^n_{j-\frac{1}{2},k} + E^n_{j,k+\frac{1}{2}} + E^n_{j,k-\frac{1}{2}})$$

$$- \frac{\Delta t}{2\Delta x}(F^n_{j+\frac{1}{2},k} - F^n_{j-\frac{1}{2},k}) - \frac{\Delta t}{2\Delta y}(G^n_{j,k+\frac{1}{2}} - G^n_{j,k-\frac{1}{2}}) \tag{45}$$

$$E_{j,k}^{n+1} = E_{j,k}^{n} - \frac{\Delta t}{\Delta x}\left(\tilde{F}_{j+\frac{1}{2},k}^{n+\frac{1}{2}} - \tilde{F}_{j-\frac{1}{2},k}^{n+\frac{1}{2}}\right) - \frac{\Delta t}{\Delta y}\left(\tilde{G}_{j,k+\frac{1}{2}}^{n+\frac{1}{2}} - \tilde{G}_{j,k-\frac{1}{2}}^{n+\frac{1}{2}}\right)$$

The amplification matrix for Equation 45 is:

$$G = I - i(\cos\alpha + \cos\beta)\frac{\Delta t}{\Delta x}(A \sin\alpha + B \sin\beta)$$

$$- 2\left[\frac{\Delta t}{\Delta x}(A \sin\alpha + B \sin\beta)\right]^2 \qquad (46)$$

where

$$\alpha = \tfrac{1}{2}k_x\Delta x$$

and

$$\beta = \tfrac{1}{2}k_y\Delta y$$

The stability criterion for the scheme given by Equation 45 is the same as that found for the original Lax-Wendroff scheme; namely,

$$\frac{\Delta t}{\Delta x} \leq \frac{1}{\sqrt{8}\left|\sigma_{max}\right|} \qquad (47)$$

Richtmyer's method requires approximately twice as much computing time as does Lax's method for the same mesh size. Added storage space is necessary for storing the variables $\tilde{E}_{j,k}^{n+\frac{1}{2}}$ at each mesh point, but the storage required is still less than that needed for the original Lax-Wendroff scheme.

Burstein's Method

Burstein (5), (6) also developed a two step version of the Lax-Wendroff scheme which is analogous to the one developed by Richtmyer (43).

Burstein's method as applied to Equation 20 is as follows:

$$\tilde{E}^{n+1}_{j,k} = \tfrac{1}{4}(E^n_{j+\frac{1}{2},k+\frac{1}{2}} + E^n_{j+\frac{1}{2},k-\frac{1}{2}} + E^n_{j-\frac{1}{2},k+\frac{1}{2}} + E^n_{j-\frac{1}{2},k-\frac{1}{2}})$$

$$- \frac{\Delta t}{2\Delta x}(F^n_{j+\frac{1}{2},k+\frac{1}{2}} - F^n_{j-\frac{1}{2},k+\frac{1}{2}} + F^n_{j+\frac{1}{2},k-\frac{1}{2}} - F^n_{j-\frac{1}{2},k-\frac{1}{2}})$$

$$- \frac{\Delta t}{2\Delta y}(G^n_{j+\frac{1}{2},k+\frac{1}{2}} - G^n_{j+\frac{1}{2},k-\frac{1}{2}} + G^n_{j-\frac{1}{2},k+\frac{1}{2}} - G^n_{j-\frac{1}{2},k-\frac{1}{2}})$$

$$- \frac{\Delta t}{4}(H^n_{j+\frac{1}{2},k+\frac{1}{2}} + H^n_{j+\frac{1}{2},k-\frac{1}{2}} + H^n_{j-\frac{1}{2},k+\frac{1}{2}} + H^n_{j-\frac{1}{2},k-\frac{1}{2}}) \qquad (48)$$

$$E^{n+1}_{j,k} = E^n_{j,k} - \frac{\Delta t}{4\Delta x}(F^n_{j+1,k} - F^n_{j-1,k} + \tilde{F}^{n+1}_{j+\frac{1}{2},k+\frac{1}{2}} - \tilde{F}^{n+1}_{j-\frac{1}{2},k+\frac{1}{2}}$$

$$+ \tilde{F}^{n+1}_{j+\frac{1}{2},k-\frac{1}{2}} - \tilde{F}^{n+1}_{j-\frac{1}{2},k-\frac{1}{2}})$$

$$- \frac{\Delta t}{4\Delta y}(G^n_{j,k+1} - G^n_{j,k-1} + \tilde{G}^{n+1}_{j+\frac{1}{2},k+\frac{1}{2}} - \tilde{G}^{n+1}_{j+\frac{1}{2},k-\frac{1}{2}}$$

$$+ \tilde{G}^{n+1}_{j-\frac{1}{2},k+\frac{1}{2}} - \tilde{G}^{n+1}_{j-\frac{1}{2},k-\frac{1}{2}})$$

$$- \frac{\Delta t}{2}(H^n_{j,k} + \tilde{H}^{n+1}_{j,k}) \qquad (49)$$

where

$$\tilde{H}^{n+1}_{j,k} = \Sigma(\tilde{H}^{n+1}_{j\pm\frac{1}{2},k\pm\frac{1}{2}})$$

The amplification matrix for this scheme is:

$$G = I + iA\frac{\Delta t}{\Delta x}(\frac{3}{4}\sin\alpha + \frac{1}{4}\sin\alpha\cos\beta) + iB\frac{\Delta t}{\Delta x}(\frac{3}{4}\sin\beta$$

$$+ \frac{1}{4}\sin\beta\cos\alpha) + \frac{1}{2}(A\frac{\Delta t}{\Delta x})^2(\cos\alpha - 1)(1 + \cos\beta)$$

$$+ \frac{1}{2}(B\frac{\Delta t}{\Delta x})^2(\cos\beta - 1)(1 + \cos\alpha) - \frac{AB+BA}{2}(\frac{\Delta t}{\Delta x})^2\sin\alpha\sin\beta \qquad (50)$$

This results in the same stability condition that is found for the Lax-Wendroff scheme; namely,

$$\frac{\Delta t}{\Delta x} \leq \frac{1}{|\sigma_{max}| \sqrt{8}} \tag{47}$$

This scheme, as Burstein points out, centers all quantities at the point (j, k, t + $\Delta t/2$) by the averaging procedure used in Equation 48 which is what is done by the Taylor's expansion used for the Lax-Wendroff scheme. As a result of this averaging procedure, additional storage space for the variables $\tilde{E}_{j,k}$, $\tilde{F}_{j,k}$, $\tilde{G}_{j,k}$ and $\tilde{H}_{j,k}$ over Lax's method is required and the computation time is substantially increased.

Lapidus (26) presents another interesting version of the Lax-Wendroff scheme in his paper. It is a predictor -corrector scheme that uses a Lax predictor for the first step. The second step is similar to Richtmyer's (43), but Lapidus computes an average value based on four points for the derivatives.

Burstein (6) in solving multidimensional, time-dependent, shocked flow problems derived a variation of the Lax-Wendroff difference scheme which included an explicit "triple viscosity term." This added term has a stabilizing effect on the solution and allows the maximum possible time step. This fact is reflected by the greater bound derived for the ratio $\Delta t/\Delta x$.

The "triple viscosity term" which is simply added to Equation 36 is, in differential form:

$$\left\{ -\frac{\Delta t^3}{4}\left[(AB^2 + B^2A)\frac{\partial^3}{\partial x \partial y^2} + (A^2B + BA^2)\frac{\partial}{\partial x^2 \partial y}\right] \right.$$

$$\left. + \frac{\Delta t^4}{8}(A^2B^2 + B^2A^2)\frac{\partial^4}{\partial x^2 \partial y^2} \right\} E \qquad (51)$$

where A and B are matrices and where the partial derivatives operate on the dependent variable E.

In differenced form Equation 51 becomes:

$$\left\{ -\frac{1}{8}\left(\frac{\Delta t}{\Delta x}\right)^3\left[(AB^2 + B^2A)(\Delta x + \nabla x)\Delta y \nabla y + (BA^2 + A^2B)(\Delta y + \nabla y)\Delta x \nabla x\right] \right.$$

$$\left. + \frac{1}{8}\left(\frac{\Delta t}{\Delta x}\right)^4(A^2B^2 + B^2A^2)\Delta x \nabla x \Delta y \nabla y \right\} E^n \qquad (52)$$

where Δ, ∇ are the usual forward and backward difference operators and $\Delta x = \Delta y$.

Obviously, the computation of such a term is time consuming because of the large number of matrix multiplications.

The amplification matrix for Equation 51 under the assumptions, $\alpha \approx \sin \alpha$ and $\alpha^2 \approx 2(1 - \cos \alpha)$, is:

$$G' = \frac{A^2B^2 + B^2A^2}{8}\alpha^2\beta^2 - i\left(\frac{AB^2 + B^2A}{4}\alpha\beta^2 + \frac{A^2B + BA^2}{4}\alpha^2\beta\right) \qquad (53)$$

Burstein (6) shows that the difference equation will be stable if

$$\frac{\Delta t}{\Delta x} \leq \frac{1}{|\sigma_{max}(A)|} \text{ and } \frac{\Delta t}{\Delta y} \leq \frac{1}{|\sigma_{max}(B)|} \qquad (54)$$

which has increased the upper bound on the ratio $\Delta t/\Delta x$ by a factor of $\sqrt{8}$ over the Lax-Wendroff scheme.

Strang's Method

Strang (49), (50), developed a predictor-corrector difference scheme which yields the same artificial viscosity term derived by Burstein (6) by analytically substituting the predictor into the corrector. However, when solving problems this operation is performed numerically by the computer, and the artificial viscosity term is, therefore, considered to be implicit. This fact eliminates the calculation of the term in Equation 52. Strang follows the development used by Leith (29) in generalizing his one-dimensional scheme to two dimensions. Strang's scheme, though, is applicable to a sequence of partial differential equations whereas Leith could only solve a scalar equation.

Strang's scheme for the following linear system,

$$E_t + AE_x + BE_y = 0 \tag{55}$$

where E is a vector of dependent variables is:

$$E^{n+1} = \frac{1}{2}(M_x M_y + M_y M_x)E^n \tag{56}$$

where M_x, M_y are Lax-Wendroff difference operators in the x and y directions respectively and are given by the following equations:

$$M_x E^n_{j,k} = E^n_{j,k} - \frac{\Delta t}{2\Delta x} A(E^n_{j+1,k} - E^n_{j-1,k}) + \frac{1}{2}(\frac{\Delta t}{\Delta x} A)^2(E^n_{j+1,k} - 2E^n_{j,k} + E^n_{j-1,k})$$

$$M_y E^n_{j,k} = E^n_{j,k} - \frac{\Delta t}{2\Delta y} B(E^n_{j,k+1} - E^n_{j,k-1})$$

$$+\tfrac{1}{2}\left(\frac{\Delta t}{\Delta x}\,B\right)^2\left(E^n_{j,k+1} - 2E^n_{j,k} + E^n_{j,k-1}\right)$$

where A and B are assumed constant.

Gourlay and Morris' Method

Gourlay and Morris (21) developed a multistep version of Strang's technique which is applicable to the conservation-law form of the gas-dynamic equations. It, too, possesses the same stability criterion as Burstein's scheme.

For Equation 18, Gourlay and Morris' scheme is as follows:

$$\left.\begin{aligned} E^{n+1}_{a1_{j,k}} &= \tfrac{1}{2}\left(E^n_{j,k+1} + E^n_{j,k-1}\right) - \frac{\Delta t}{2\Delta y}\left(G^n_{j,k+1} - G^n_{j,k-1}\right) \\ E^{n+1}_{b1_{j,k}} &= \tfrac{1}{2}\left(E^n_{j+1,k} + E^n_{j-1,k}\right) - \frac{\Delta t}{2\Delta x}\left(F^n_{j+1,k} - F^n_{j-1,k}\right) \end{aligned}\right\} \text{1st Step} \qquad (57)$$

$$\left.\begin{aligned} E^{n+1}_{a2_{j,k}} &= E^n_{j,k} - \frac{\Delta t}{\Delta y}\left[G(E_{a1})^{n+1}_{j,k+1} - G(E_{a1})^{n+1}_{j,k-1}\right] \\ E^{n+1}_{b2_{j,k}} &= E^n_{j,k} - \frac{\Delta t}{\Delta x}\left[F(E_{b1})^{n+1}_{j+1,k} - F(E_{b1})^{n+1}_{j-1,k}\right] \end{aligned}\right\} \text{2nd Step} \qquad (58)$$

$$\left.\begin{aligned} E^{n+1}_{a3_{j,k}} &= \tfrac{1}{2}\left(E^{n+1}_{a2_{j+1,k}} - E^{n+1}_{a2_{j-1,k}}\right) - \frac{\Delta t}{2\Delta x}\left[F(E_{a2})^{n+1}_{j+1,k} - F(E_{a2})^{n+1}_{j-1,k}\right] \\ E^{n+1}_{b3_{j,k}} &= \tfrac{1}{2}\left(E^{n+1}_{b2_{j,k+1}} - E^{n+1}_{b2_{j,k-1}}\right) - \frac{\Delta t}{2\Delta y}\left[G(E_{b2})^{n+1}_{j,k+1} - G(E_{b2})^{n+1}_{j,k-1}\right] \end{aligned}\right\} \text{3rd Step} \qquad (59)$$

$$\left.\begin{aligned} E^{n+1}_{a4_{j,k}} &= E^{n+1}_{a2_{j,k}} - \frac{\Delta t}{\Delta k}\left[F(E_{a3})^{n+1}_{j+1,k} - F(E_{a3})^{n+1}_{j-1,k}\right] \\ E^{n+1}_{b4_{j,k}} &= E^{n+1}_{b2_{j,k}} - \frac{\Delta t}{\Delta y}\left[G(E_{b4})^{n+1}_{j,k+1} - G(E_{b4})^{n+1}_{j,k-1}\right] \end{aligned}\right\} \text{4th Step} \qquad (60)$$

$$E_{j,k} = \tfrac{1}{2}(E^{n+1}_{a4} + E^{n+1}_{b4}) \qquad (61)$$

This scheme does not require the computations associated with Strang's scheme which use the Jacobians A and B but merely requires the evaluation of the conservative variables F and G. It requires approximately twice as much computing time as does Richtmyer's scheme, but the stability characteristics are theoretically $\sqrt{8}$ times better due to the pseudo-viscous term which is implicit in the formulation.

MacCormack's Method

MacCormack (31) developed a two step method which is of second order in both time and space, and it can be considered a version of the Lax-Wendroff scheme. Its basic differences are that the derivatives of the partial differential equations are replaced by either forward or backward differences rather than the conventional central difference and that the term usually averaged in the predictor is now evaluated at the pivotal mesh point.

As applied to Equation 18 MacCormack's method is as follows:

$$\begin{aligned} \tilde{E}^{n+1}_{j,k} &= E^{n}_{j,k} - \frac{\Delta t}{\Delta x}(F^{n}_{j+1,k} - F^{n}_{j,k}) - \frac{\Delta t}{\Delta y}(G^{n}_{j,k+1} - G_{j,k}) \\ E^{n+1}_{j,k} &= \tfrac{1}{2}\left[E^{n}_{j,k} + \tilde{E}^{n+1}_{j,k} - \frac{\Delta t}{\Delta x}(\tilde{F}^{n+1}_{j,k} - \tilde{F}^{n+1}_{j-1,k}) - \frac{\Delta t}{\Delta y}(\tilde{G}^{n+1}_{j,k} - \tilde{G}^{n+1}_{j,k-1})\right] \end{aligned} \qquad (62)$$

The tilde appearing over certain quantities indicates an intermediate evaluation of that variable.

In this version forward differences are used in the predictor and backward differences in the corrector. However, there exist three other combinations which will yield a second order method of the same form. For example, if instead of using forward differences in the predictor and backward differences in the corrector, the reverse procedure could be followed. Another possibility is to use a forward difference for the x-derivative and a backward difference for the y-derivative in the predictor and the opposite in the corrector. Application of these different forms to the solution of the same problem yields slightly different results as will be shown later. For this reason MacCormack's method is termed a preferential difference scheme.

The amplification matrix for Equation 62 is as follows:

$$G = I + i\frac{\Delta t}{\Delta x}(A \sin\alpha + B \sin\beta) - \tfrac{1}{2}\left(\frac{\Delta t}{\Delta x}\right)^2\left[(1 - e^{-i\alpha})A + (1 - e^{-i\beta})B\right] x \left[(1 - e^{+i\alpha})A + (1 - e^{i\beta})B\right] \tag{63}$$

where $\alpha = k_x\Delta x$, $\beta = k_y\Delta y$, and equal spacing is assumed ($\Delta x = \Delta y$).

In one-dimension the stability condition is

$$\frac{\Delta t}{\Delta x} \leq \frac{1}{|\sigma_{max}|} \tag{64}$$

which is the one usually obtained. For two-dimensions MacCormack obtains

the relation

$$\frac{\Delta t}{\Delta x} \leq \frac{(\Delta t)^{\frac{1}{4}}}{|\sigma_{max}|} \tag{65}$$

This is not the usual form obtained, but it is shown in this study that the stability of this method is comparable to the other predictor-corrector techniques.

For the purpose of differencing Equation 20 which contains the additional term, it was found satisfactory in this study to simply add the following quantities to the predictor and corrector of Equation 46:

$$\begin{aligned} &\text{Predictor;} \quad -H^{n}_{j,k}\,\Delta t \\ &\text{Corrector;} \quad -\tfrac{1}{2}H^{n}_{j,k}\,\Delta t \end{aligned} \tag{66}$$

Programming MacCormack's method is quite simple and requires the same amount of storage as Richtmyer's second order method. The necessary computing time is somewhat reduced when MacCormack's method is used because only integer indices appear in the difference scheme, thus requiring no storage shifting.

SOLUTION OF THE MODIFIED BURGER'S EQUATION

Introduction

In this section the solution of a simple initial value problem based on a modified version of Burger's equation is developed using a variety of the numerical algorithms introduced in this and the preceding sections.

The parabolic partial-differential equation

$$u_t + uu_x = \mu u_{xx} \tag{67}$$

where $\mu > 0$ was first introduced by J. M. Burgers in (22) as the simplest model for the differential equations describing fluid flow problems. It can be seen that a close analogy exists between the nonlinearity of the left side of Equation 67 and the terms which appear in the inviscid gas-dynamic equations. For the analysis performed in this study, the viscosity term on the right hand side of Equation 67 is set equal to zero which results in the following equation in conservation-law form:

$$u_t + (\tfrac{1}{2}u^2)_x = 0 \tag{68}$$

In order to simulate certain flow conditions (such as shocks and rarefactions) which do occur in the solutions of the gas-dynamic equations, the initial conditions for the modified Burger's equation are varied as given in Table 1. The discontinuities which appear in the initial data are assumed to be spread over one mesh interval, for example; u_1, u_2, ..., $u_{j+1}=u_i$ and u_{j+2}, ..., $u_m = u_f$.

The exact solution of Equation 2 for the position of a right moving

Table 1. Initial conditions for modified Burger's equation

Wave	Right Moving	Left Moving	Standing
Shock	$u_i = 1.0,\ x < k$	$u_i = 0.0,\ x < k$	$u_i = 0.5,\ x < k$
	$u_f = 0.0,\ x \geq k$	$u_f = -1.0,\ x \geq k$	$u_f = 0.5,\ x \geq k$
Rarefaction	$u_i = 0.0,\ x < k$	$u_i = -1.0,\ x > k$	--
	$u_f = 1.0,\ x \geq k$	$u_f = 0.0,\ x \geq k$	--

"shock" starting at x = 0 when t = 0 is x = t/2. The exact value for u is:

$$u(x,t) = \begin{cases} 1 \text{ for } x/t < 1/2 \\ 0 \text{ for } x/t > 1/2 \end{cases} \tag{69}$$

The exact solution for u in a right moving "rarefaction" with the same starting location is:

$$u(x,t) = \begin{cases} 0 \text{ for } x < 0 \\ x/t \text{ for } 0 < x < t \\ 1 \text{ for } t < x \end{cases} \tag{70}$$

These solutions can be generalized for the analogous left moving waves.

The solution for the standing "shock" wave is:

$$u(x,t) = \begin{cases} 0.5 \text{ for } x < 0 \\ -0.5 \text{ for } 0 < x \end{cases} \tag{71}$$

In the actual solution of gas-dynamic problems, the choice of a coordinate system and independent variable of integration determines whether

shocks which form will appear as moving or standing waves. For example, in spherical coordinates when integrating with respect to r, the conical shock which forms about a cone in supersonic flow is fixed with respect to θ in the converged solution, and is therefore considered a standing wave. In a body coordinate system, such as the one used later for the solution of the same problem, the shock is moving with respect to y as the integration procedes in x for the converged solution. These facts motivate the study in this section of the effects various finite difference schemes have on standing and moving waves. The study of left and right moving waves is performed to demonstrate the effects the preferential difference schemes have on the solution.

For the physical flow problem of a cone at angle of attack in a supersonic flow field, which is discussed in a later section, the conical shock which forms varies in intensity with respect to the meridional angle. The maximum eigenvalue associated with the gas-dynamic equations occurs in the meridional plane where the shock is the strongest, and according to the theory defining the amplification matrix, it is this point which governs stability and the ratio $\Delta x/\Delta y$ where x is now the independent variable of integration. The smallest associated eigenvalue occurs in the meridional plane which contains the weakest part of the shock, and this region therefore has less of a tendency to become unstable for a given $\Delta x/\Delta y$. Theoretically it allows for the possibility of a larger value of $\Delta x/\Delta y$ in this region.

It is possible to simulate this effect of varying shock intensities in a fixed mesh by studying the simple Burger's model using a fixed "shock" strength and various ratios of $\Delta t/\Delta x$. For the purposes of this study a value of $\Delta t/\Delta x$ corresponding to the maximum allowable for a stable solution ($\Delta t/\Delta x = 1$) and a value equal to half that ($\Delta t/\Delta x = 0.5$) are employed.

Difference Schemes Revisited

In the previous section, which described various algorithms, all of the difference schemes presented are considerably simplified when applied to one-dimensional, time-dependent problems. When applied to a linear equation, e.g. Equation 2 where A is a constant matrix, they reduce to a form attributable to either Lax (27), Fromm (16), or Lax-Wendroff (28). Many other forms of difference schemes can be written which are fundamentally the same as those already presented with regards to their applicability to linear equations. The differences between these various numerical algorithms become apparent when applied to nonlinear problems.

In this section modifications of some of the difference schemes are described. The methods are presented for the one-dimensional, time-dependent Equation 1.

The scheme developed by Fromm (16) in its present form is not applicable to conservation-law form equations. However, it can be easily modified. The following two-step scheme reduces to Fromm's scheme for the linear case and involves only three adjacent mesh points:

$$\tilde{E}_j^{n-\frac{1}{2}} = \tfrac{1}{4}(E_{j-1}^n + 2E_j^n + E_{j+1}^n) - \frac{\Delta t}{4\Delta x}(F_{j-1}^n - F_{j+1}^n)$$

$$E_j^{n+1} = E_j^n - \frac{\Delta t}{\Delta x}(\tilde{F}_{j-1}^{n-\frac{1}{2}} - \tilde{F}_j^{n-\frac{1}{2}} - \tfrac{3}{2}F_{j-1}^n + F_j^n + \tfrac{1}{2}F_{j+1}^n) \tag{72}$$

A variation of MacCormack's preferential difference scheme given by Equation 6 is as follows:

$$\tilde{E}_j^{n+1} = E_j^n - \frac{\Delta t}{\Delta x}(F_{j+1}^n - F_j^n)$$

$$E_j^{n+1} = E_j^n - \frac{\Delta t}{2\Delta x}(\tilde{F}_j^{n+1} - \tilde{F}_{j-1}^{n+1} + F_{j+1}^n - F_j^n) \tag{73}$$

Equation 73 will be referred to as the Lax-Wendroff (A) method.

If instead of using a forward difference in the predictor and a backward difference in the corrector of Equation 73, the reverse procedure is tried, it results in the following scheme:

$$\tilde{E}_j^{n+1} = E_j^n - \frac{\Delta t}{\Delta x}(F_j^n - F_{j-1}^n)$$

$$E_j^{n+1} = E_j^n - \frac{\Delta t}{2\Delta x}(\tilde{F}_{j+1}^{n+1} - \tilde{F}_j^{n+1} + F_j^n - F_{j-1}^n) \tag{74}$$

This scheme will be referred to as the Lax-Wendroff (B) method.

A new second order, fractional time step, finite difference technique was developed during the course of this study. It falls under the same class of preferential difference schemes as do MacCormack's methods in that there exist variations, each of which yields slightly different solutions.

The first variation of the new scheme is as follows:

$$\tilde{E}_j^{n-\frac{1}{2}} = E_j^n - \frac{\Delta t}{2\Delta x}\left[-(F_{j+1}^n - F_j^n)\right]$$

$$E_j^{n+1} = E_j^n - \frac{\Delta t}{\Delta x}\left[-(\tilde{F}_j^{n+\frac{1}{2}} - \tilde{F}_{j-1}^{n-\frac{1}{2}}) + \tfrac{1}{2}F_{j+1}^n + F_j^n - \tfrac{3}{2}F_{j-1}^n\right] \qquad (75)$$

A negative forward difference is used in the predictor to yield an intermediate value of the dependent variable, E, at t- $\Delta t/2$. These intermediate values are used in a negative backward difference in conjunction with two differently weighted, forward differences in the corrector to yield a value of the dependent variable at t + Δt. This scheme is designated the Lax-Wendroff (C) method.

Substituting the predictor into the corrector of Equation 75 for a linear partial differential equation yields the following equation:

$$E_j^{n+1} = E_j^n - \frac{A}{2}\frac{\Delta t}{\Delta x}(E_{j+1}^n - E_{j-1}^n) + \tfrac{1}{2}(A\frac{\Delta t}{\Delta x})^2(E_{j+1}^n - 2E_j^n + E_{j-1}^n) \qquad (76)$$

Equation 76 can be recognized as a second order Taylor series expansion in time with second order spatial differences replacing the time derivatives. The scheme given by Equation 75 is, therefore, of second order in both time and space.

The amplification matrix for Equation 75 is:

$$G = I - A\frac{\Delta t}{\Delta x}(\tilde{G}_{n-1} - \tilde{G}_n - \tfrac{3}{2}e^{-i\alpha} + 1 + \tfrac{1}{2}e^{i\alpha}) \qquad (77)$$

where

$$\tilde{G}_{n-1} = e^{-i\alpha} - \frac{A}{2}\frac{\Delta t}{\Delta x}(e^{-i\alpha} - 1)$$

and

$$\tilde{G}_n = 1 - \frac{A}{2}\frac{\Delta t}{\Delta x}(1 - e^{i\alpha})$$

Equation 77 can be rewritten as:

$$G = I - \frac{A}{2}\frac{\Delta t}{\Delta x}(e^{i\alpha} - e^{-i\alpha}) + \tfrac{1}{2}(A\frac{\Delta t}{\Delta x})^2(e^{i\alpha} - 2 + e^{-i\alpha}) \tag{78}$$

or

$$G = I - A\frac{\Delta t}{\Delta x}\sin\alpha + (A\frac{\Delta t}{\Delta x})^2(\cos\alpha - 1) \tag{79}$$

The stability criterion is the same as that found for the other schemes studied, and is:

$$\frac{\Delta t}{\Delta x} \leq \frac{1}{|\sigma_{max}|} \tag{80}$$

The second variation of this new scheme which will be called Lax-Wendroff (D) and which possesses opposite spatial differencing to that of Equation 75 is:

$$\begin{aligned} \tilde{E}_j^{n-\frac{1}{2}} &= E_j^n - \frac{\Delta t}{\Delta x}\left[-(F_j^n - F_{j-1}^n)\right] \\ E_j^{n+1} &= E_j^n - \frac{\Delta t}{\Delta x}\left[-(\tilde{F}_{j+1}^{n-\frac{1}{2}} - \tilde{F}_j^{n-\frac{1}{2}}) + \frac{3}{2}F_{j+1}^n - F_j^n - \tfrac{1}{2}F_{j-1}^n\right] \end{aligned} \tag{81}$$

The new finite difference schemes developed in this study can be generalized to two spatial dimensions for problems which require it.

Numerical Solution

The numerical solution of the modified Burger's equation was programmed in Fortran IV and then solved on the IBM 1800 computer system of the Theoretical Branch at NASA's Ames Research Center. The 1800 has a storage capacity of 32K, 16 bit words. Linked with the 1800 is an IBM 2250 display tube (C.R.T.) which provides a visual observation of solutions as they develop. The 2250 display unit consists of a 21-inch cathode ray tube with

a display area of 12 inches by 12 inches. It has an alphanumeric keyboard, a programmed keyboard and a light pen for use as interrupt and programmed message sending devices. The unit is capable of generating and maintaining displays containing points, vectors and characters from data sent by the 1800. All of the numerical solutions obtained for this particular problem were output on the C.R.T. and then recorded using a Poloroid Land Camera.

In order to study a variety of numerical differencing schemes, a generalized two-step difference equation is used to integrate the equation $E_t + F_x = 0$. For the modified Burger's equation E and F are scalars equal to u and $u^2/2$, respectively.

The generalized, fractional time-step, difference equations are as follows:

$$\tilde{E}^{n+\zeta} = a_{11}E^n_{j-1} + a_{12}E^n_j + a_{13}E^n_{j+1} - \frac{\Delta t}{\Delta x}(a_{21}F^n_{j-1} + a_{22}F^n_j + a_{23}F^n_{j+1}) \tag{82}$$

$$E^{n+1}_j = a_{31}E^n_{j-1} + a_{32}E^n_j + a_{33}E^n_{j+1} + a_{41}\tilde{E}^{n+\zeta}_{j-q} + a_{42}\tilde{E}^{n+\zeta}_{j} + a_{43}\tilde{E}^{n+\zeta}_{j+q}$$
$$- \frac{\Delta t}{\Delta y}(a_{51}\tilde{F}^{n+\zeta}_{j-q} + a_{52}\tilde{F}^{n+5}_j + a_{53}\tilde{F}^{n+\zeta}_{j+q} + a_{61}F^n_{j-1} + a_{62}F^n_j + a_{63}F^n_{j+1}) \tag{83}$$

The tilde which appears over E in Equation 82 indicates an intermediate value of that variable. The position in time at which Equation 82 predicts the variable $\tilde{E}$ depends upon the values of $a_{2,m}$. In order that the term involving $a_{2,m}$ represent a derivative, a simple Taylor series analysis shows that

$$a_{21} + a_{22} + a_{23} = 0$$

and that

$$a_{21} a_{23} \neq 0$$

The time location of the predictor is $t + \zeta\Delta t$ (superscript $n + \zeta$ on $\tilde{E}$) where ζ is given by the following equation:

$$\zeta = -a_{21} + a_{22}$$

The tilde appearing over F in Equation 81 implies that the conservative variable F is evaluated using the intermediate values of $\tilde{E}$. The constant q which appears as a subscript in Equations 82 and 83 is either equal to $\frac{1}{2}$ or 1 depending on the difference scheme used. The coefficients, $a_{l,m}$, appearing before all terms in Equations 82 and 83 represent a sequence of constants which describe a particular difference scheme. In order to simplify the description of a particular numerical algorithm, this sequence of numbers can be written in matrix form for easy input to the computer.

Consider for example Burstein's (5) predictor-corrector version of the Lax-Wendroff difference scheme in one spacial dimension which can be written as follows:

$$\tilde{E}^{n+1}_{j+\frac{1}{2}} = \tfrac{1}{2}(E^n_{j+1} + E^n_j) - \frac{\Delta t}{\Delta x}(-F^n_j + F^n_{j+1})$$

$$E^{n+1}_j = E^n_j - \frac{\Delta t}{2\Delta x}\left(-\tilde{F}^{n+1}_{j+\frac{1}{2}} + \tilde{F}^{n+1}_{j+\frac{1}{2}} + \frac{-F^n_{j-1} + F^n_{j+1}}{2}\right) \qquad (84)$$

If $q = \frac{1}{2}$, the matrix of coefficients describing Equation 84 is:

$$a_{l,m} = \frac{1}{100}\begin{vmatrix} 0 & 50 & 50 \\ 0 & -100 & 100 \\ 0 & 100 & 0 \\ 0 & 0 & 0 \\ -50 & 50 & 0 \\ -25 & 0 & 25 \end{vmatrix}$$

Ten different numerical algorithms are used in the solution of Equation 68 and they include Lax's method, the original Lax-Wendroff method, Richtmyer's single and double time step methods, MacCormack's methods, two new methods derived in this study, Burstein's method, and a version of Fromm's method. The original Lax-Wendroff method, which necessitates the numerical evaluation of the Jacobian A, cannot be written in the form of the generalized, predictor-corrector equation and is therefore programmed separately. The coefficient matrices and the value of q for the difference schemes mentioned above are given in Appendix A.

To begin the integration of Equation 68 a sequence of mesh points (M in number) in the x-direction is assigned initial values according to those prescribed in Table 1. The values of the dependent variables at the end points of the mesh are held constant throughout the entire integration procedure. The computation is terminated well before the wave has a chance to reach these extremities. The constants which describe the difference scheme to be used are input through the alphanumeric keyboard on the C.R.T.

In order to correlate the results obtained for the different numerical

schemes, the number of mesh points (40), the location of the initial discontinuity and the total integration time are the same for each algorithm tested. For right-moving waves the discontinuity is initially spread between the tenth and eleventh mesh points, and for left-moving waves it is spread between the thirtieth and thirty-first mesh points. For the standing wave it lies between the twentieth and twenty-first mesh points. Using the ratio $\Delta t/\Delta x = 1.0$, the number of time steps integrated is twenty-five while for the ratio $\Delta t/\Delta x = 0.5$ it is fifty.

Stability Study

A stability analysis based on amplification matrix theory is performed for Equation 2 in order to determine the largest value the ratio $\Delta t/\Delta x$ can assume and still yield a stable solution when differenced according to one of the schemes mentioned above.

Equation 68 can be written in the following general form:

$$E_t + AE_x = 0 \tag{85}$$

where $E = u$, and A is the derivative of $(\frac{1}{h} u^h)$ with respect to u which simply equals u^{h-1}, (h = 2 for the modified Burger's equation).

The stability criteria for the methods considered in this paper as applied to one-dimensional, time-dependent problems is stated as follows:

$$\frac{\Delta t}{\Delta x} \leq \frac{1}{|\sigma_{max}|} \tag{25}$$

where σ_{max} is the maximum eigenvalue of the matrix A. In this case

$$|\sigma_{max}| = |u_{max}^{h-1}|$$

and therefore

$$\frac{\Delta t}{\Delta x} \leq \frac{1}{|u_{max}^{h-1}|} \tag{86}$$

Results are only presented for the particular form of Equation 85 which represents the modified Burger's equation. In all but one of the cases used in analyzing a particular method, the quantity $|u_{max}|$ is equal to one. Therefore, for these cases the ratio $\Delta t/\Delta x$ according to amplification matrix theory should be less than or equal to unity in order to obtain a stable solution.

An experimental stability analysis was performed for some of the methods tested in this study, and it was found that the ratio $\Delta t/\Delta x$ given by Equation 86 compared excellently with the experimentally determined stability bound.

Numerical Results

The numerical results obtained for each of the cases listed in Table 1 for the two values of $\Delta t/\Delta x$ are presented in a single figure for easy comparison with the other difference schemes.

The results obtained using Lax's method, the only first order scheme studied, are given in Figure 1. The "shocks" obtained for a $\Delta t/\Delta x$ of 1.0 are spread over five to six mesh intervals, while for a $\Delta t/\Delta x$ of 0.5, they are spread over ten to twelve mesh intervals. This smearing effect

is characteristic since the coefficient of artificial viscosity is inversely proportional to $\Delta t/\Delta x$. The exact shock location, which is not shown for comparison in this figure, is predicted quite well by the numerical solution. The right and left moving rarefaction waves agree well with the exact solution for the larger value of $\Delta t/\Delta x$.

The effects of the original, single-step, second order, Lax-Wendroff difference scheme on the modified Burger's equation can be seen in Figure 2. For the left and right moving "shock" waves, using a $\Delta t/\Delta x$ of 1.0, there is an undershoot and overshoot respectively succeeding each shock. This is characteristic with all Lax-Wendroff type schemes. The "shock" itself is spread over two to three mesh intervals, which is considered to be a well defined "shock". Decreasing the ratio $\Delta t/\Delta x$ to 0.5 causes a slight oscillation in the solution to appear after the shock has passed. However, the shock still remains as crisp as for a $\Delta t/\Delta x$ of 1.0. The standing waves for both values of $\Delta t/\Delta x$ are not altered in any way from the values they possessed initially. All "rarefaction" waves are predicted poorly by this scheme.

Two versions of Richtmyer's method were programmed. These included the single and double time-step techniques, and the results for each are shown in Figures 3 and 4, respectively. From Figure 4 it can be seen that all waves except the standing waves are predicted correctly. The large overshoot and undershoot which is seen for the standing waves increases linearly with time and never damps. This would seem to imply that this

difference scheme is not desirable for use in the solution of problems which possess standing shocks as the converged solution.

The results obtained by using the modified versions of MacCormack's method termed the Lax-Wendroff (A) and (B) methods are shown in Figures 5 and 6. These methods are termed preferential difference schemes and the fact that they are preferential can be seen by comparing the right and left moving "shocks" for a $\Delta t/\Delta x$ of 1.0 in either figure. This terminology is chosen since the methods yield results that differ depending on the direction of the shock. In analyzing such methods, a shock is said to be moving in the preferred direction when its over and undershoot are minimized. For the Lax-Wendroff (A) method, which uses a forward difference in the predictor and a backward difference in the corrector, the right moving shock is predicted much better than the left moving one because it possesses no characteristic overshoot and therefore approximates the exact solution in a more exact fashion. The Lax-Wendroff (B) scheme which uses a backward difference in the predictor and a forward difference in the corrector has the opposite effects. The standing waves in all cases reproduced the initial data. These schemes have the opposite effect on the "rarefaction" waves from that which they have on the "shock" waves. Namely, using the Lax-Wendroff (A) scheme yields better results for the left moving "rarefactions" and using the Lax-Wendroff (B) scheme yields better results for the right moving "rarefaction". The effect of lowering the ratio $\Delta t/\Delta x$ is the same as it is for the previously discussed second-

order schemes, except the amplitude of the oscillations is not as large.

The results obtained for the new schemes developed in this paper called the Lax-Wendroff (C) and (D) methods are shown in Figures 7 and 8. Again, the preferential effects are the same as they were for the Lax-Wendroff (A) and (B) methods. There are two cases for which this scheme becomes unstable using $\Delta t/\Delta x = 1.0$. These can be seen in the figures. The reason for the instability can be attributed to an excessively large overshoot which occurs when the method is used on "shocks" moving in the non-preferred direction. If the ratio is lowered, however, the solution will stabilize. The "rarefaction" waves for these schemes more closely approximate the exact solution than do the Lax-Wendroff (A) and (B) schemes.

The effects of Burstein's method are shown in Figure 9. Burstein's scheme is not a preferential scheme and, therefore, yields good results for all waves including the standing wave. The overshoot succeeding the shock is less than that found using the original Lax-Wendroff and Richtmyer's methods. This fact was stated by Burstein (4). However, the overshoot is greater than that found using a perferential difference scheme on a "shock" moving in the preferred direction.

The results of applying Fromm's method to the modified Burger's equation are shown in Figure 10. These results are somewhat misleading, and it should be emphasized that Fromm's method was not designed for the analysis of flows possessing discontinuities such as shocks. Further, it is,

by construction, unstable when the convective velocity changes sign. In other words the method is highly preferential, and the form of the method given in Appendix A is unstable if u is ever negative. This, at once, excludes the appropriateness of its use on most of the cases listed in Table 1 and is clearly evident from the results shown in Figure 10. Fromm's method, however, possesses the unusual and rather appealing characteristic of being able to excellently resolve a right moving shock for all values of $\Delta t/\Delta x$ from 0.1 to 1.0 as can be seen in Figure 11. This characteristic is advantageous for gas-dynamic problems in which the shock intensity varies, and the assumptions of Fromm's method are met.

Figure 12 compares the solutions of some of the methods mentioned and discussed above as applied to a right moving "shock" wave. Superimposed on these solutions is the location of the exact wave.

SUPERSONIC WEDGE FLOW

Introduction

The problem of supersonic flow over a wedge is by no means a difficult one to solve, and it serves only in this study as a stepping stone for the solution of more complicated conical flow problems. Selected finite difference schemes used to solve the modified Burger's equation (Equation 68) are programmed to solve the non-linear Eulerian equations constrained by wedge flow boundary conditions. Since Equation 68 is representative of the gas-dynamic equations, correlations between effects of the numerical differencing schemes on it and on the nonlinear Eulerian equations are sought. The supersonic wedge flow problem is also chosen so that the numerical technique used in solving conical flow problems could be properly developed and demonstrated and so that easy comparison of the numerical results obtained could be made with the exact theory. In analyzing the results of the various algorithms on the wedge flow problem, characteristics of the numerical solutions such as crispness of the shock and the effect of varying the ratio $\Delta x/\Delta y$ above and below its stability limit are sought. Ease of programming, required storage apace, and computation time are also noted in order to select an "optimum" numerical difference scheme for solving the cone at angle of attack and the conical wing-body at angle of attact problems.

The problem of supersonic flow over a wedge or conically shaped bodies can be solved by using the flow equations in their unsteady form and inte-

grating them with respect to time until the steady state is reached. The time-dependent equations are hyperbolic and the problem is a well posed initial value problem involving time and two spatial directions as the independent variables.

The basis for the solution of general conical flow problems (the wedge being a special case) used in this study resides in the fact that in one of the coordinate directions a characteristic length does not exist. By using this fact the steady flow equations can be solved if they are hyperbolic with respect to that coordinate direction. In the case of supersonic wedge flow the gas-dynamic equations are x-hyperbolic if u (the x-component of velocity) is greater than the local speed of sound. This is substantiated by the fact that the eigenvalues of the gas-dynamic equations derived in Appendix C are real. The x-coordinate in the steady flow equations is thus analogous to time in the unsteady equations, and therefore the problem is well posed. Since this is so, integration of the governing partial differential equation may be performed with respect to the x-coordinate. If time is eliminated as one of the independent variables in the problem, the amount of storage space, numerical computations, and resulting computer time are reduced.

Derivation of Equations

In Cartesian coordinates the two-dimensional gas-dynamic equations under the assumptions of steady, inviscid, non-heat-conducting and adiabatic flow

conditions are:

$$\frac{\partial}{\partial x}(\rho u) + \frac{\partial}{\partial y}(\rho v) = 0 \tag{87}$$

$$\frac{\partial}{\partial x}(P + \rho u^2) + \frac{\partial}{\partial y}(\rho uv) = 0 \tag{88}$$

$$\frac{\partial}{\partial x}(\rho uv) + \frac{\partial}{\partial y}(P + \rho v^2) = 0 \tag{89}$$

$$\frac{\partial}{\partial x}(Eu + Pu) + \frac{\partial}{\partial y}(Ev + Pv) = 0 \tag{90}$$

which represent the conservation of mass, x and y momentum, and energy respectively where

$$E = \frac{P}{\gamma-1} + \rho \frac{u^2+v^2}{2} \tag{91}$$

is the energy per unit volume.

Two forms of the energy equation are used in the solution of this problem. In the first case the energy equation is used in its differential form as given by Equation 90. Authors such as Moretti (36), Bohachevsky (3), Emery (12), Burstein (6), and Lapidus (26) who are interested in transient solutions to the time-dependent flow equations and possible application of real gas effects must use this form.

In the second case the energy equation is used in its integrated form since the steady flow equations are used. The total enthalpy of the flow field is constant and the energy equation can be written as follows:

$$\frac{\gamma}{\gamma-1}\frac{P}{\rho} + \frac{q^2}{2} = \frac{c_{0_\infty}^2}{\gamma-1} \tag{92}$$

In one special case Babenko (1) solved a conical flow problem using the

steady flow equations but with the differential form of the energy equation. This study shows that the same end results are obtained regardless of the form of the energy equation. The integrated form does eliminate the numerical integration of one partial differential equation and therefore reduces the computation time.

In this study Equations 87 through 92 are nondimensionalized with respect to freestream stagnation conditions, i.e., pressures are nondimensionalized with respect to gamma times the stagnation pressure, density with respect to stagnation density, velocities with respect to stagnation speed of sound and lengths with respect to some length, L, which is set equal to unity for the numerical computation.

Determination of Gas-Dynamic Variables from Conservative Variables

Equations 87 through 91 are of the general conservation form proposed for differencing by Lax (28) and can be represented by:

$$\frac{\partial E_1}{\partial x} + \frac{\partial F_1}{\partial y} = 0 \qquad (93)$$

in which E_1 and F_1 represent the conservative variables. According to the scheme proposed below, E_1 is the dependent variable of integration.

The conservative variables, F_1, can be determined indirectly from the variables of integration, E_1. The procedure is outlined below for both forms of the energy equation. In this procedure it is necessary to first determine the flow variable P, ρ, u, v, and E (energy) from the E_1 conservative variables. This entails the solution of four simultaneous alge-

braic equations. These are:

$$a = \rho u \tag{94}$$

$$b = P + \rho u^2 \tag{95}$$

$$c = \rho u v \tag{96}$$

and in addition for the differential form of the energy equation

$$d = Eu + Pu \tag{97}$$

or for the integrated form of the energy equation

$$P = \rho\left(1 - \frac{\gamma-1}{2} q^2\right) \tag{98}$$

in which a, b, c, and d are temporarily assumed constant.

The solutions are:

$$v = c/a \tag{99}$$

$$u = \frac{be \pm \sqrt{b^2e^2 - a(2e-1)(2d-c^2/a)}}{2a(1-f)} \tag{100}$$

using the differential energy equation and

$$u = \frac{b \pm \sqrt{b^2 - 4a^2(1-f)(1-fv^2)}}{2a(1-f)} \tag{101}$$

using the integrated energy equation. For both cases

$$\rho = a/u \tag{102}$$

$$P = b - \rho u^2 \tag{103}$$

where

$$e = \frac{\gamma}{\gamma-1}$$

and

$$f = (\gamma-1)/2$$

The sign before the radical in Equations 100 and 101 must be positive if u (the x-component of velocity) is supersonic and negative if u is subsonic. In the applications outlined in this study the Mach number is chosen well above the maximum for shock detachment, and therefore the x component of velocity is everywhere supersonic.

Exact Solution

For steady supersonic flow over a wedge the gas-dynamic variables are constant on either side of the straight shock. This implies that all derivatives of the flow variables with respect to either coordinate direction in the shock layer are zero. In addition the exact inviscid boundary condition at the body requires that the flow must be parallel to the body.

To determine the exact pressure on the surface of the wedge and the exact location of the shock wave for comparison with the numerical solution the following equations found in NACA Report 1135 (38) were used:

$$\frac{P_w}{P_\infty} = \frac{2\gamma M_\infty^2 \sin^2\theta - (\gamma-1)}{\gamma+1} \tag{104}$$

where P_w denotes pressure on the wedge and θ represents the shock angle.

As is indicated in the report, the shock angle θ is found by solving numerically the following polynomial:

$$\sin^6\theta + b \sin^4\theta + c \sin^2\theta + d = 0 \tag{105}$$

where

$$b = -\frac{M_\infty^2 + 2}{M_\infty^2} - \gamma \sin^2\delta$$

$$c = \frac{2M_\infty^2 + 1}{M_\infty^4} + \frac{(\gamma+1)^2}{4} + \frac{\gamma-1}{M_\infty^2} \sin^2\delta$$

$$d = -\frac{\cos^2\delta}{M_\infty^4}$$

This set of equations yields three roots, one of which corresponds to a decrease in entropy and should therefore be disregarded according to the second law of thermodynamics, and two others corresponding to strong and weak solutions. Of these two the weak solution is the one of interest.

Method of Solution

The body may be oriented with respect to the coordinate directions in two ways. In the first case the top surface of the body is canted at the wedge angle with respect to the x axis while the free stream is parallel to the axis. For this wedge orientation the mesh points do not lie on the body. Hence the mesh for the flow region above the wedge is irregular. Burstein (6) solved the time-dependent flow equations for the problem of a wedge in a channel using an irregular mesh. He experienced stability difficulties in applying the boundary conditions at the surface of the body because of this fact. He also found that for surfaces oriented parallel to the coordinate directions application of the boundary conditions was facilitated and no instabilities were experienced.

The second possibility and the one used in this study orients the body in such a manner that its top surface coincides with the x-axis (Figure 13).

The free-stream velocity is thus canted at the wedge angle with respect to the x-axis. The entire computing region is covered by a rectangular mesh which facilitates application of the boundary conditions at the body.

A section of the flow field extending from x = 1 to x = 2 and from the body to the free stream is the region of integration (Figure 13). Guessed values of the flow variables are used to initialize the mesh points in the y direction at x = 1. The differenced equations are then integrated from x = 1 to x = 2 at which time under the conical flow assumption, the distance between the shock and the body should have doubled. This can be seen from Figure 13 since by similar triangles the distance d_1 is equal to half the distance d_2. The flow variables are then "stepped back" to x = 1.

The values of the flow variables existing at the odd numbered mesh points at x = 2 are used as initial data for the mesh points at x = 1. For example the flow variables at the fifth mesh point at x = 2 lie along the same ray as the third mesh point at x = 1 and should therefore be the same under the conical flow assumption. Only half of the mesh points at x = 1 are reinitialized by this procedure. The rest are assigned free-stream values. The integration from x = 1 to x = 2 is then repeated. This entire procedure is continued until there is little change between the flow variables at x = 2 for two subsequent cycles. The solution is then assumed to have converged.

It might be noted that it is not necessary to terminate the integration

at x = 2. For example, the integration may be continued to x = 3 and then stepped back taking every third point as initial data at x = 1. This, however, would entail using a larger number of mesh points in the y direction in order to completely capture the shock at x = 3 and therefore increase computing time. It is also possible to terminate the integration at some value of x less than x = 2. This would necessitate interpolation of the flow variables in order to reinitialize the values at x = 1.

It is necessary to choose a sufficient number of mesh points in the y direction so that at x = 2 the shock wave is completely captured and the upper portion of the integration region is truly in the free stream.

Numerical Boundary and Initial Conditions

It is necessary to specify boundary conditions at y_{max} (Figure 13), which lies entirely in the free stream, and at the body. At $y = y_{max}$ the free-stream pressure, density, and velocities are specified and remained fixed throughout the integration. The mesh point just below the one at y_{max} is the last to be integrated while the first to be integrated is the mesh point directly above the body. The values of the flow variables at the body are set equal to the values at one mesh point above the body. This might be thought of as being a zeroth order extrapolation but in the case of wedge flow, it is an exact boundary condition. The normal velocity component or y component at the body is set equal to zero since the flow is parallel to the body.

Two different schemes are tried for initializing the flow variables

at the mesh points in the y direction at x = 1. In the first case guesses are made based on linear theory as to the location of the shock and the values of the flow variables in the shock layer. In the second case all mesh points are initially assigned values equal to those in the free stream except at the body where the normal velocity component is set equal to zero. Both schemes yield the same results, but as should be expected the first one converges more rapidly.

The free-stream pressure, density, and velocity can be written as a function of the ratio of specific heats and free-stream Mach number as follows:

$$\bar{P}_\infty = \frac{1}{\gamma}\left(1 + \frac{\gamma-1}{2} M_\infty^2\right)^{-\frac{\gamma}{\gamma-1}} \tag{106}$$

$$\bar{\rho}_\infty = \left(1 + \frac{\gamma-1}{2} M_\infty^2\right)^{-\frac{1}{\gamma-1}} \tag{107}$$

$$\bar{q}_\infty = M_\infty\left(1 + \frac{\gamma-1}{2} M_\infty^2\right)^{-1/2} \tag{108}$$

where the bar over the variable implies that the quantity is nondimensional.

The free-stream velocity in this problem is canted with respect to the x axis at an angle equal to the wedge angle. The free-stream velocity can be written in vector form as:

$$\vec{\bar{q}}_\infty = \bar{q}_\infty(\cos\delta\,\hat{i} - \sin\delta\,\hat{j}) \tag{109}$$

where δ equals the wedge angle.

Computer Program

The computer program for the solution of supersonic flow over a wedge uses the generalized, two-step predictor-corrector difference equation described earlier. The procedure allows for the use of a number of different numerical schemes. A resume of the computer program including the function of its subroutines is given in Appendix B. The program in its final form was stored on the disk of the IBM 1800 as a core load for easy accessibility.

In using the program it is necessary to initialize certain constants which govern the computation before the actual integration procedure is initiated. These constants are fed into the computer through the alphanumeric keyboard on the C.R.T. These constants are:

NX - the integer number of steps taken between x=1 and x=2 (the integration step size $\Delta x = 1/(NX-1)$,

NY - The integer number of mesh points in the y direction,

DXDY - the ratio $\Delta x/\Delta y$ which governs the stability of the solution (This will be discussed below in greater detail.),

NSTEP - the integer number one or two depending on whether one or two steps in x is made after one complete integration,

NPRT - a zero will print nothing while one will print both initial and converged values of the flow variables,

A(L,M) - the matrix of coefficients describing numerical differencing scheme used,

DELTA - the wedge angle in degrees,

XMACH - the free-stream Mach number

The quantity Δy, the distance between mesh points in the y direction, is determined using NX and DXDY. The quantity DXDY should be as large as possible without causing instabilities, and therefore, there exists only one optimum possible value of it for a given flow situation. In order for the shock to be completely captured it is therefore necessary to adjust the value of Δy or NY so that y_{max} (Figure 13) extends well into the free stream. The quantity Δy can only be adjusted through the parameter NX by the following relation:

$$\Delta y = \frac{1}{(NX-1)DXDY} \tag{110}$$

y_{max}, therefore, becomes:

$$y_{max} = \frac{NY-1}{(NX-1)DXDY} \tag{111}$$

Equations 110 and 111 are based on the fact that the integration starts at $x = 1$ and terminates at $x = 2$. Hence, by adjusting either NY or NX, y_{max} can have any value desired.

To determine the location of the shock formed as a result of the numerical solution some scheme based on the physical properties of the flow field had to be devised. Since it is well known that the flow properties are constant throughout the shock layer for supersonic wedge flow, by averaging the pressure of the free stream with that at the surface of the wedge a value can be found which corresponds to the pressure at the center

of the shock wave ($P_{sh_{avg}}$). By scanning the values of the pressure at each mesh point, a pressure can be found which is closest to $P_{sh_{avg}}$. This locates the integer mesh point of the shock. Using linear interpolation a fraction of the mesh interval can be found which yields the exact pressure $P_{sh_{avg}}$. Multiplying Δy by the exact fractional mesh point location the distance between the shock and the body for a given x can be found.

Knowing the exact pressure distribution and shock wave location for a wedge in supersonic flow, a visual comparison of the numerical solution as it develops can be made using the C.R.T. The C.R.T. might then be thought of as a numerical wind tunnel. For purposes of study and analysis still or motion pictures can be made from the displays which appear. Displayed after each integration step on the C.R.T. (e.g., see Figure 16) are the exact and numerical solutions of the pressure distribution as a function of y (the distance normal to the body) for a given x location, the section at which the pressure distribution plot is made, the exact and numerical location of the shock wave, a cross sectional view of the body shape and an arrow indicating the direction of flow in the free stream. The Mach number and wedge angle are also indicated. In the fourth row of the upper left-hand display there appears the number 000810. The last two digits of this number indicate the number of times the equations have been integrated since starting at x = 1, and the middle two digits indicate the number of times the step-back procedure has occurred.

Stability Analysis for Flow Over a Wedge

As was mentioned previously, one of the necessary inputs to initiate integration is the value of $\Delta x/\Delta y$ (DXDY). It is this quantity which governs the stability of the numerical soltuion. If the value chosen for this quantity is too large, the solution becomes oscillatory and diverges. If the value chosen is too small the system is dissipative and this results in a smeared shock. Therefore, the optimum choice for this ratio is the largest permissible value which allows the solution to remain stable.

Two techniques for the determination of the quantity $\Delta x/\Delta y$ will be discussed in this section. The first of these involves simply a sequence of trial-and-error experiments in which different values of $\Delta x/\Delta y$ are tried for a given flow situation, and the optimum one is selected based on stability of the resulting solutions. Figure 15 shows the results of such an experiment performed on the C.R.T. for flow at Mach numbers of 2 and 3 over 5, 10, and 15 degree wedges. Two values are plotted for $\Delta x/\Delta y$ for each combination indicating stable and unstable soltuions. MacCormack's (A) differencing scheme was used in this experiment. Instabilities which did occur appeared to form in the shock layer and not in the free stream, e.g., see Figure 19 for the case of $\Delta x/\Delta y$ of 1.3. A family of parametric curves could conceivably be constructed based on experiments such as the one above which would yield the desired value of $\Delta x/\Delta y$ for any given flow situation. This would, however, involve a large block of computer time.

The second technique which can be used to predict a value of $\Delta x/\Delta y$

involves the use of amplification matrix theory. Many authors resort to the use of this theory because of its ability to conservatively and quickly predict the stability boundary. The method, as mentioned before, is based on a locally linear analysis of the gas-dynamic equations coupled with a discrete harmonic analysis of the linear difference scheme which yields the amplification matrix. According to the von Neumann necessary condition for stability (43) the eigenvalues of the amplification matrix should not exceed unity in absolute value. This results in the following equation for $\Delta x/\Delta y$:

$$\frac{\Delta x}{\Delta y} < \frac{1}{|\sigma_{max}|} \tag{112}$$

where σ_{max} is the maximum eigenvalue of the coefficient matrix of the gas-dynamic equations.

This eigenvalue was determined in Appendix C and is repeated here:

$$|\sigma_{max}| = \left| \frac{-uv \pm c\sqrt{u^2+v^2-c^2}}{u^2-c^2} \right| \tag{113}$$

It can be rewritten more simply as:

$$|\sigma_{max}| = \frac{|uv| + c\sqrt{u^2+v^2-c^2}}{u^2-c^2} \tag{114}$$

Substituting Equation 114 into Equation 112 results in the following equation:

$$\frac{\Delta x}{\Delta y} = \frac{u^2 - c^2}{|uv| + c\sqrt{u^2+v^2-c^2}} = \frac{M_u^2 - 1}{M_u M_v + \sqrt{M^2 - 1}} \tag{115}$$

The only flow variables known a priori are those associated with

the initialization procedure. Most of the cases solved in this study were started impulsively using free-stream values as the initial guess for the flow variables. A ratio $\Delta x/\Delta y$ can be determined using the free-stream variables. For the cases considered above if the free-stream conditions are used in Equation 115, some rather conservative values are predicted for $\Delta x/\Delta y$. These are plotted as the dashed line in Figure 15 along with the experimentally determined values.

For the case of Mach 2 flow over a wedge the values of $\Delta x/\Delta y$ predicted using amplification matrix theory fall a little below the experimental results. However, for Mach 3 flow the curve based on theory lies well below that found by experiment.

Using the same stable value of $\Delta x/\Delta y$, a numerical solution to the problem is found which approximates the exact solution. A local maximum eigenvalue in the shock layer can then be determined using the numerical values of the flow variables there. This yields another value of $\Delta x/\Delta y$. These values are plotted as the solid line in Figure 15 for the same cases considered above.

From these results it can be seen that there is a better correlation with the experiment for the ratios determined using variables in the shock layer than using the variables of the free stream. This is in direct contradiction to what one would expect using amplification matrix theory.

According to amplification matrix theory and based on the fact that the maximum eigenvalue occurs in the free stream any instabilities which might

occur should appear first in the free stream. As was mentioned previously in the experimental study, the instabilities which occurred appeared to form in the shock layer and not in the free stream.

It can be concluded that the optimum way to determine the maximum permissible values of $\Delta x/\Delta y$ is by a combination of the above techniques. Using a value of $\Delta x/\Delta y$ based on the free-stream variables as an initial guess and then proceeding experimentally by incrementing its value is one possibility.

There are two possible explanations for the considerable disagreement between the amplification matrix theory and the experiment. The usual and most often used explanation is that the equations which are actually used in the numerical solution are nonlinear and the amplification matrix is based on a linear analysis. Therefore, the disagreement is a result of the nonlinear effects. This is probably part of the reason. Another part, and possibly a greater part, is that use of the step-back principle seems to enhance stability.

A motion picture study was made which demonstrated the fact that an unstable solution could be made stable by stepping the flow field back in about half as many steps as was previously used. The case considered was Mach 2 flow over a 15 degree wedge. The value of $\Delta x/\Delta y$ was 1.26, and this caused the solution using Lax's method to become unstable before integrating the required 22 steps to reach $x = 2$. The number of steps was then decreased to 12, and the integration was again initiated. This time

the solution was stable and resulted in quite a sharp shock for Lax's method.

At "step-back" (x = 2) the values of the flow variables at every other mesh point are disregarded, and, therefore, oscillations which are sometimes present are smoothed and damped somewhat by this procedure. It is therefore believed that stepping the flow field back does effect the stability and hence the value of $\Delta x/\Delta y$.

Numerical Results

The problem of supersonic flow over a wedge is solved using seven of the numerical differencing schemes described in this study. The schemes and their associated coefficient matrices are listed in Appendix A. In experimenting with four representative differencing schemes selected from the seven, certain characteristics of the solutions are noted. One of these includes the number of mesh intervals it takes to completely capture the shock. Others include how well the shock location is predicted, how close the pressure distribution agrees with the exact solution and what the effects are on the solution of varying the ratio $\Delta x/\Delta y$ in both directions from its optimum value.

For the experiment a 15 degree wedge in Mach 2 flow is selected. NX is chosen as 16 and NY as 30. This allows for a sufficient number of points to completely capture the shock and describe the shock layer for all values of $\Delta x/\Delta y$. The cases considered are all started impulsively using the free-stream conditions as the initial data. Table 2 compares the numerically determined pressure coefficients with the exact theory for some of

Table 2. Comparison of numerical and exact solutions for wedge flow

Mach Number	Wedge Angle	Method	Pressure Coefficient Numerical	Exact	Percent Error
2	15°	Lax	0.42686	0.42666	0.05
2	15°	MacCormack (A)	0.42647	0.42666	0.04
2	15°	Richtmyer single time step	0.42647	0.42666	0.04
2	15°	Richtmyer double time step	0.42611	0.42666	0.13
2	15°	Burstein	0.42647	0.42666	0.04
2	15°	Lax-Wendroff (C)	0.42817	0.42666	0.35
2	10°	MacCormack (A)	0.25534	0.25234	1.19
2	5°	MacCormack (A)	0.11264	0.11156	0.96
3	15°	MacCormack (A)	0.28820	0.28913	0.30
3	10°	MacCormack (A)	0.16817	0.16737	0.50
3	5°	MacCormack (A)	0.07206	0.073180	1.6

the difference schemes that are used.

For wedge flow Lax's method is the only first order difference scheme that is tried. Figure 16 shows the results of this method. A value of 1.2 for $\Delta x/\Delta y$ is found to be the optimum and to yield the most satisfactory results. The shock is spread over approximately four mesh intervals, and its location agrees quite well with the exact shock location. The pressure distribution throughout the shock layer also agrees well with the exact

theory. Bohachevsky (2) used Lax's method to calculate detached shocks and found them to be spread over six to eight mesh intervals. This is the usual result of investigators who use Lax's method. The finer shock found in this study is probably a result of using the step-back principle.

When a value of 1.3, slightly above optimum, is used for $\Delta x/\Delta y$ the solution becomes unstable. Using a value of 0.8, well below optimum, results in a shock which is spread over seven mesh intervals, the center of which though coincides with the exact shock location. The pressure distribution compares quite well with the exact theory.

Richtmyer's double time step method, a predictor-corrector version of the Lax-Wendroff scheme, is used next, and the results are shown in Figure 17. For a $\Delta x/\Delta y$ of 1.1 the solution is not unstable, but the results are oscillatory in the shock layer. The shock wave is "crisp" and covers only two mesh intervals. If $\Delta x/\Delta y$ is set equal to 1.0 the pressure distribution throughout the shock layer becomes smooth. The shock is spread over three mesh intervals while its location varies somewhat from the exact location. Setting $\Delta x/\Delta y$ equal to 0.6 yields an undesirable solution in all respects.

Richtmyer's single time step scheme is employed next and the results of using it on the wedge flow problem for the same three $\Delta x/\Delta y$ ratios used previously are shown in Figure 18. For a $\Delta x/\Delta y$ of 0.6 the shock is spread over three mesh intervals. However, there exists a slight oscillation near the shock on the body side. This is characteristic with second order methods. The dissipation effect, i.e. the smeared shock wave effect, how-

ever, is not as predominant as it is in Lax's first order method. The overshoot in pressure observed for a $\Delta x/\Delta y$ of 1.0 is characteristic of the Lax-Wendroff type schemes.

The results of using MacCormack's (A) method are shown in Figure 19. For $\Delta x/\Delta y = 1.0$ no overshoot is observed, but small oscillations throughout the shock layer are found. The scheme does not appear to be as dissipative for $\Delta x/\Delta y = 0.6$ as are the previous two second order schemes. The oscillations at the shock have a smaller amplitude for this method than they do for the previously studied second order methods.

The three remaining schemes exhibited characteristics similar to either Richtmyer's single time step method or MacCormack's (A) method, and results are only presented for a value of $\Delta x/\Delta y$ of 1.0. These results appear in Figure 20 for the Lax-Wendroff (C) method, Burstein's method, and MacCormack's (B) method.

It might be pointed out that as predicted by Burstein (5) and demonstrated in this experiment, the overshoot in pressure at the shock is reduced when using this scheme.

All of the results observed in the solution of supersonic flow over a wedge using the nonlinear Eulerian equations correlate with the results observed using the modified Burger's equation. By comparing similar flow situations the correlations are readily recognized. The shocks captured in both problems exhibited the same characteristics, i.e., the dissipation or smearing effect, and the typical overshoot and undershoot behavior. This,

therefore, enables one to use a simple one-dimensional time dependent equation to analyze finite difference schemes and their particular characteristics.

Different flow configurations were run in which solutions for 5, 10, and 15 degree wedges in Mach 2 and Mach 3 flow were found. The results are given in Figures 21 and 22. The pressure coefficients are compared with the exact theory in Table 2. MacCormack's (A) method was used for these solutions.

Flow situations were also set up using negative wedge angles which resulted in Prandtl-Meyer expansions about the leading edge. MacCormack's (A) was used, and it yielded excellent results.

It can be concluded from this study of wedge flow that the step-back principle proposed for the solution of conical flow problems used in conjunction with a second order numerical differencing scheme yields acceptable results.

CONE AT INCIDENCE

Introduction

When the angle of attack of a cone in a supersonic flow field is increased such that supersonic cross-flow velocities result, there exists the possibility of embedded shock waves forming on the lee side of the cone. There is at present no inviscid theory which describes this flow situation, and it is the purpose of this section to demonstrate the existence and formation of the aforementioned embedded shocks.

Rainbird (39) in his experimental study of cones at incidence found embedded shocks in Mach 1.8 flow for an angle of attack equal to 1.82 times the cone half-angle. The shock was relatively weak and appeared near the 120° meridional plane. Cooke (7) developed an implicit finite-difference method for the compressible laminar case of cones at large yaw. In applying his method to circular cones, he was restricted by the lack of knowledge of the inviscid flow field at large relative incidences. It should be pointed out that at such large incidences the viscous effects, which are present in the physical situation, are predominant, and the inviscid theory developed in this section can, therefore, be used as near surface conditions in determining the external flow for boundary layer calculations.

The cone at small incidence problem is not a new one and has been investigated by Ferri (14), Stocker and Mauger (48), Kopal (24) and Melnik (33) to mention a few.

Most of these early solutions of the gas-dynamic equations describing conical flow fields introduced a series of simplifying assumptions, which

sometimes yielded analytical solutions. The assumptions imposed, however, are sometimes not justified and the error introduced cannot as a rule be determined. Recent numerical solutions have been obtained by Emery (12), Babenko (1), Gonidou (19), Rakich (40), and Moretti (35). Most of these people use finite difference techniques which are capable of solving the complete gas-dynamic equations with a high order of accuracy.

Emery (12) solved the problem of a cone at zero angle of attack using the time-dependent form of the gas-dynamic equations. He differenced the equations in spherical coordinates according to Lax's method and in cylindrical coordinates according to Rusanov's method. Difficulties were experienced in differencing the apex of the cone since it is a singular point of the flow and of the coordinate system. Emery found, however, that suitable results could be obtained by employing a backward difference at this point which simply had the effect of neglecting it.

Babenko, et al. (1) designed a method to determine the flow field about smooth three-dimensional bodies in supersonic flow fields and in so doing demonstrated the technique for a pointed circular cone. His technique termed "the method of establishment" differences the steady flow equations in non-conservative form and applies the Rankine-Hugoniot equations at the conical shock. The scheme utilizes the fact that the flow near an infinite cone is self-similar and therefore independent of the radial coordinate direction. The integration is performed with respect to this coordinate direction and is assumed to have converged when the flow variables become independent of it. Babenko's technique in contrast to the "step back principle" used in this study integrates the gas-dynamic equations until r, the radial coordinate, becomes large, while the step back

principle integrates the flow equations between two particular points.

Babenko's results are tabulated for various Mach numbers, cone angles, and angles of attacks.

Gonidou (19) used Babenko's "method of establishment" in obtaining numerical results for circular and elliptical cones at angle of attack. He determined the flow fields about a 9° circular cone in Mach 7 flow for 5°, 7°, 9°, and 11° angle of attack. Gonidou found that for the 11° case the shock wave remained closed on the lee side of the cone and approached the local Mach wave. He experienced numerical instabilities when he tried to increase the angle of attack beyond 11° and it was, therefore, not possible to observe whether or not evanescence of the lee shock occurred.

Rakich (40) presented a three-dimensional method of characteristic technique for solving the blunted and pointed circular cone problem. Calculations were performed for a 15° half-angle sphere-cone at angles of attack up to 20°. He compared these results with those for the pointed cone at 10° angle of attack and demonstrated that the effects of bluntness do persist at a large distance downstream.

Moretti (35) in solving the problem considered the conical motion as the asymptote (with respect to r in spherical coordinates) of a non-conical one. He assigned initial values to the flow variables at $r = r_o$ and computed the flow from there on as dependent on θ, ϕ, and r, until an asymptotic state, independent of r, developed. He used the original Lax-Wendroff finite difference technique in conjunction with a method of characteristics at the shock and on the body. His scheme was limited to angles of attack less than the cone half-angle.

In this section the problem of a cone at large incidences is solved

using the three-dimensional steady flow gas-dynamic equations which are hyperbolic with respect to the independent variable of integration. The actual conical flow equations are elliptic for small incidences and mixed for large incidences and become ill-suited when numerical procedures of the type discussed in this study are used for their solution. Using the "step back principle" established in the solution for supersonic flow over a wedge described in a previous section in conjunction with one of the numerical differencing techniques described earlier, the problem of a cone at incidence can be formulated and subsequently solved.

The physical argument for the existence of a conical flow described by the above technique is that the flow in the shock layer is constrained by two boundaries, the free stream which is uniform and the body which is a cone, each of which is conical, i.e., possesses no characteristic length in one coordinate direction. The constrained flow must therefore itself be conical.

Derivation of Equations

Under the assumption of steady flow for a perfect, inviscid and non-heat conducting gas the basic flow equations in vector notation are:

Conservation of Mass;

$$\nabla\cdot(\rho\bar{q}) = 0 \tag{116}$$

Conservation of Momentum;

$$\nabla\left(\frac{\bar{q}\cdot\bar{q}}{2}\right) + (\nabla x\bar{q})x\bar{q} + \frac{\nabla P}{\rho} = 0 \tag{117}$$

Conservation of Energy;

$$q\cdot\nabla H_t = 0 \tag{118}$$

In solving boundary value problems one of the most difficult problems that is encountered is satisfying the boundary conditions at the body. For this reason a body oriented coordinate system is chosen (Figure 23). In this coordinate system x denotes distance along the body, y denotes distance normal to the body, and ϕ is the meridional angle measured from the windward side.

The transformation of Equations 116 and 117 using the aforementioned coordinate system yields:

Continuity;

$$\frac{\partial}{\partial x}(\rho u r) + \frac{\partial}{\partial y}(\rho v r H) + \frac{\partial}{\partial \phi}(\rho w H) = 0 \tag{119}$$

Momentum in x direction;

$$\frac{u}{H}\left(\frac{du}{\partial x} + \frac{v}{R_b}\right) + r\left(\frac{\partial u}{\partial y} + \frac{w}{r}\left(\frac{\partial u}{\partial \phi} - \frac{w}{H}\frac{\partial r}{\partial x}\right) + \frac{1}{\rho H}\frac{\partial P}{\partial x} = 0\right. \tag{120}$$

Momentum in y direction;

$$\frac{u}{H}\left(\frac{\partial v}{\partial x} - \frac{u}{R_b}\right) + v\frac{\partial v}{\partial y} + \frac{w}{r}\left(\frac{\partial v}{\partial \phi} - w\frac{\partial r}{\partial y}\right) + \frac{1}{\rho}\frac{\partial P}{\partial y} = 0 \tag{121}$$

Momentum in ϕ direction;

$$\frac{u}{H}\frac{\partial w}{\partial x} + v\frac{\partial w}{\partial y} + \frac{w}{r}\left(\frac{u}{H}\frac{\partial r}{\partial x} + v\frac{\partial r}{\partial y} + \frac{\partial w}{\partial \phi}\right) + \frac{1}{\rho r}\frac{\partial P}{\partial \phi} = 0 \tag{122}$$

where H is the metric coefficient $1 + y/R_b$. The energy equation is used in its integrated form as was done by Kutler (25), thereby facilitating numerical computation.

Lax (27) originally showed that the determination of flow fields containing strong shocks may be found if the governing equations are written in conservation form which is defined mathematically to be $E_\xi + F_\eta + G_\zeta + H = 0$ where ξ, η, and ζ represent generalized coordinates and physically to be an expression of the conservation of a physical quantity such as mass, momentum, etc. He demonstrated for a simple one-dimensional,

time-dependent partial differential equation that the wave speed was predicted more accurately if the P.D.E. was differenced in conservative form. Gary (43) obtained the same result for a one-dimensional shock wave. In his study he used the original Lax-Wendroff technique for differencing the flow equations in conservative form and a modified version of it for the non-conservative form.

In conjunction with the continuity equation (Equation 119) which is in conservative form Equations 120, 121, and 122 are transformed to the conservation-law form and are written as follows:

Momentum in x direction;

$$\frac{\partial}{\partial x}\left[r(P + \rho u^2)\right] + \frac{\partial}{\partial y}(Hr\rho uv) + \frac{\partial}{\partial \phi}(H\rho uw) - (P + \rho w^2)\frac{\partial r}{\partial x} + \rho uv \frac{r}{R_b} = 0 \tag{123}$$

Momentum in y direction;

$$\frac{\partial}{\partial x}(r\rho uv) + \frac{\partial}{\partial y}\left[rH(P + \rho v^2)\right] + \frac{\partial}{\partial \phi}(H\rho vw) - (P + \rho w^2)H\frac{\partial r}{\partial y} - (P + \rho u^2)\frac{r}{R_b} = 0 \tag{124}$$

Momentum in ϕ direction;

$$\frac{\partial}{\partial x}(r\rho uw) + \frac{\partial}{\partial y}(rH\rho vw) + \frac{\partial}{\partial \phi}\left[H(P + \rho w^2)\right] + \rho uw \frac{\partial r}{\partial x} + \rho vwH \frac{\partial r}{\partial y} = 0 \tag{125}$$

For a conically shaped body with a circular cross section R_b becomes infinite and the metric coefficient H equals one. The flow equations become:

Continuity;

$$\frac{\partial}{\partial x}(\rho ur) + \frac{\partial}{\partial y}(\rho vr) + \frac{\partial}{\partial \phi}(\rho w) = 0 \tag{126}$$

Momentum in x direction;

$$\frac{\partial}{\partial x}\left[r(P + \rho u^2)\right] + \frac{\partial}{\partial y}(r\rho uv) + \frac{\partial}{\partial \phi}(\rho uw) - (P + \rho w^2)\sin \sigma = 0 \tag{127}$$

Momentum in y direction;

$$\frac{\partial}{\partial x}(r\rho uv) + \frac{\partial}{\partial y}\left[r(P + \rho v^2)\right] + \frac{\partial}{\partial \phi}(\rho vw) - (P + \rho w^2)\cos \sigma = 0 \tag{128}$$

Momentum in ϕ direction;

$$\frac{\partial}{\partial x}(r\rho uw) + \frac{\partial}{\partial y}(r\rho vw) + \frac{\partial}{\partial \phi}(P + \rho w^2) + \rho w(u \sin \sigma + v \cos \sigma = 0 \tag{129}$$

where σ equals the cone half-angle, and the cylindrical radius

$$r = x \sin \sigma + y \cos \sigma \tag{130}$$

Equations 126, 127, 128, 129, and the energy equation are next non-dimensionalized as in Kutler (25). Pressure and density are non-dimensionalized with respect to stagnation conditions, velocities are non-dimensionalized with respect to maximum adiabatic velocity, while distances are non-dimensionalized with respect to some length, L. This procedure results in the following form of the gasdynamic equations:

Continuity;

$$\frac{\partial}{\partial x}(\rho ur) + \frac{\partial}{\partial y}(\rho vr) + \frac{\partial}{\partial \phi}(\rho w) = 0 \tag{131}$$

Momentum in x direction;

$$\frac{\partial}{\partial x}\left[r(kP + \rho u^2)\right] + \frac{\partial}{\partial y}(r\rho uv) + \frac{\partial}{\partial \phi}(\rho uw) - (kP + \rho w^2)\sin \sigma = 0 \tag{132}$$

Momentum in y direction;

$$\frac{\partial}{\partial x}(r\rho uv) + \frac{\partial}{\partial y}\left[r(kP + \rho v^2)\right] + \frac{\partial}{\partial \phi}(\rho vw) - (kP + \rho w^2)\cos \sigma = 0 \tag{133}$$

Momentum in ϕ direction;

$$\frac{\partial}{\partial x}(r\rho uw) + \frac{\partial}{\partial y}(r\rho vw) + \frac{\partial}{\partial \phi}(kP + \rho w^2) + \rho w(u \sin \sigma + v \cos \sigma) = 0 \tag{134}$$

Energy;

$$P = \rho(1 - q^2) \tag{135}$$

where $k = \frac{\gamma - 1}{2\gamma}$

Equations 131, 132, 133, and 134 can be represented in a general form by the following equation:

$$\frac{\partial E_1}{\partial x} + \frac{\partial F_1}{\partial y} + \frac{\partial G_1}{\partial \phi} + H_1 = 0 \tag{136}$$

where E_1, F_1, and G_1 are the conservation variables and H_1 is the additional term whose appearance depends upon the choice of coordinate system.

It was found in the present study that when the governing flow equations are differenced according to schemes which average the dependent variable of integration in the predictor, that eliminating the cylindrical radius, r (Equation 130), by differentiation of the equations facilitates the analytical determination and subsequent numerical computation of necessary correction factors. These will be discussed further in a later section.

The final form of the E_1, F_1, G_1, and H_1 conservation variables is:

$$E_1 = \begin{vmatrix} \rho u \\ kP + \rho u^2 \\ \rho uv \\ \rho uw \end{vmatrix} \qquad F_1 = \begin{vmatrix} \rho v \\ \rho uv \\ kP + \rho v^2 \\ \rho vw \end{vmatrix} \tag{137}$$

$$G_1 = \frac{1}{r}\begin{vmatrix} \rho w \\ \rho uw \\ \rho vw \\ kP + \rho w^2 \end{vmatrix} \qquad H_1 = \frac{\rho}{r}\begin{vmatrix} u \sin\sigma + v\cos\sigma \\ (u^2 + w^2)\sin\sigma + uv\cos\sigma \\ uv\sin\sigma + (v^2 - w^2)\cos\sigma \\ 2uw\sin\sigma + 2vw\cos\sigma \end{vmatrix}$$

Determination of Gas-Dynamic Variables From Conservative Variables

The flow variables P, ρ, u, v, and w are determined from the conservative variables E_1 in an analogous fashion as was done for the wedge. There are two differences, these being the addition of another dependent variable (w the cross flow velocity component) and the quantities used to non-dimensionalize the flow variables. These differences result in the following set of five algebraic equations for the five unknown flow variables:

$$a = \rho u \tag{138}$$

$$b = kP + \rho u^2 \tag{139}$$

$$c = \rho uv \tag{140}$$

$$d = \rho uw \tag{141}$$

$$P = \rho(1 - q^2) \tag{142}$$

Again a, b, c, and d are known after one step. The solution of these five equations is:

$$v = c/a \tag{143}$$

$$w = d/a \tag{144}$$

$$u = (-B + \sqrt{B^2 - 4AC})/2A \tag{145}$$

$$\rho = a/u \tag{146}$$

$$P = \rho(1 - q^2) \tag{147}$$

where

$$A = 1 - k$$

$$B = -b/a$$

$$C = k(1 - m^2)$$

$$k = (\gamma - 1)/2\gamma$$

$$m = v^2 + w^2$$

The plus sign appearing before the radical was chosen because u (the x component of velocity) is supersonic throughout the entire field of integration.

Exact Boundary Conditions

The flow field about a cone at incidence possesses a plane of symmetry which passes through the $\phi = 0$ and 180° meridional plane. With respect

to these planes the pressure, density, and tangential and normal velocity components are considered even functions. The cross flow velocity component is identically zero in these planes.

At the surface of a cone for zero incidence the pressure, density, and tangential velocity component have zero slopes with respect to the distance normal to the body, while the normal and cross-flow velocity components themselves are zero. This is shown in Appendix D.

For a cone at incidence the boundary conditions are more complicated in that there exists a vortical layer near the body's surface with singularities at the planes of symmetry. Ferri (14) was the first to show that these singularities did exist, and he introduced the concept of a vortical layer surrounding the cone. Explicit relations describing the derivatives of the flow variables with respect to y (distance normal to the body) cannot be found.

Ferri introduced the fact that the entropy on the body is constant and equal to the value of the entropy in the windward meridional plane ($\phi = 0^{o}$). He also stated that all lines of constant entropy converge at the leeward meridional plane ($\phi = 180^{o}$) thereby yielding a nodal point in entropy at that point.

Babenko (1) in solving the cone at incidence problem made use of the fact that the density and radially, tangential velocity component on the body at the nodal point were multivalued. The value that these functions assumed depended on the direction in which the vortical singularity was approached. Babenko's results yielded two values for the density and tangential velocity component which was a result of approaching the nodal point in both the cross-flow direction and in a direction normal to the

axis of revolution.

Method of Solution

The procedure for solving the cone at angle of attack problem is the same as it is for the wedge except the problem is more complicated by the increased dimensionality. However, the flow field about a cone at incidence has a plane of symmetry which lies parallel to the free stream velocity vector. This simplifies the problem in that only half the flow field surrounding the cone need be determined.

For the purpose of solving this problem a rectangular mesh is chosen in which Δy and $\Delta\phi$ are constant (Figures 14 and 25). In the y direction the mesh begins one mesh point below the body ($y = \Delta y$ or $j = 1$) and extends to a point well into the free stream ($y = y_{max}$ or $j = NY2$). In the ϕ direction the mesh begins at $\phi = -\Delta\phi$ ($k = 1$) and terminates at $\phi = 180^{\circ} + \Delta\phi$ ($k = NPHI3$). The reason for extending the mesh one point below the body and one point beyond the plane of symmetry is for easy application of the boundary conditions at these points. This will be discussed later. The computing region or region of integration for this problem, therefore, extends from $j = 2$ to $j = NY2$ in the y-direction and $k = 2$ to $k = NPHI3$ in the ϕ direction.

As was done for the wedge, the integration is started at $x = 1$ and continued to $x = 2$ at which position the step-back procedure is performed. It is essentially the same as that for the wedge except it is performed in two dimensions and therefore at each meridional location. Values of the gas-dynamic variables corresponding to free stream conditions are used to reinitialize the unfilled mesh points at $x = 1$.

It should be pointed out that in the coordinate system chosen for the solution of this problem the flow variables at a constant distance y from the body vary as a function of x. The line y = constant is obviously not a ray originating from the vertex of the cone, unless the constant is zero. In this case the ray lies along the body, and the flow variables should be constant as a function of x. It is found in the numerical determination of the flow field that the flow variables at the body vary somewhat for a converged solution as the integration proceeds from $x = 1$ to $x = 2$. The numerical scheme employed for the solution of this problem uses values of the flow variables above the body to determine values at the body. Since the points above the body are functions of x, this is reflected in the values of the flow variables at the body. Therefore, a solution is assumed to have converged when at $x = 2$ the difference between the flow variables for two subsequent cycles is less than some predetermined constant.

Numerical Boundary and Initial Conditions

Boundary conditions are applied at the extremities of the mesh shown in Figure 14. At the planes of symmetry, i.e., at $\phi = 0^{\circ}$ and $\phi = 180^{\circ}$, the cross-flow velocity component, w, is set equal to zero. The pressure, density, and two other velocity components are considered even functions with respect to these planes, and therefore, the values of these variables at $k = 1$ ($\phi = -\Delta\phi$) are set equal to the values of these variables at $k = 3$($\phi = \Delta\phi$). The cross-flow velocity component can be considered as an odd function, and, therefore, its value at $k = 1$ is set equal to the negative of its value at $k = 3$ and equal to zero at $k = 2$. The same

procedure is used to evaluate the mesh points at $k = NPHI3$.

The mesh in the y direction is assumed to extend far enough into the free stream so that all of the conical shock wave is captured. Values of the free stream variables are assigned to the sequence of mesh points at $j = NY2$ (Figure 14). These remain fixed during the entire integration procedure, and are the free stream values used in the reinitialization at $x = 1$ after step-back occurs.

At the body the reflection principle, as suggested by Bohachevsky (2), supplies the necessary boundary conditions. This, as was done at the plane of symmetry, assumes that pressure, density, tangential, and cross-flow velocity components are locally even functions, while the normal velocity component is a locally odd function with respect to the body. The values of the flow variables at $j = 1$, one mesh point below the body's surface, are assigned values equal to those at $j = 3$, one mesh point above the body's surface, according to the above scheme. At the body, $j = 2$, the normal velocity component is set equal to zero. The use of the reflection principle at the body is an exact boundary condition in the case of a cone at zero angle of attack. This is proven in Appendix D. However, at an angle of attack it is no longer exact since at meridional locations other than the plane of symmetry, the assumed even function variables do possess a finite slope. The accuracy of the numerical solutions obtained using the reflection principle, though, seems to substantiate its use.

The entropy at the body is not assumed constant in this problem and no special differencing is employed in the region of the vortical singularity. The effect of this on the numerical solution is an averaging of the two values of the variables described in Babenko (1) at the leeward

plane of symmetry.

The values of the flow variables in the free stream are used as initial data for the entire computing region. As a function of Mach number and ratio of specific heats, the free stream conditions are as follows:

$$\bar{P}_\infty = P_\infty / P_{o_\infty} = \left(1 + \frac{\gamma - 1}{2} M_\infty^2\right)^{-\frac{\gamma}{\gamma-1}} \tag{148}$$

$$\bar{\rho}_\infty = \rho_\infty / \rho_{o_\infty} = \left(1 + \frac{\gamma - 1}{2} M_\infty^2\right)^{-\frac{1}{\gamma-1}} \tag{149}$$

$$\bar{q}_\infty = q_\infty / q_{max} = \left(\frac{\frac{\gamma-1}{2} M_\infty^2}{1 + \frac{\gamma-1}{2} M_\infty^2} \right)^{1/2} \tag{150}$$

where the bar above the variable indicates that it is dimensionless.

In order to determine the values of the free stream velocity components with respect to the given coordinate system a transformation matrix is derived relating the unit vectors of the Cartesian system to the unit vectors of the body-oriented system. The following equation results:

$$\begin{vmatrix} i \\ j \\ k \end{vmatrix} = |A| \begin{vmatrix} i_x \\ i_y \\ i_\phi \end{vmatrix} \tag{151}$$

where

$$A = \begin{vmatrix} \cos\sigma & -\sin\phi & 0 \\ \sin\sigma\cos\phi & \cos\sigma\cos\phi & -\sin\phi \\ \sin\sigma\sin\phi & \cos\sigma\sin\phi & \cos\phi \end{vmatrix} \tag{152}$$

The free stream velocity for an arbitrary angle of attack can be expressed vectorially in Cartesian coordinates as:

$$\vec{q}_\infty = q_\infty(\cos\alpha\,\hat{i} - \sin\alpha\hat{j}) \tag{153}$$

Using Equation 22 this results in the following equation for the free-stream velocity in body-oriented coordinates:

$$\begin{aligned}\vec{q}_\infty = q_\infty[&(\cos\alpha\cos\sigma - \sin\alpha\sin\sigma\cos\phi)\hat{i}_x \\ &+ (-\cos\alpha\sin\sigma - \sin\alpha\cos\sigma\cos\phi)\hat{i}_y \\ &+ (\sin\alpha\sin\phi)\hat{i}_\phi]\end{aligned} \tag{154}$$

From the above equation, it is seen that the free-stream velocity is a function of only the single independent variable ϕ; α and σ being constant for a given flow situation.

Correction Factors

All of the difference schemes used in this study replace the partial derivative with respect to x appearing in the partial differential equations by a forward difference approximation. For example, in the P.D.E.

$$\frac{\partial u}{\partial x} = a\frac{\partial u}{\partial y} \tag{155}$$

the term $\frac{\partial u}{\partial x}$ is replaced by $\frac{u^{n+1} - u^n}{\Delta x}$. Equation 155 is then written as

$$u^{n+1} = u^n + a\Delta x\frac{\partial u^n}{\partial y} \tag{156}$$

In all of the predictor-corrector difference schemes considered in this study except MacCormack's (31) and the one derived in this study, the term u^{n} in Equation 156 is replaced by a quantity which is averaged over the neighboring mesh points. In the body-oriented coordinate system used for the cone problem and in the spherical coordinate system used later in the wing-body problem, the free-stream velocity components are functions of their location in the mesh. In body coordinates u_{∞} and v_{∞} vary as $\cos \phi$ while w_{∞} varies as $\sin \phi$. This means that differencing schemes which average neighboring points will not retain a uniform free stream. For this reason the differencing scheme must be modified so that flow initially uniform will remain so unless disturbed. In order to achieve this, certain correction factors are needed.

It should also be pointed out that some error is also introduced in recapturing the free-stream conditions due to the difference expressions which replace the remaining partial derivatives in the flow equations. However, the order of this error is less than that due to the averaging process explained above.

Correction factors are determined which minimized the error introduced by both sources mentioned above. To determine the correction factors the partial differential equations are differenced using values in the free stream at an arbitrary meridional plane. The terms necessary to make the equation identically zero, which it should be in the free stream, are the correction factors. These correction factors are given in Appendix E for Lax's method.

Computer Program

The problem of a cone at incidence is programmed for both the IBM 1800 and 7094 computer systems. The 1800 is used mainly for determining the stability bounds with the results being displayed on the C.R.T. Since its storage space is rather limited, the maximum number of mesh points possible is 360 which is usually sufficient for cones at small angles of attack. When a greater number of mesh points is needed for cones at larger angles of attack, the IBM 7094 is employed. Approximately 1850 mesh points could be used, and this was found sufficient for the cases tested.

A resume of the computer program including the function of its subroutines is given in Appendix F. The program is capable of solving the cone problem using three finite difference schemes. These include Lax's, Equation 9, Richtmyer's Equation 45, and MacCormack's, Equation 62. A restart tape is generated after each step-back occurs. This allows the program to be terminated at any time and restarted using the data last recorded after a step-back cycle occurred. This restart tape option is employed for two reasons. First of all long computer runs can be broken down into a sequence of short runs, and secondly certain constants can be changed before beginning the integration again.

The constants which describe the problem to be solved and govern the computer program itself are input through data cards. These constants along with their descriptions are:

XMACH - the free-stream Mach number,

GAMMA - the ratio of specific heats,

SIGMA - the cone half-angle,

ALPHA - the angle of attack,

DXDY - the ratio $\Delta x/\Delta y$ which governs the stability of the solution (This is discussed below.),

NPHI - the number of intervals in the phi direction between 0 and 180° ($\Delta\phi = 180/NPHI$),

NX - the number of intervals in the x direction between $x = 1$ and $x = 2$ ($\Delta x = 1.0/NX$),

NY - the even number of intervals in the y direction ($\Delta y = \Delta x/(\Delta x/\Delta y) = 1.0/(NX \cdot DXDY)$),

NITER - the number of times step back occurs,

NDATA - the control variable which determines restart tape option, 0 implies read, 1 implies don't read,

METHD - the finite difference scheme used (-1, MacCormack; 0, Lax; 1, Richtmyer)

DXDY, NX, NITER, and METHD are the constants which may be charged when using a restart tape.

As in the wedge problem, it is necessary to choose the values of DXDY, NX, and NY such that y_{max} ($y_{max} = NY/(NX \cdot DXDY)$) is large enough to capture the entire shock wave. For cones at small incidences in which the solutions are known from other inviscid theories, y_{max} can be chosen such that it is large enough to extend into the free stream on the lee side of the cone. For cones at larger incidences with the same free-stream conditions in which no solutions exist y_{max} can be determined approximately by extrapolating the curve of y_{max} versus α for small angles of attack.

In numerically solving the cone at angle of attack problem it is necessary to store the values of the five dependent variables P, ρ, u, v,

and w and the sixteen conservative variables E_l, F_l, G_l, and H_l ($l = 1,4$) at each mesh point for each time step. In addition for the predictor-corrector schemes used in this analysis, it is necessary to store the four conservative variables, E_l, at each mesh point for both the predicted and corrected values. This is a total of 29 data words for each mesh point so that, for example, a 10 by 10 mesh requires 2900 storage locations. For grids which are considerably finer and, therefore, involves a greater number of mesh points, the amount of storage space is drastically increased and can easily exceed the available storage capacity of the computer.

The quantity of storage space required for the conservative variables can be sizably reduced at the sacrifice of added computation time by the following technique. Rather than storing the conservative variables for the entire flow field, only the terms which are used to integrate a particular column of mesh points are stored. The others are calculated as they are needed.

The finite difference formulas require only three values of the conservative variables to integrate a particular column of mesh points with respect to x, two on either side of the pivotal point and one at the pivotal point itself. Therefore if a sequence of mesh points in the y direction, e.g. at ϕ_o, is to be integrated, it is only necessary to have available the values of the conservative variables for each mesh point in the y direction at $\phi_o - \Delta\phi$, ϕ_o, and $\phi_o + \Delta\phi$. After the integration of a complete sequence of mesh points in the y direction is performed at ϕ_o, integration is begun at $\phi_o + \Delta\phi_o$, and it is only necessary to calculate the conservative variables at $\phi_o + 2\Delta\phi_o$ since those at

ϕ_o and $\phi_o + \Delta\phi_o$ are known from the last integration sequence. This is easily performed since the dependent variables for the entire mesh are known.

With this as the basis, the storage space required can be reduced since it is necessary to store the dependent variables at all mesh points and only the conservative variables at the pivotal point and the two mesh points on either side of it for each mesh point in the y direction. For the example of the 10 by 10 mesh mentioned earlier the number of storage locations necessary using the new scheme is now 1420. This is more than a 50 percent reduction with only a slight increase in computer time.

Choice of Numerical Method

The choice of a finite difference scheme to solve the cone at angle of attack problem is based on the results obtained in the previous two sections in conjunction with certain optimum properties in the technique of constructing programs. These optimum properties include ease of programming, storage space requirements, and length of computing time. In demonstrating the effects that certain schemes have on the solution of the cone problem, the equations are not only solved in a body-oriented coordinate system but also in a spherical coordinate system, which is used subsequently for the solution of the wing-body problem.

Difference schemes which depend on values of the conservative variables at t and $t + 5\Delta t$ in the corrector are eliminated immediately from consideration under the storage space criterion. These schemes include that due to Burstein, Equations 48 and 49 and those derived in this study, Equations 72, 73, 74, 75, and 81.

The original Lax-Wendroff scheme, Equation 40, is not considered because of the analytical and subsequent numerical difficulties associated with the determination and calculation of the coefficient matrices A and B.

The schemes left for consideration include Lax's, Equation 9, a first order method, and Richtmyer's, Equation 45, and MacCormack's, Equation 62, both second order methods. In solving the modified Berger's equation and the supersonic wedge flow problem these methods yielded good results.

Lax's method requires the least amount of storage space, a minimum of computing time, and is rather simple to program for the three-dimensional cone problem. Lax's method does require the use of correction factors which is a disadvantage. The result of using Lax's method to solve the cone problem at zero angle of attack in Mach 7 flow for the body-oriented coordinate system is shown in Figure 27. By comparing with Babenko's (1) results, which are used as a reference wherever possible, it can be seen that the shock is spread over six to seven mesh intervals, and the pressure distribution throughout the shock layer is not predicted very well.

The result of using Lax's method for a spherical coordinate system is shown in Figure 28 and is comparable to the result found for the body coordinate system.

Applying Lax's method to a cone in Mach 5 flow at 2.5° angle of attack yields the results shown in Figure 29. The pressure distribution throughout the shock layer at both the 0° and 180° planes is presented. These two planes contain the strongest and weakest parts of the conical shock respectively. For the $\phi = 0^{\circ}$ plane the pressure of the body happens to be predicted well, but the pressure distribution throughout the shock layer varies considerably from the exact solution. The shock is spread over

several mesh intervals, and its location would be taken closer to the body if Babenko's results were not superimposed. For the $\phi = 180^{\circ}$ plane the pressure distribution throughout the shock layer and the shock position are both quite unsatisfactory.

The solution obtained using Lax's method for cones at angle of attack are not satisfactory. This can be attributed first to the fact that it is a first order method and secondly to the fact that it is highly dissipative.

In order to increase the accuracy of the solution, Richtmyer's double-time step method, Equation 45, a second order scheme which uses Lax's method as the predictor and hence its correction factors, is employed. Utilization of this scheme approximately double the computation time but requires only a slight increase in storage space.

The result of applying Richtmyer's method to a cone at zero angle of attack is shown in Figure 30. From this it can be seen that the pressure at the body agrees well with the inviscid theory of Babenko while the pressure distribution throughout the shock layer is approximated by a small amplitude, oscillatory wave.

When using the double-time step method of Richtmyer (42), adjacent mesh points are completely uncoupled from one another in the field, and if they are also uncoupled at the body (which they are in this case), two unrelated solutions are actually being computed simultaneously. If every other point is plotted (as Richtmyer suggested) the solution would be smoother but still unsatisfactory. The single time step version of Richtmyer's predictor-corrector scheme would give much more accurate results for the same mesh spacing because it does not uncouple adjacent

points. However, it is more difficult to program than the method discussed next and appeared from the results in the previous sections, to offer no advantage in accuracy over it. Therefore, no calculations of cone flow using Richtmyer's single time step version are carried out.

MacCormack's method, Equation 62, is a second order scheme which requires no correction factors, a minimum of computing time for the accuracy attained and a smaller block storage space than that required by Richtmyer's method. The method is as simple to program as Richtmyer's double time step technique and utilizes every mesh point.

Applying MacCormack's method in body coordinates to the cone at zero angle of attack yields the results shown in Figure 31. It can be seen that the inviscid solution of Babenko is approximated quite closely throughout most of the flow field by this method with the shock itself being spread over about two mesh intervals and the typical numerical oscillation preceding the shock contained within about six intervals.

The results of applying MacCormack's method to the cone problem for spherical coordinates is shown in Figures 32 and 33 for two different flow configurations. Again the results are quite good.

The manner in which the numerical solution approximates Babenko's solution in Figure 32 is characteristic of the results obtained for a spherical coordinate system, i.e., the oscillations preceding and succeeding the shock. Under certain unknown conditions results such as those shown in Figure 33 are possible. Here there is only a slight oscillation on the body side near the shock and the shock itself is quite crisp. The best possible solution is to capture the shock in a single mesh interval.

Results obtained for the wing-body problem demonstrate this unique possibility.

MacCormack's method, as was stated previously, is a preferential method and therefore yields slightly different solutions depending on the variation used. The different variations were experimented with, and as predicted earlier from the analysis using the modified Berger's equation, the one yielding the best shock solution is MacCormack's (A) method which uses forward differences in the predictor and backward differences in the corrector. The results of using MacCormack's (A) and (B) methods are shown in Figure 34 for a 10° cone at 2.5° angle of attack in Mach 5 flow. The difference between the two variations occurs in the amplitude of the oscillations near the shock.

The remaining two variations of MacCormack's method, applicable only to multidimensional problems, yielded results similar to those shown in Figure 34.

It should be reiterated, however, that the variation which yielded the best "shock" solution for the modified Burger's equation also yielded the worst "rarefaction" solution. It is for this reason that MacCormack's (B) method is selected to solve the cone at angle of attack problem. In any event, the difference between solutions calculated by the two variations is small.

Stability Study

A simple stability study was performed using the IBM 1800-2250(C.R.T.) system for a cone at incidence to determine the largest value that $\Delta x/\Delta y$ could assume and still yield a stable solution. The analysis was

performed for Mach 5 flow over a 10^{o} half-angle cone at angles of attack of 0.0^{o}, 2.5^{o}, 5.0^{o} and 7.5^{o}. The mesh consisted of 32 points in the y direction and 12 points in the ϕ direction. MacCormack's method was used to difference the equations. The results of this experiment are shown in Figure 26.

To make a theoretical comparison based on amplification matrix theory it is necessary to know the eigenvalues of the coefficient matrices of the gas-dynamic equations. These are given in Appendix C for both the A and B matrices encountered in the three-dimensional steady flow equations. For the angles of attack considered in this study, the stability of the solution is governed by the maximum eigenvalues of the matrix A and hence the ratio $\Delta x/\Delta y$. The ratio $\Delta x/\Delta\phi$ which also appears in the differenced equations is not as critical as $\Delta x/\Delta y$ since the maximum eigenvalue of the entire flow field occurs in the matrix A.

Burstein (5) has pointed out in his paper that his method is capable of exceeding the stability limit given by Equation 47. He mentioned that it is possible to use the following equation to predict the stability bound in multidimensional problems:

$$\frac{\Delta x}{\Delta y} \leqslant \frac{1}{c\sigma_{max}}$$

where the constant c is close to unity instead of $\sqrt{8}$ normally used for the Lax-Wendroff type schemes.

The curve based on this equation is shown in Figure 26. The maximum eigenvalues used in this equation are found to occur in the free stream at the $\phi = 0^{o}$ meridional plane. The differences between the experimental and theoretical stability boundaries has been discussed previously in the

section on wedge flow and the same conclusions apply here.

It might be pointed out that in the experimental study when instabilities are first observed, they appear as small oscillations in the free stream and are nowhere near the shock.

Numerical Results

In this section numerical results are presented which describe the flow field about a 10° half-angled cone in Mach 5 flow for angles of attack ranging from 0° to 15°. These flow conditions were arbitrarily chosen but are of interest because of an unusual relationship that exists among the shock shapes for different incidences.

Figure 35 is a sketch of the shock shapes that result for the cone at 2.5°, 5.0°, and 7.5° angle of attack. From this sketch it can be seen that the distance between the shock and the body for a particular meridional angle, ϕ, is independent of the angle of attack. This characteristic is peculiar to this particular set of initial conditions and in general does not exist for different configurations.

For the 10° cone in Mach 5 flow Babenko (1) presents results for 0.0°, 2.5°, 5.0°, and 7.5° angle of attack. In order to demonstrate the reliability of the method of solution presented in this study (i.e., the step back principle), these cases are run for comparison. The mesh sizes used in solution of these cases along with other pertinent constants are listed in Table 3.

A tabulated form of pressures and densities at the body is presented in Table 4. These results are compared with those given by Babenko (1). It should be reemphasized that Babenko presents two values of the density

Table 3. Characteristics of mesh used in cone solutions

α	NX	NY	NPHI	$\Delta x/\Delta y$	$\Delta x/\Delta \phi$
0	44	30	1	2.850	0.007
2.5	48	30	9	2.200	0.060
5.0	38	30	20	2.200	0.168
7.5	38	30	20	1.900	0.168
9.0	48	40	20	1.800	0.133
10.0	48	40	20	1.700	0.133
12.0	50	40	25	1.500	0.159
14.0	50	40	36	1.300	0.229
15.0	44	40	36	1.300	0.260

in the 180° meridional plane at the body as a result of the vortical singularity. These two limiting values are a result of approaching the singularity in the normal and cross-flow directions, and both are listed in Table 4. The effect of the boundary conditions used in this study is to smooth the discontinuous variables near the vortical singularity, and therefore the results are compared with the average of the two values given.

The pressure and density distributions at the body as a function of the meridional angle, ϕ, are compared with Babenko's results in Figures 36 and 37 respectively. From the pressure plot, in which it is hard to discern any difference between the two theories, it can be seen that there exists a point near the 80° meridional plane for which the pressure at the body is independent of the angle of attack. For the 7.5° pressure plot the pressure reaches a minimum near the 155° meridional plane.

Table 4. Comparison of pressure results with those of Babenko (1) for cone flow

Angle of Attack	Present Results	Babenko	Percent Error
$\alpha = 0^\circ$	$P = 0.004369$	$P = 0.004370$	0.0
$\alpha = 2.5^\circ$	$P_0 = 0.005439$	$P_0 = 0.005426$	0.2
	$P_{90} = 0.004326$[a]	$P_{90} = 0.004325$	0.2
	$P_{180} = 0.003531$	$P_{180} = 0.003528$	0.1
$\alpha = 5.0^\circ$	$P_0 = 0.006682$	$P_0 = 0.006698$	0.2
	$P_{90} = 0.004200$	$P_{90} = 0.004199$	0.0
	$P_{180} = 0.002898$	$P_{180} = 0.002889$	0.3
$\alpha = 7.5^\circ$	$P_0 = 0.008172$	$P_0 = 0.008178$	0.1
	$P_{90} = 0.004014$	$P_{90} = 0.004035$	0.5
	$P_{180} = 0.002435$	$P_{180} = 0.002425$	0.4
$\alpha = 0^\circ$	$\rho = 0.02045$	$\rho = 0.02051$	0.3
$\alpha = 2.5^\circ$	$\rho_0 = 0.02348$	$\rho_0 = 0.02366$	0.8
	$\rho_{90} = 0.02005$[a]	$\rho_{90} = 0.02012$	0.3
	$\rho_{180} = 0.01752$	$\rho_{180} = 0.01771$[b] / 0.01756[c] / 0.01740[d]	0.2
$\alpha = 5.0^\circ$	$\rho_0 = 0.02685$	$\rho_0 = 0.02700$	0.6
	$\rho_{90} = 0.01937$	$\rho_{90} = 0.01934$	0.2
	$\rho_{180} = 0.01520$	$\rho_{180} = 0.01538$[b] / 0.01509[c] / 0.01480[d]	1.0
$\alpha = 7.5^\circ$	$\rho_0 = 0.03015$	$\rho_0 = 0.03036$	0.7
	$\rho_{90} = 0.01808$	$\rho_{90} = 0.01833$	1.4
	$\rho_{180} = 0.01318$	$\rho_{180} = 0.01358$[b] / 0.01316[c] / 0.01274[d]	0.2

[a] Linearly interpolated

[b] Limiting value in normal direction

[c] Average value

[d] Limiting value in cross-flow direction

The variations between the two theories for density plots is probably a result of the smoothing approximation associated with the vortical singularity.

To describe the remaining flow field between the free stream and the body, pressure and density distribution plots as a function of the distance normal to the body are presented for the previously mentioned cases.

Figure 31 is a pressure distribution for the zero angle of attack case. The shock is spread over about two mesh intervals, and its location agrees well with that predicted by Babenko. The pressure distribution throughout the layer is also predicted quite well in view of the anticipated, characteristic oscillations near the shock.

Figures 38 and 39 describe the pressure and density distributions for the cone at 2.5° angle of attack with the meridional angle, ϕ, a parameter. These numerical solutions agree well with Babenko's results.

Figures 40 and 41, and 42 and 43 show the pressure and density distributions for the 5.0° and 7.5° angle of attack cases. In the 180° plane for the 7.5° case the shock is spread over four to five mesh intervals while in 0° plane it is spread over two mesh intervals. This is characteristic since the leeward shock is the weaker of the two.

The angle of attack is now increased until the formation of a distinct embedded shock appears on the leeward side of the cone. Cone solutions are found for incidences of 9°, 10°, 12°, 14°, and 15°. Detailed results of the flow field are presented for the 9° and 15° cases.

The pressure and density distributions as a function of ϕ for the 9° case are shown in Figures 44 and 45 respectively. Detailed pressure and density plots which describe the shock layer are shown in Figures 46

through 49. The shock in the leeward plane is spread over five to six mesh intervals.

In order to demonstrate the appearance of embedded shocks, a plot of pressure versus meridional angle with the angle of attack as a parameter is shown in Figure 50. A distinct pressure minimum occurs near $\phi = 140^{\circ}$ for $\alpha = 9^{\circ}$ and moves to $\phi = 150^{\circ}$ for $\alpha = 15^{\circ}$. A recompression wave becomes well defined for $\alpha = 12^{\circ}$ and forms into a weak shock with a noticeable increase in entropy for $\alpha = 14^{\circ}$. At $\alpha = 15^{\circ}$ the embedded shock is slightly stronger and occurs near the 155° meridional plane. It is spread over approximately two mesh intervals.

Figure 51 is a detailed pressure plot of the region surrounding the embedded shock. As the distance normal to the body is increased the intensity of the shock decreases. The embedded shock tends to bend toward the leeward side of the cone which is in agreement with the experimental results given by Rainbird (39).

Figures 52 and 53 are pressure and density plots as a function of the meridional angle, ϕ, for the 15° case. In the density plot there is a slight oscillation near the leeward plane. This is probably a result of the approximation used to capture the vortical singularity.

Figures 54 and 55, and 56 and 57 are pressure and density plots respectively throughout the shock layer. From these figures it can be seen that the number of mesh points describing the shock layer for the windward side of the cone is relatively small compared to the mesh points in the leeward side. This is a result of the closeness to the body of the windward shock. It should also be pointed out that the free-stream velocity which is a function of the independent variables varies somewhat from

its initial value. This variance is most critical in the 90° meridional plane for large incidences and is a result of the difference expressions which approximate the y and ϕ spatial derivatives.

Evanescence of the shock wave did not occur for the incidences tested. The weakest part of the conical shock wave occurs in the 180° meridional plane for $\alpha = 15^{\circ}$. A slight compression wave in this plane is observed which lies near the free stream Mach cone as shown in Figure 54. This was also observed by Gonidou (19) for smaller incidences. The pressure then expands as it approaches the body, and is well below the free stream pressure at the body.

CONICAL WING-BODY COMBINATION AT INCIDENCE

Introduction

Interest in orbital gliders and long range hypersonic cruise and boost vehicles has stimulated both theoretical and experimental work on flow fields about such configurations. A logical and somewhat practical means of obtaining favorable interference effects to increase the maximum lift-drag ratios at hypersonic speeds for these configurations is suggested by Eggers and Syvertson (11). Their suggestion is to mount a half cone beneath a thin, highly swept delta wing (Figure 58). For the resulting conical wing-body configuration at angle of attack, the wing receives additional lift from the superimposed flow field of the body. The wing itself should extend out at least as far as the body shock wave to preserve momentum from the body. Any portion of the wing which extends beyond the body shock does not serve to increase the downward momentum of the air influence by the body. It will, however, add to the forward momentum through friction forces. Thus optimum configurations are, therefore, obtained when the wing leading edge and shock generated by the conical body coincide.

Experimental data on the conical wing-body or "flat-top" configurations are plentiful. Investigators such as Dunavant (9), Savin (45), and Randall, et al. (41) have determined surface pressure distributions for various flat-top configurations operating under various flow conditions. Lift-drag data has been obtained by Fetterman (15), Johnston, et al. (23), Small, et al. (47), Goebel (18), and Syvertson, et al. (51).

There exists, however, relatively few theoretical studies of the flow fields about such configurations. Migotsky and Adams (34) developed a method for predicting the aerodynamic forces on flat-top configurations. Since it is based on linear theory, its validity is necessarily restricted to the low supersonic speed range. Savin (45) developed a semiempirical method which is based on the inviscid conical flow equations. The agreement he obtains between his theory and experimental data is remarkable considering his theory is in error in that calculated pressures on the wing do not reduce to those at zero incidence where they are known from the flow about a complete cone.

Mandl (32) combines the theory of linearized characteristics, introduced by Ferri (13), with the hypersonic small disturbance approximation and derives explicit expressions for the shock shape, the flow field, the surface pressure distribution, and the aerodynamic forces for a conical wing-body combination traveling at hypersonic speeds. The method of linearized characteristics considers the flow about the body to be a perturbation of a known basic nonlinear flow which in this case is considered to be that about a circular cone at zero incidence.

In all of the theoretical investigations performed for this type of configuration, certain simplifying assumptions are made at the outset. In the present study these assumptions are eliminated, and the complete three-dimensional, steady flow, nonlinear Eulerian equations are solved using MacCormack's (31) method; the same finite difference technique selected for use in solving the cone at incidence problem.

There has been some controversy in the past about what the shock pattern for a conical wing-body combination in supersonic flow actually

looks like. Savin (45) in his theoretical analysis assumed a continuous single-shock pattern like that shown in Figure 59. Mandl, on the other hand, developed his theory based on the double-shock pattern shown in Figure 60. For this case the body shock impinges on the wing's surface while the shock generated by the leading edge of the wing intersects the body shock causing a vortex sheet to form between the point of intersection and the wing-body juncture. Migotsky and Adams (34) assumed the body-shock to be coincident with the leading edge of the wing or the single-shock pattern.

The technique that is used for the analysis of this problem in this study possesses the ability to allow for the formation of shock waves when and where they may occur. Therefore, there is no necessity of assuming a specific type of shock pattern as has been done by the aforementioned investigators. The results obtained in this study do show the existence of the double-shock pattern when the wing's leading edge extends beyond the position of the body shock. However, most of the cases analyzed are concerned with the optimum configuration for a maximum lift-drag ratio for which only a single shock can exist.

Included also in this study is an analysis of the effects on the resulting flow field of changing the dihedral of the delta wing while keeping all other flow conditions constant.

Where possible the results are compared with the applicable theory of Savin (45) and the experimental results of Dunavant (9) and Randall, et al. (41).

Derivation of Equations

As has been mentioned previously, in order to alleviate the numerical difficulties in assigning boundary conditions it is desirable to choose a coordinate system in which the body coincides with one of the coordinate directions. For the conical wing-body problem the body-oriented coordinate system does not conform to the above criterion. The reason is that, in general, for a given sweep angle, the wing's leading edge does not fall on a sequence of mesh points in an x-y plane. Use of the body-oriented system would therefore necessitate the use of an unequal mesh distribution.

The use of a spherical coordinate system (Figure 24), however, does allow both the conical body and planar delta wing to coincide with one of the coordinate directions and thus fall directly on the sequence of mesh points in that direction.

Employing the same assumptions and nondimensionalization procedure that was used for the cone at angle of attack, the basic flow equations written in conservation-law form for spherical coordinates are:

$$\frac{\partial E}{\partial r} + \frac{\partial F}{\partial \theta} + \frac{\partial G}{\partial \phi} + H = 0 \tag{157}$$

where

$$E = \begin{vmatrix} \rho u \\ kP + \rho u^2 \\ \rho uv \\ \rho uw \\ u(P + \rho q^2) \end{vmatrix} \quad , \quad F = \frac{1}{r} \begin{vmatrix} \rho v \\ \rho uv \\ kP + \rho v^2 \\ \rho vw \\ v(P + \rho q^2) \end{vmatrix}$$

$$G = \frac{1}{r\sin\theta}\begin{vmatrix} \rho w \\ \rho uw \\ \rho vw \\ kP + \rho w^2 \\ w(P+\rho q^2) \end{vmatrix}, \qquad H = \frac{\rho}{r}\begin{vmatrix} 2u + v\cot\theta \\ uv\cot\theta + 2u^2 - (v^2+w^2) \\ (v^2 - w^2)\cot\theta + 3uv \\ w(3u + 2v\cot) \\ 2u(P+\rho q^2)/\rho + (P+\rho q^2)v\cot\theta/\rho \end{vmatrix} \tag{158}$$

In the above equations the differential form of the energy equation is replaced by the integrated form given by the following equation:

$$P = \rho(1 - q^2) \tag{159}$$

Exact Boundary Conditions

In determining the flow field about a flat-top, wing-body configuration at angle of attack, one is mainly interested in the compression side of the body. Under the assumption of a supersonic leading edge, the flow fields for the expansion and compression sides of the body are independent of each other. Therefore, only half the flow field need be determined. Further, because there exists a plane of symmetry in the problem at the windward plane, only half the compression side is left to be determined.

The usual inviscid boundary conditions are applied at the body's surface. On the cone the normal velocity component, v, is set equal to zero, while on the wing the cross-flow velocity component, w, is equated to zero. In the plane of symmetry and at the wing-body juncture both the normal and cross-flow velocity components are zero.

In this problem, as in the cone at incidence problem, there exists a vortical layer near the surface of the cone. The vortical singularity, however, now falls at the point of the wing-body juncture. The entropy

on the cone's surface and the wing's surface is constant for the single shock pattern but the two constants are not the same. The magnitude of the entropy on the body is equal to that in the windward plane just behind the shock. The magnitude of the entropy on the wing is equal to the value just behind the body shock which is coincident with the leading edge of the wing. In the case of a double-shock pattern, the entropy on the wing is constant between the leading edge and the impinging body shock and a different constant between the body shock and the wing body juncture. For the problem solved in this study no restrictions are placed on the value the entropy can assume anywhere in the flow field.

Method of Solution

The procedure for solving the conical wing-body combination at angle of attack in spherical coordinates is similar to that used in the solution of the cone at incidence problem in that the flow variables are stepped back. However, in this case they are stepped back after every iteration.

The basic approach is to integrate the steady flow, gas-dynamic equation with respect to the radial coordinate, r, in the vicinity of $r = 1$ until an asymptotic state is reached. Precisely what this means is that the integration of the flow equations for one cycle begins at $r = 1$ and ends $r = 1 + \Delta r$ at which time the flow field is stepped back to $r = 1$ and the cycle repeated. This procedure is continued until there is little change in the magnitude of the gas-dynamic variable with respect to r. The conical flow field is then assumed to have converged.

For the purpose of differencing the gas-dynamic equations according to MacCormack's scheme, the portion of the flow field which is of interest

is covered by the mesh shown in Figure 61. As in the cone problem, the mesh is extended one interval beyond each of the boundaries for easy application of the boundary conditions. The cone's surface corresponds to the mesh points at $j = 2$ from $k = 2$ to $k = PHWNG$. The meridional plane in which the wing is located ($\phi = PHWNG$) can be varied to effect a change in the dihedral of the wing. The wing angle, λ, is chosen so that it falls on a mesh point for some θ = constant. The computing region, therefore, for this problem extends from $j = 2$ to $j = NTHE1$ in the θ-direction to from $k = 2$ to $k = PHWNG$ in the ϕ-direction.

The same equations (Equations 138-147) that were used in the cone problem for the determination of the flow variables from the conservative variables are used here for the wing-body problem.

The version of MacCormack's method which uses forward differences to replace the spatial derivatives in the predictor and backward differences in the corrector is used for the solution of this problem since it yielded the best results for problems which involve shocks only.

Numerical Boundary and Initial Conditions

Boundary conditions are applied at the extremeties of the mesh shown in Figure 61. As was done in the cone problem at the plane of symmetry ($\phi = 0^{\circ}$), the crossflow velocity component is set equal to zero while the pressure, density, and remaining two velocity components are considered even functions with respect to this plane, which means that the flow variables for $k = 1(\phi = -\Delta\phi)$ are evaluated using the flow variables of $k = 3(\phi = \Delta\phi)$.

The conditions of evenness or oddness described earlier for the cone problem is used in determining the boundary conditions at the surface of both the body and the wing.

The mesh in the θ-direction extends far enough into the free stream to completely capture the shock and/or shocks generated by the conical wing-body combination. At the sequence of mesh points for $\theta = \theta_{max}$ (j = NTHE2) values of the free stream variables are assigned to these points and held constant throughout the entire integration procedure.

The values of the flow variables in the free stream are used as initial data for the entire computing region. The free-stream pressure, density, and velocity magnitude are given by Equations 148, 149, and 150 respectively.

To determine the free-stream velocity components, the matrix in Equation 152 is used with σ replaced by θ. This results in the following equation for the free-stream velocity in spherical coordinates:

$$\begin{aligned} q_\infty = q_\infty \Big[& (\cos\alpha\cos\theta - \sin\alpha\sin\theta\cos\phi) i_r \\ + & (-\cos\alpha\sin\theta - \sin\alpha\cos\theta\cos\phi) i_\theta \\ + & (\sin\alpha\sin\phi) i_\phi \Big] \end{aligned} \tag{160}$$

In spherical coordinates for a constant angle of attack the free-stream velocity is a function of θ and ϕ.

Computer Program

The conical wing-body at angle of attack problem is programmed for both the IBM 7094 and 1800 computer systems. Still and motion picture

results are obtained from the IBM 2250 display tube. Selected pressure coefficient plots are displayed along with the predicted shock shape (see for example Figure 62).

A resume of the computer program including the function of its various subroutines is given in Appendix G. The program is capable of generating a restart tape after any specified number of integration cycles. The same storage-space saving technique that is used in the cone problem is used here.

The constants which describe the problem to be solved and govern the computer program itself are input through data cards. These constants along with their descriptions are as follows:

XMACH - the free-stream Mach number,

GAMMA - the ratio of specific heats,

SIGMA - the conical-body half angle,

ALPHA - the angle of attack,

DR - the integration step size in the radial direction,

DTHE - the length of a mesh interval in the theta direction,

NTHE - the number of intervals in the theta direction,

NPHI - the number of intervals in the phi direction,

NWING - the integer variable which determines the desired wing angle (NWING multiplied by DTHE plus SIGMA equals the wing angle, lambda),

PHWNG - the meridional angle at which the wing is located,

NBACK - the number of iterations before data is output,

NITER - the maximum number of data sets output,

NDATA - the control variable which determines restart tape option, 0 implies read, 1 implies don't read.

For this problem it is usually sufficient to extend the mesh four to six mesh intervals beyond the leading edge of the wing.

The approximate value of the mesh ratio, $\Delta r/r\Delta\theta$, for a particular flow situation is found by using the following equation:

$$\Delta r/r\Delta\theta = 1/|\sigma_{max}| \tag{161}$$

where σ_{max} is the largest eigenvalue of Equation C19 which uses the flow properties at θ_{max} in the ϕ equal zero plane.

Numerical Results

In this section numerical results are presented for various conical wing-body figurations operating under different flow conditions. Most of the results are compared with available experimental data or other inviscid theories when applicable. The numerical results obtained using inviscid theory on the average compare favorably with the experimental data.

For all of the problems solved in this study a 30 by 11 mesh was used. Each calculation required approximately 15 minutes of computer time on the IBM 7094, computer system.

In an experiment by Dunavant to determine the heat transfer to a conical wing-body combination, surface pressure measurements were taken

at various sections along the body and the wing. The results obtained using the inviscid theory developed in this study are compared with those of Dunavant for a 5° cone mounted beneath a 15° wing (75° sweep) in Mach 6.8 flow for angles of attack equal to 3.7° and 6.0°.

Figure 62 is a sequence of photographs which reveal the development of the flow field for an angle of attack of 3.7°. The body shock lifts off the body and proceeds to its equilibrium position which in this case is not coincident with the leading edge of the wing. In the pressure coefficient plot for ϕ = CONST, the constant is zero degrees. The last photograph in Figure 62 shows a small pressure rise near the leading edge. This is the shock generated by the wing. Because it is not as strong as the body shock, it is spread over a greater number of mesh points as would be expected. The program which plots the shock shape on the C.R.T. is only capable of plotting the strongest shock, and for this reason the wing shock does not appear. The jaggedness of the shock shape is a result of the approximation used to predict the shock's location.

Figure 63 shows the converged solution for the same body at an angle of attack of 6.0°. As a result of increasing the angle of attack, the shock in the windward plane moves closer to the body and the part in the plane of the wing moves farther from the body. The body shock impinges on the wing but is still not coincident with the leading edge, so there is subsequently a weak wing shock as is indicated by the small pressure rise seen in Figure 63.

A comparison with Dunavant's results for surface pressure distributions is given in Table 5. It is found that the greatest disagreement

occurs in the windward plane, and that the best agreement occurs on the lee-part of the body and on the wing.

Table 5. Comparison of present results with Dunavant's experiments for the surface pressure distribution (P/P_∞)

	$\alpha = 3.7^\circ$			$\alpha = 6.0^\circ$		
Location	Present Results	Experiment	Percent Error	Present Results	Experiment	Percent Error
Body						
$\phi = 0^\circ$	2.65	2.31	12.8	3.50	3.22	10.9
30°	2.57	2.35	8.6	3.34	3.16	5.4
60°	2.45	2.33	4.9	3.09	3.08	0.3
Wing						
$\theta = 6^\circ$	2.41	2.18	9.1	3.04	3.05	0.3
8°	2.36	2.26	4.2	3.01	3.00	0.3
10°	2.29	2.13	7.0	2.96	3.02	2.0
12°	2.38[a]	2.05	13.8	3.05[a]	3.05	0.0

[a]Taken from overshoot portion of body shock

It should be stressed that for these relatively small angles of attack the viscous forces are not predominant near the wing-body juncture and the agreement with experiment is better than that which can be expected for larger incidences.

The pressure, as expected, is a maximum on the cone in the windward plane and decreases with increasing ϕ. It is relatively uniform on the wing's surface with a somewhat larger than usual overshoot near the body shock. Dunavant in his experiment found no evidence to indicate impinge- of the body shock on the wing. However, the present results obtained by

inviscid theory indicate that the body shock does impinge on the wing at an angle, θ, greater than 12°. This is the location of the pressure probe furthest from the body in Dunavant's experimental study and this indicates that the impingement of the body shock on the wing could not have been detected in his experiment.

From a Schlieren photograph in Dunavant's report the windward shock is seen to lie approximately 3.5° above the cone's surface for the 6.0° angle of attack case. The inviscid theory of this study places the windward shock at approximately 3.2° above the body.

The theory developed by Savin (45) for determining the flow field about conical, flat-top, wing-body configurations is based on the assumptions of high supersonic Mach numbers, slender configurations, supersonic leading edges with single attached shocks, and small angles of attack.

The results obtained using the inviscid theory developed in this study are compared with Savin's theoretical results for a particular configuration. Since Savin's theory is based on the assumption of a single attached shock at the leading edge, it is more appropriate to consider a case in which the body shock is coincident with the leading edge rather than a case which would result in a double shock pattern.

To satisfy this criterion the test conditions chosen consisted of a 5.71° cone with an 11.98° wing angle at 1.142° angle of attack in Mach 6.021 flow. Table 6 lists the results of the pressure distribution at the three points on the body given by Savin and the corresponding values found using the present theory.

Table 6. Comparison of present results with Savin's theory for the surface pressure distribution (P/P_∞)

Location	Present results	Savin's theory	Percent error
Body ($\phi = 0^\circ$)	1.91	1.96	2.6
Wing-body juncture	1.82	1.85	1.6
Wing leading edge	1.62[a]	1.68	3.7

[a]Determined by averaging and extrapolation near leading edge shock

The surface pressure distribution is shown in Figure 64 along with the results obtained by Savin. The pressure at every other mesh point is plotted on the surface of the wing. Also shown in Figure 64 is the pressure distribution at the surface of the cone for a case in which there is no wing. It can be seen that near the windward plane the pressures on the cone and on the conical wing-body are relatively close to each other. The same can be said about the location of the shock wave in this region.

The effect of adding the wing to the cone is to increase the pressure on all surfaces and subsequently move the shock farther from the body. The particular configuration tested here, in which the body shock coincided with the wing's leading edge, is referred to as an optimum configuration in that it results in a maximum lift-over-drag ratio, $(L/D)_{max}$.

To determine the effects of positive and negative dihedral on the resulting flow field of a wing-body combination a 5.73° conical body at 4.585° angle of attack in Mach 6 flow is calculated. The wing angle is varied in such a manner so as to keep the body shock coincident with the leading edge of the wing.

For the 0° dihedral case, i.e., the wing located in the 90° meridional plane, the results can be compared with those of Savin. The comparison is given numerically in Table 7. The surface pressure distribution for this case is shown in Figure 65. For this case the wing angle is 14.39°. Savin predicted the body shock would be coincident with the leading edge for a wing angle of 13.94°.

Table 7. Comparison of present results with Savin's theory for the surface pressure distribution (P/P_{∞})

Location	Present results	Savin's theory	Percent error
Body ($\phi = 0^{\circ}$)	2.69	2.84	5.6
Wing-body juncture	2.44	2.39	2.0
Wing leading edge	2.29[a]	2.33	1.7

[a]Determined by averaging and extrapolation near leading-edge shock

Figure 66 is a sequence of photographs taken from the C.R.T. which shows the development of the flow field for the 0° dihedral case. In the last photograph the shock in the ϕ = CONST plane is captured within one mesh interval.

When a 5° dihedral is added to the wing to form the wing-body combination shown in Figure 67, the surface pressure distribution is found to decrease over the entire body when compared to the 0° dihedral case. This can be seen in Figure 65. It is necessary to increase the wing angle (decrease the sweep) in order to keep the body shock coincident with the leading edge. Figure 67 is a photograph of the converged solution for 5° dihedral case.

Adding a -5° dihedral to the wing-body combination has the opposite effect. The surface pressure distribution over the entire body is increased and the wing angle has to be decreased in order to keep the body shock coincident with the leading edge. This is also shown in Figure 65. Figure 68 is a photograph from the C.R.T. of the converged solution for this case. Again the shock in the windward plane is captured within one mesh interval.

Also shown in Figure 65 is the surface pressure distribution for the cone alone under the same flow conditions. It can be seen from this figure that near the windward plane the pressure for the three cases tested is close to the pressure of the equivalent cone.

Randall (41), et al., performed an experiment at Arnold Engineering Development Center to determine the surface pressure distribution on several sharp, leading edged, conical wing-body combinations. To compare the inviscid theory developed in this study with the experimental results of A.E.D.C. a 12.5° cone mounted beneath a 25° delta wing in Mach 5.08 flow is calculated. Results are obtained for angles of attack of 0° and 11°. Both the experimental and theoretical surface pressure distributions for these two cases are shown in Figure 69.

For the zero angle of attack case the surface pressure on the body compare favorably with the experimental. However, on the wing there is considerable disagreement. The location of the body shock which impinges on the wing as predicted by the inviscid theory does not agree well with that given by the experiment.

For the 11° angle of attack case the surface pressures over the entire body agree well with the experimental results. For this case the body shock fell very close to the wing's leading edge.

RECOMMENDATIONS FOR FURTHER STUDY

Several possible extensions to the problems solved in this analysis can be suggested.

Numerical techniques that can be used to calculate transonic and supersonic flow fields with shocks have been developed and are being widely and successfully used on a variety of specific problems. Their adaptability to general airplane shapes, however, is still in a primitive state, a result which appears to be due to both limited computer capacity and a lack of understanding of the basic laws which govern the really optimum approaches. Part of the analysis presented in this study investigated, in a fundamental way, the latter of the two deficiencies. Future investigations of this type should be based on three key aspects: one, to explore the desirability of using the solution matrix (Lomax, 30) rather than the amplification matrix as a basis for correlating the stability of various methods; another, to consider generalization of the method of relaxation to flows with shocks using, insofar as possible, the solution matrix as a guide; and finally to incorporate into the numerical technique a cathode ray tube which can be used to monitor the calculations in a variety of ways as they proceed.

One of the most troublesome problems encountered in using the aforementioned techniques for the solution of gas dynamic problems is satisfying the boundary conditions at the surface of the body. Possible extensions to the analysis presented in this study should include an investigation which presents a systematic study of the effect of numerically approximated,

boundary conditions on the accuracy, stability and efficiency of methods designed for simplified airplane configurations whose flow fields contain multiple shock waves. Incorporated into such a study should be the effect of transformations which focus numerical grids into specified areas, as well as coordinate transformations which result, for example, in shock moving or shock fixed calculations.

A direct extension to the conical wing-body problem solved in this study might be to analyze the expansion side of this type of configuration (flat-bottom configuration). The flow field about such a body would include shock-expansion interactions and the usual vortical singularities associated with conical flow problems. In the analysis one should investigate the effects of Mach number, angle of attack and meridional location of the planar wing on the subsequent flow field. Among the practical applications of a study of this type is the effect of lateral spreading of initial shocks on supersonic boom signatures.

ACKNOWLEDGMENTS

The author wishes to express his appreciation to Dr. M. L. Millett who was instrumental in initiating my graduate studies; to Dr. D. A. Anderson for his guidance and helpful suggestions throughout my graduate school career; to Dr. V. J. Rossow who set up the Iowa State University-NASA Ames Research Center, cooperative, work-study program which resulted in this paper; to Dr. H. E. Bailey and Mr. J. V. Rakich for their technical advice; to Margaret Covert and Dr. W. A. Reinhardt for their assistance in the use of the IBM 1800 and 7094 computer systems; to Dr. E. W. Anderson for his administrative and technical advice, for his faith and the feeling of security he instilled and in general for his unending help throughout my college career; to Mr. Harvard Lomax for his creative suggestions, technical advice, and close supervision; to Mrs. Beverly A. Webb and Mrs. Nadine Omlid for the typing of the manuscript; and to my wife, Judi, for her moral and spiritual help in times of need.

BIBLIOGRAPHY

1. Babenko, K. I., Voskresenskiy, G. P., Lyubimov, A. N., and Rusanov, V. V. Three-dimensional flow of ideal gas past smooth bodies. National Aeronautics and Space Administration Technical Translation F-380. 1966.

2. Bohachevsky, I. O. and Mates, R. E. A direct method for calculation of the flow about an axisymmetric blunt body at angle of attack. American Institute of Aeronautics and Astronautics Journal 4: 776-782. 1966.

3. Bohachevsky, I. O. and Rubin, E. L. A direct method for computation of nonequilibrium flows with detached shock waves. American Institute of Aeronautics and Astronautics Journal 4: 600-607. 1966.

4. Burstein, S. Z. Difference methods for the inviscid and viscous equations of a compressible gas. Journal of Computational Physics 2: 178-196. 1967.

5. Burstein, S. Z. Finite-difference calculations for hydrodynamic flows containing discontinuities. Journal of Computational Physics 2: 198-222. 1967.

6. Burstein, S. Z. Numerical methods in multidimensional shocked flows. American Institute of Aeronautics and Astronautics Journal 2: 2111-2117. 1964.

7. Cooke, J. C. Supersonic laminar boundary layers on cones. Royal Aircraft Establishment Technical Report 66347. 1966.

8. DeJarnette, F. R. Application of Lax's finite difference method to nonequilibrium hypersonic flow problems. National Aeronautics and Space Administration Technical Report R-234. 1966.

9. Dunavant, J. C. Heat transfer to a delta-wing-half-cone combination at Mach numbers of 7 and 10. National Aeronautics and Space Administration Technical Note D-2199. 1964.

10. Eggers, A. J., Allen, H. J., and Neice, S. E. A comparative analysis of the performance of long-range hypervelocity vehicles. National Advisory Committee for Aeronautics Technical Note 4046. 1957.

11. Eggers, A. J. and Syvertson, C. A. Aircraft configurations developing high lift-drag ratios at high supersonic speeds. National Advisory Committee for Aeronautics Research Memorandum A55L05. 1956.

12. Emery, A. F. An evaluation of several differencing methods for inviscid fluid flow problems. Journal of Computational Physics 2: 306-331. 1968.

13. Ferri, A. The linearized characteristic method and its application to practical non-linear supersonic problems. National Advisory Committee for Aeronautics Technical Note 2515. 1951.

14. Ferri, A. Supersonic flow around circular cones at angles of attack. National Advisory Committee for Aeronautics Technical Note 2236. 1951.

15. Fetterman, D. E. Favorable interference effects on maximum lift-drag ratios of half-cone delta-wing configurations at Mach 6.86. National Aeronautics and Space Administration Technical Note D-2942. 1965.

16. Fromm, J. E. A method for reducing dispersion in convective difference schemes. Journal of Computational Physics 3: 176-189. 1968.

17. Godunov, S. K. and Ryabenki, V. S. The theory of difference schemes. John Wiley and Sons, Inc., New York, New York. c1964.

18. Goebel, T. P., Martin, J. J., and Boyd, J. A. Factors affecting lift-drag ratios at Mach numbers from 5 to 20. American Institute of Aeronautics and Astronautics Journal 1: 640-649. 1963.

19. Gonidou, R. Supersonic flows around cones at incidence. National Aeronautics and Space Administration Technical Translation F-11, 473. 1968.

20. Gourlay, A. R. and Morris, J. L. Finite-difference methods for nonlinear hyperbolic systems. Mathematics of Computation 22: 28-39. 1968.

21. Gourlay, A. R. and Morris, J. L. A multistep formulation of the optimized Lax-Wendroff method for nonlinear hyperbolic systems in two space variables. Mathematics of Computation 22: 715-719. 1968.

22. Hopf, E. The partial differential equation $u_t + uu_x = \mu u_{xx}$. Communications on Pure and Applied Mathematics 3: 201-230. 1950.

23. Johnston, P. J., Snyder, C. D., and Witcofski, R. D. Maximum lift-drag ratios of delta-wing-half-cone combinations at a Mach number of 20 in helium. National Aeronautics and Space Administration Technical Note D-2762. 1965.

24. Kopal, Z. Tables of supersonic flow around cones. MIT Department of Electrical Engineering, Center of Analysis Technical Report 1. 1947.

25. Kutler, P. Determination of the inviscid flowfield with massive blowing about a two-dimensional cylinder. American Institute of Aeronautics and Astronautics Student Journal 6: 77-81. 1968.

26. Lapidus, A. A detached shock calculation by second-order finite differences. Journal of Computational Physics 2: 154-177. 1967.

27. Lax, P. D. Weak solutions of nonlinear hyperbolic equations and their numerical computation. Communications on Pure and Applied Mathematics 7: 159-193. 1954.

28. Lax, P. D. and Wendroff, B. Difference schemes for hyperbolic equations with high order of accuracy. Communications on Pure and Applied Mathematics 17: 381-398. 1964.

29. Leith, C. E. Numerical simulation of the earth's atmosphere. In Alder, B., Fernbach, S., and Rotenberg, M., eds. Methods in computational physics. Vol. 4. Pp. 1-28. New York, New York, Academic Press, Inc. 1965.

30. Lomax, H. An operational unification of finite difference methods for the numerical integration of ordinary differential equations. National Aeronautics and Space Administration Technical Report R-262. 1967.

31. MacCormack, R. W. The effect of viscosity in hypervelocity impact cratering. American Institute of Aeronautics and Astronautics Paper No. 69-354: 1-7. 1969.

32. Mandl, P. A theoretical study of the inviscid hypersonic flow about a conical flat-top wing-body combination. American Institute of Aeronautics and Astronautics Journal 2: 1956-1964. 1964.

33. Melnik, R. E. Vortical singularities in conical flow. American Institute of Aeronautics and Astronautics Journal 5: 631-637. 1967.

34. Migotsky, E. and Adams, G. J. Some properties of wing and half-body arrangements at supersonic speeds. National Advisory Committee for Aeronautics Research Memorandum A57E15. 1957.

35. Moretti, G. Inviscid flow field past a pointed cone at an angle of attack. General Applied Science Laboratories Technical Report No. 577. 1965.

36. Moretti, G. and Abbett, M. A time-dependent computational method for blunt body flows. American Institute of Aeronautics and Astronautics Journal 4: 2136-2141. 1966.

37. Moretti, G. and Bleich, G. Three-dimensional flow around blunt bodies. American Institute of Aeronautics and Astronautics Journal 5: 1557-1562. 1967.

38. National Advisory Committee for Aeronautics, Ames Laboratory Research Staff. Equations, tables, and charts for compressible flow. National Advisory Committee for Aeronautics Report 1135. 1953.

39. Rainbird, J. W. Turbulent boundary-layer growth and separation on a yawed cone. American Institute of Aeronautics and Astronautics Journal 6: 2410-2416. 1968.

40. Rakich, J. V. and Cleary, J. W. Theoretical and experimental study of supersonic steady flow around inclined bodies of revolution. American Institute of Aeronautics and Astronautics Paper No. 69-187: 1-9. 1969.

41. Randall, R. E., Bell, D. R., and Burk, J. L. Pressure distribution tests of several sharp leading edge wings, bodies, and body-wing combinations at Mach 5 and 8. Arnold Engineering Development Center Technical Note 60-173. 1960.

42. Richtmyer, R. D. A survey of difference methods for non-steady fluid dynamics. National Center for Atmospheric Research Technical Note 63-2. 1962.

43. Richtmyer, R. D. and Morton, K. W. Difference methods for initial-value problems. John Wiley and Sons, Inc., New York, New York. c1967.

44. Roberts, K. V. and Weiss, N. O. Convective difference schemes. Mathematics of Computation 20: 272-299. 1966.

45. Savin, R. C. Approximate solutions for the flow about flat-top wing body configurations at high supersonic airspeeds. National Advisory Committee for Aeronautics Research Memorandum A58F02. 1958.

46. Scheuing, R. A. Outer inviscid hypersonic flow with attached shock waves. American Rocket Society Journal 31: 486-503. 1961.

47. Small, W. J. and Bertram, M. H. Effect of geometric modifications on the maximum lift-drag ratios of slender wing body configurations at hypersonic speeds. National Aeronautics and Space Administration Technical Note D-3276. 1966.

48. Stocker, P. M. and Mauger, F. E. Supersonic flow past cones of general cross-section. Journal of Fluid Mechanics 13: 383-399. 1962.

49. Strang, G. Accurate partial difference methods. I: Linear Cauchy problem. Archive for Rational Mechanics and Analysis 12: 392-402. 1963.

50. Strang, G. Accurate partial difference methods. II: Nonlinear problems. Numerische Mathematik 6: 47-48. 1964.

51. Syvertson, C. A., Wong, T. J., and Gloria, H. R. Additional experiments with flat-top wing-body combinations at high supersonic speeds. National Advisory Committee for Aeronautics Research Memorandum A56I11. 1957.

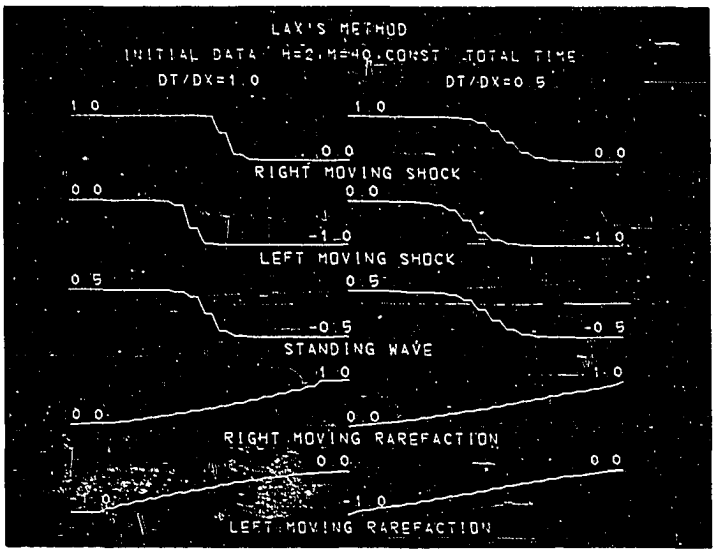

Figure 1. Lax's method

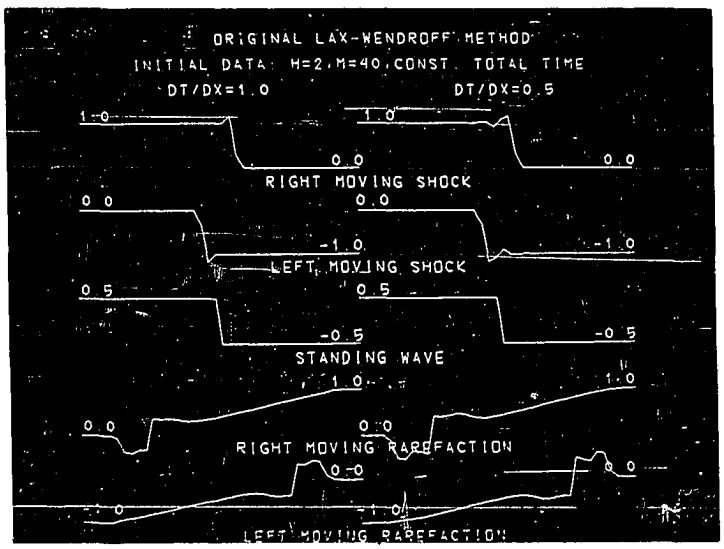

Figure 2. Original Lax-Wendroff method

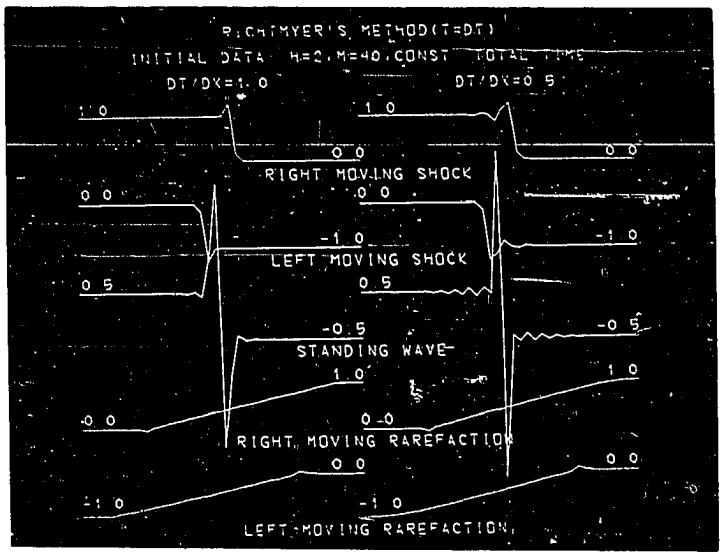

Figure 3. Richtmyer's single time step method

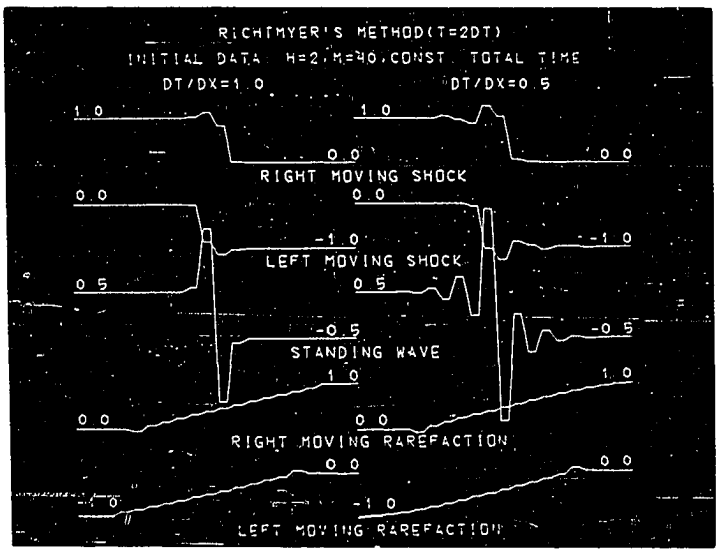

Figure 4. Richtmyer's double time step method

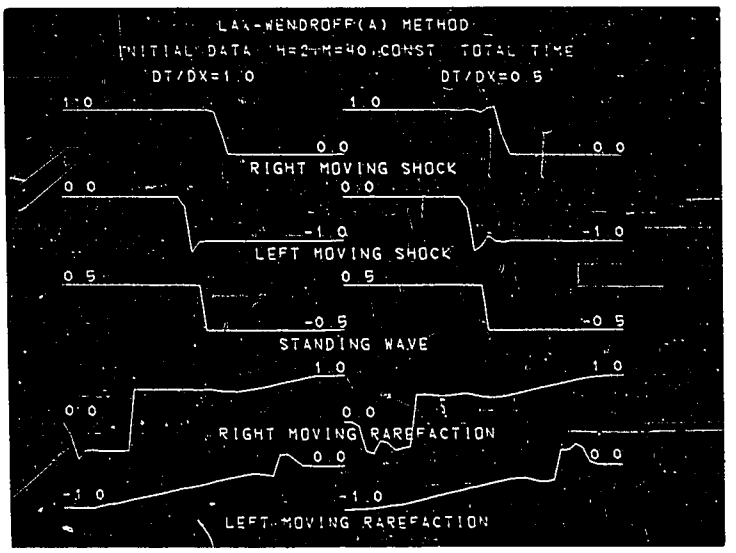

Figure 5. Lax-Wendroff (A) method

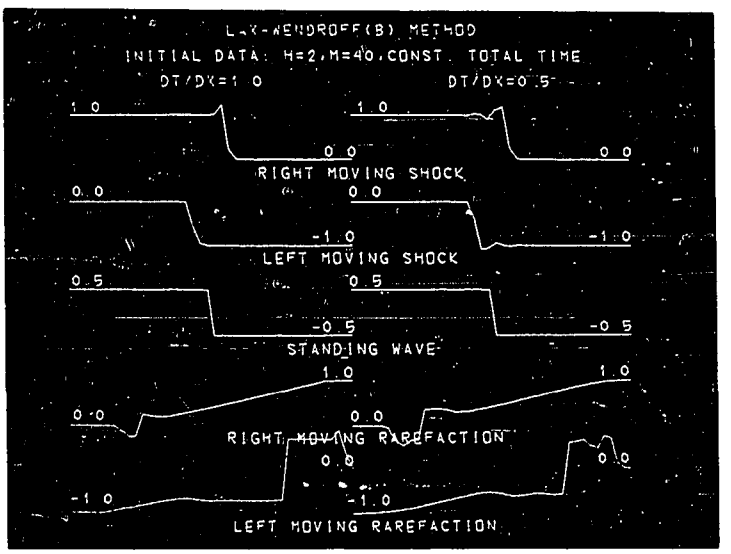

Figure 6. Lax-Wendroff (B) method

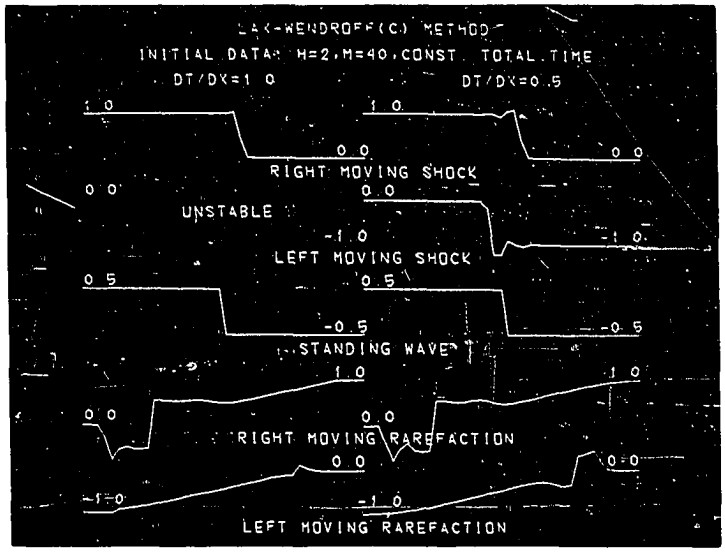

Figure 7. Lax-Wendroff (C) method

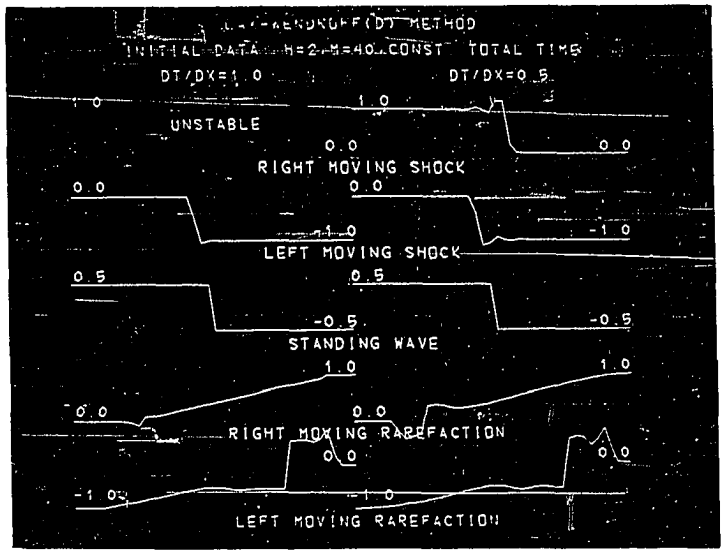

Figure 8. Lax-Wendroff (D) method

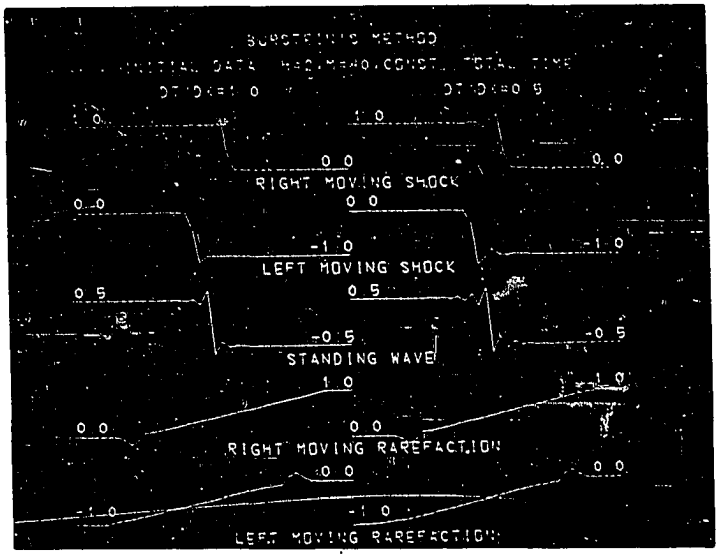

Figure 9. Burstein's method

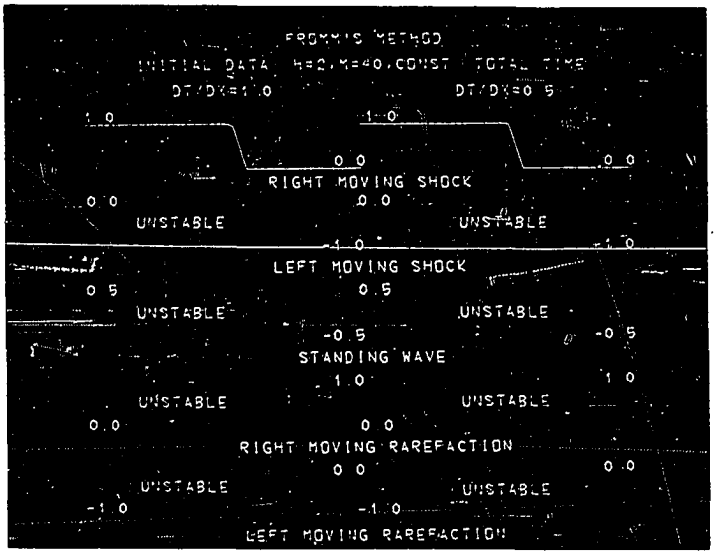

Figure 10. Fromm's method

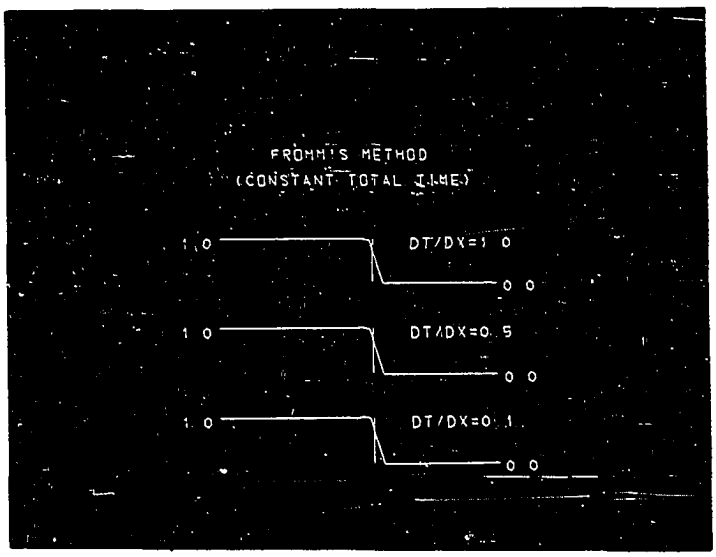

Figure 11. Fromm's method for various mesh ratios

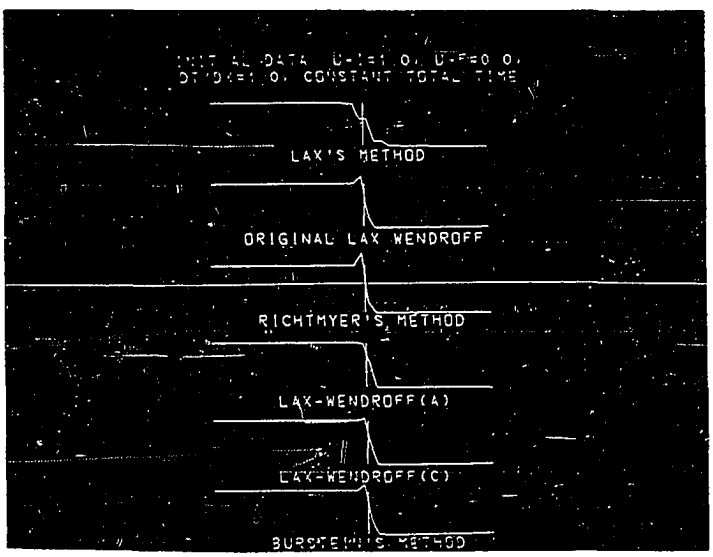

Figure 12. Comparison of selected methods with exact solution

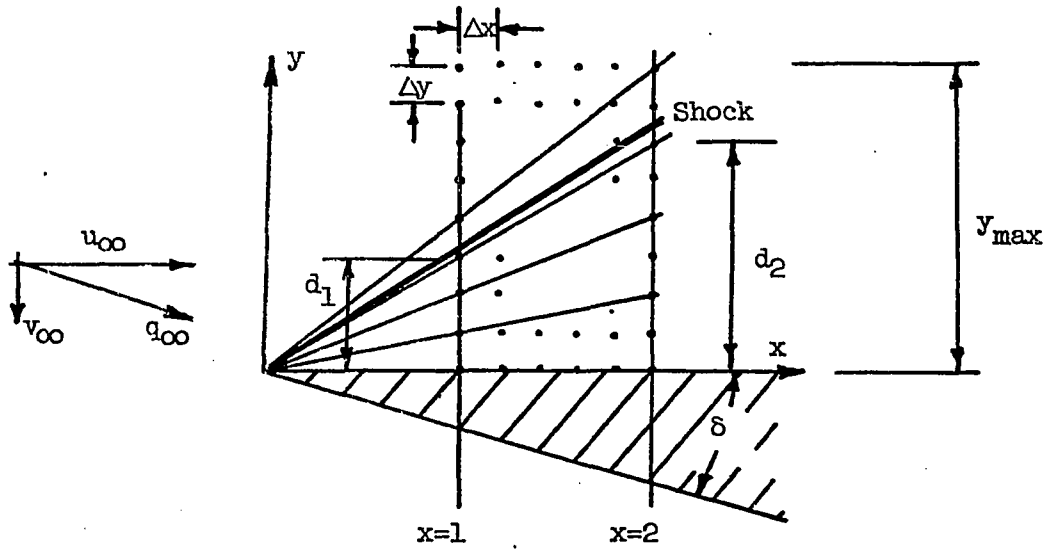

Figure 13. Coordinate system for wedge

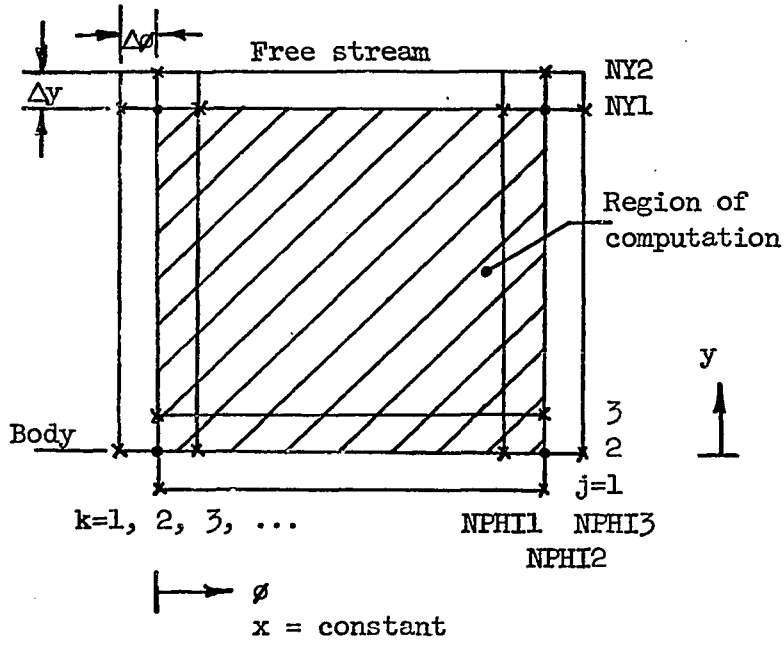

Figure 14. Mesh description for cone

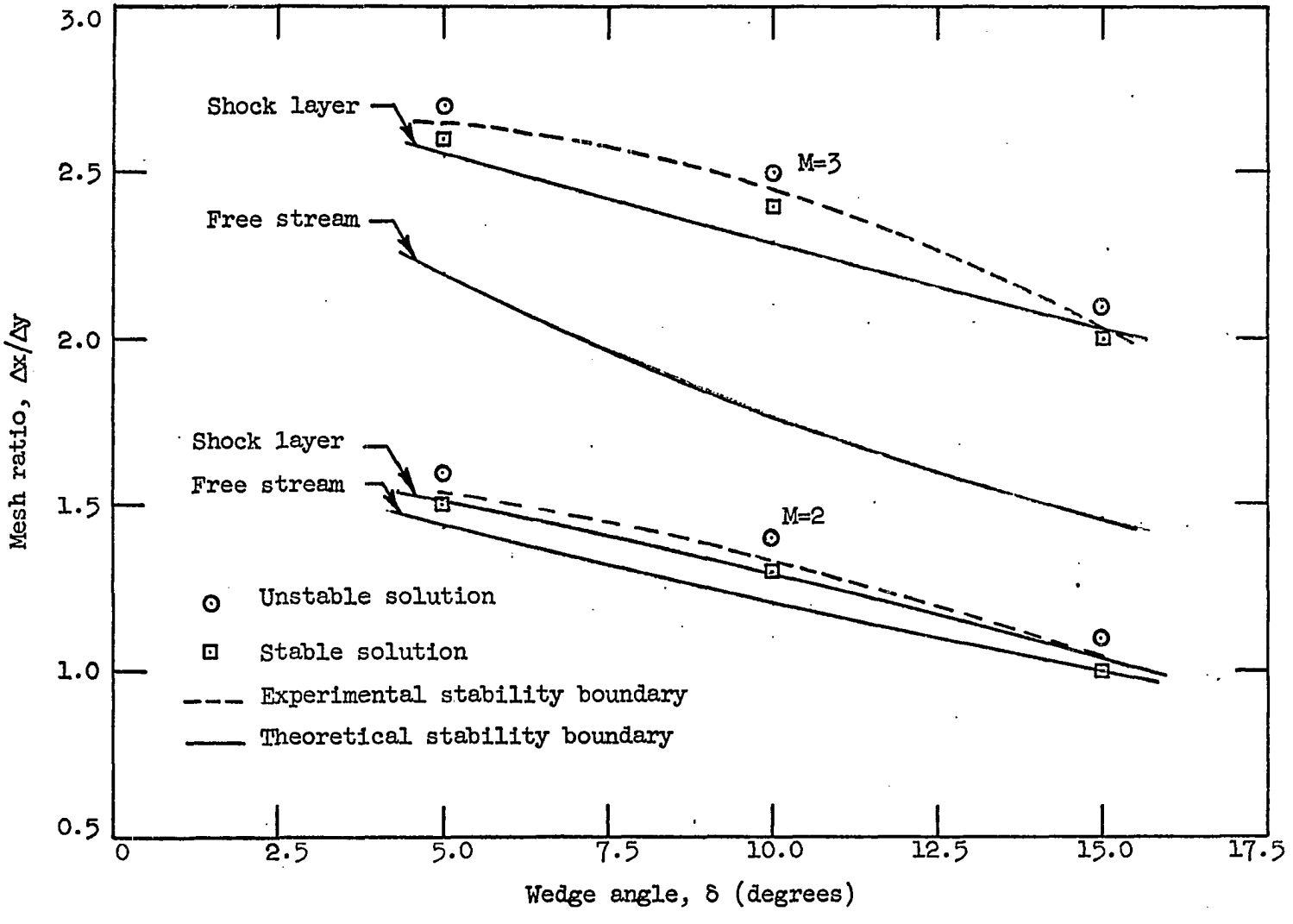

Figure 15. Comparison of experimental and theoretical stability bounds

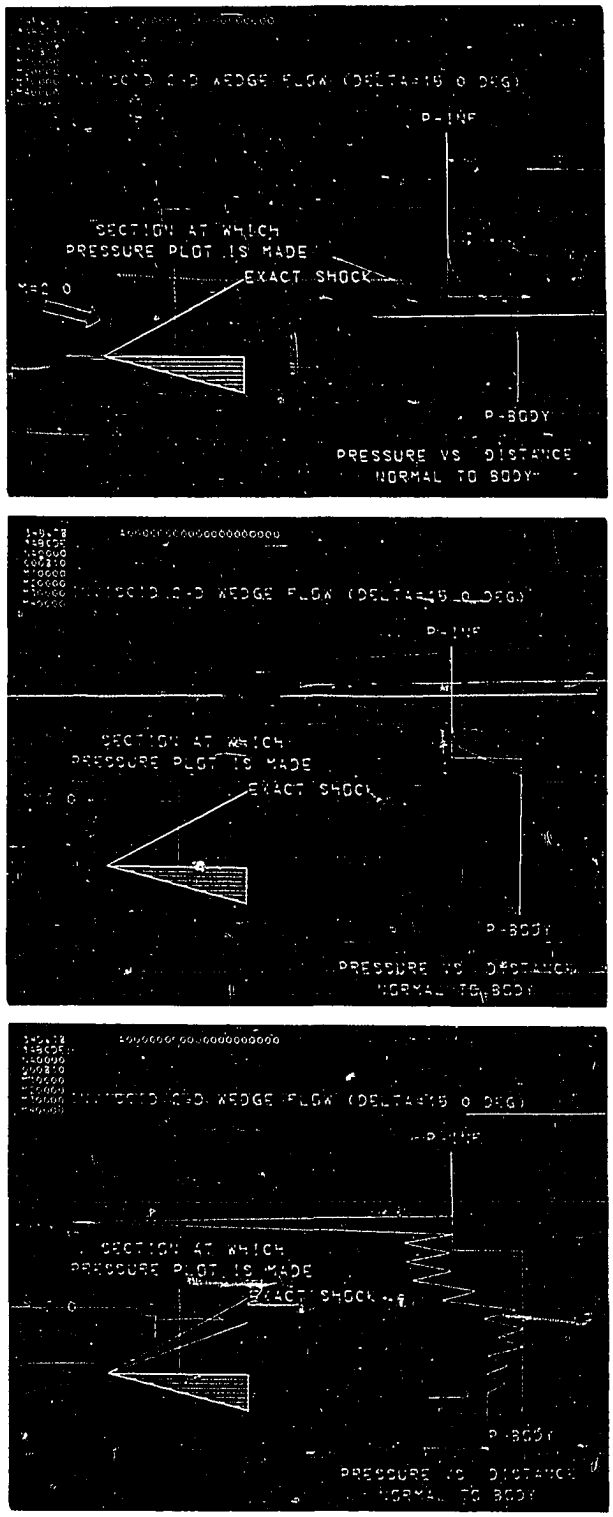

Figure 16. Lax's method ($\Delta x/\Delta y$ = 0.8, 1.2, 1.3)

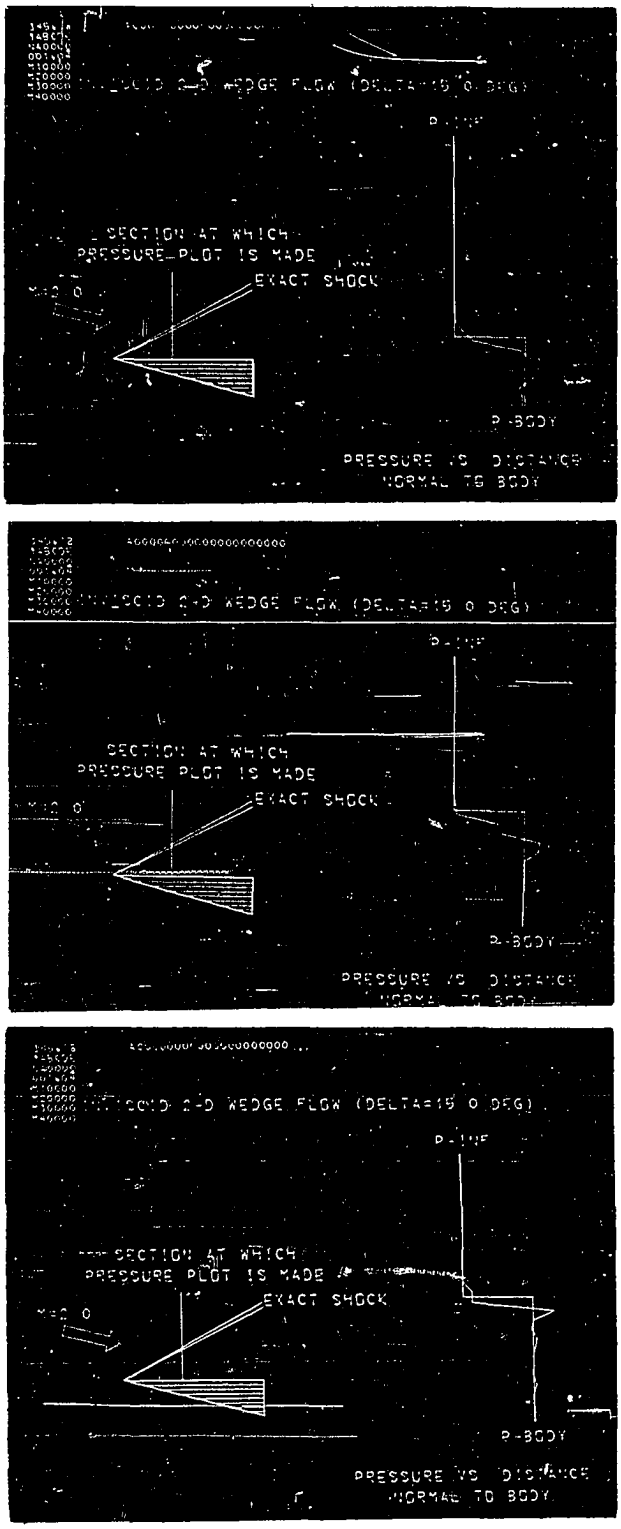

Figure 17. Richtmyer's double time step method ($\Delta x/\Delta y$ = 0.6, 1.0, 1.1)

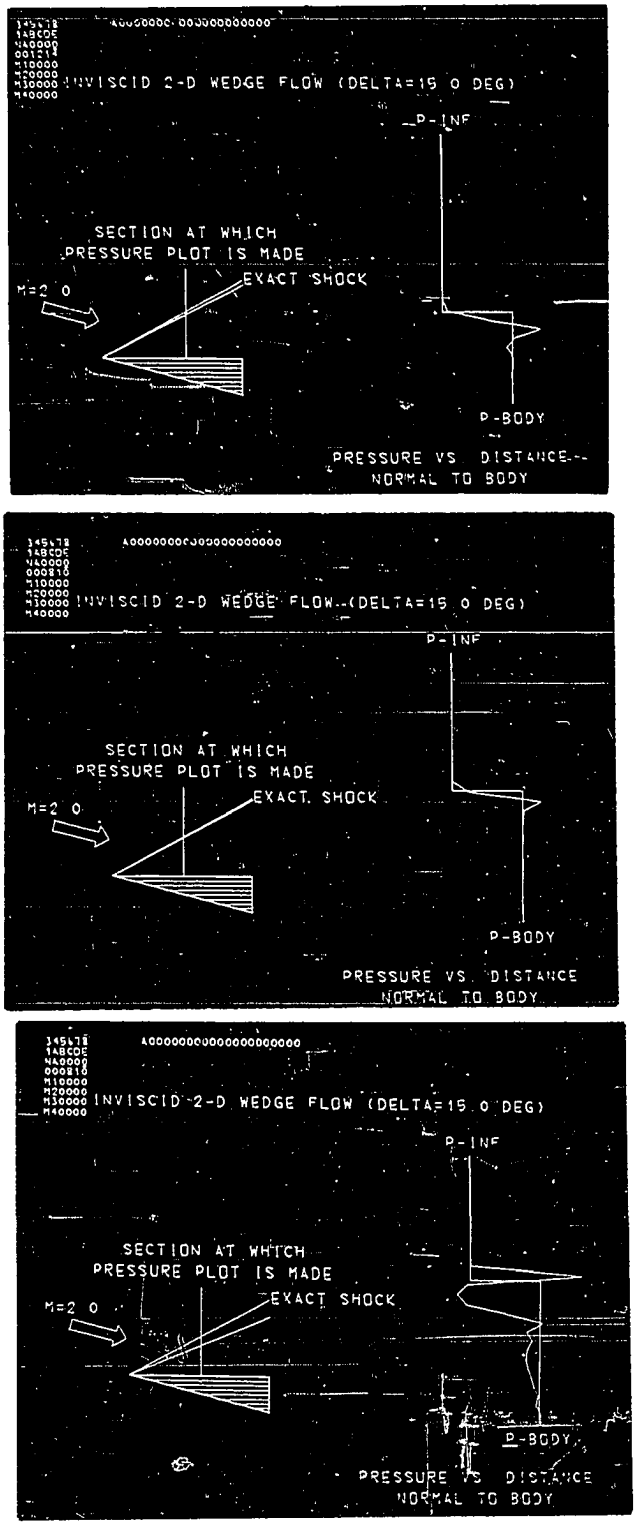

Figure 18. Richtmyer's single time step method ($\Delta x/\Delta y$ = 0.6, 1.0, 1.1)

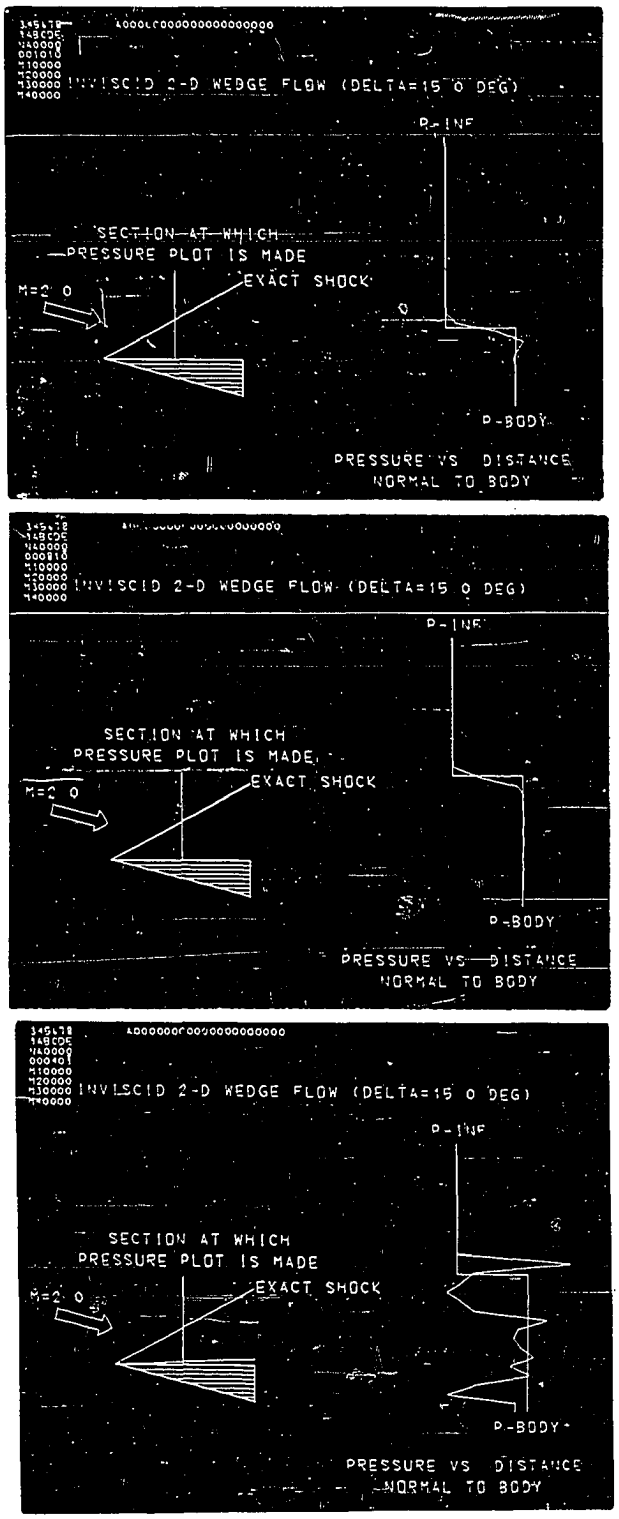

Figure 19. MacCormack's (A) method ($\Delta x/\Delta y$ = 0.6, 1.0, 1.1)

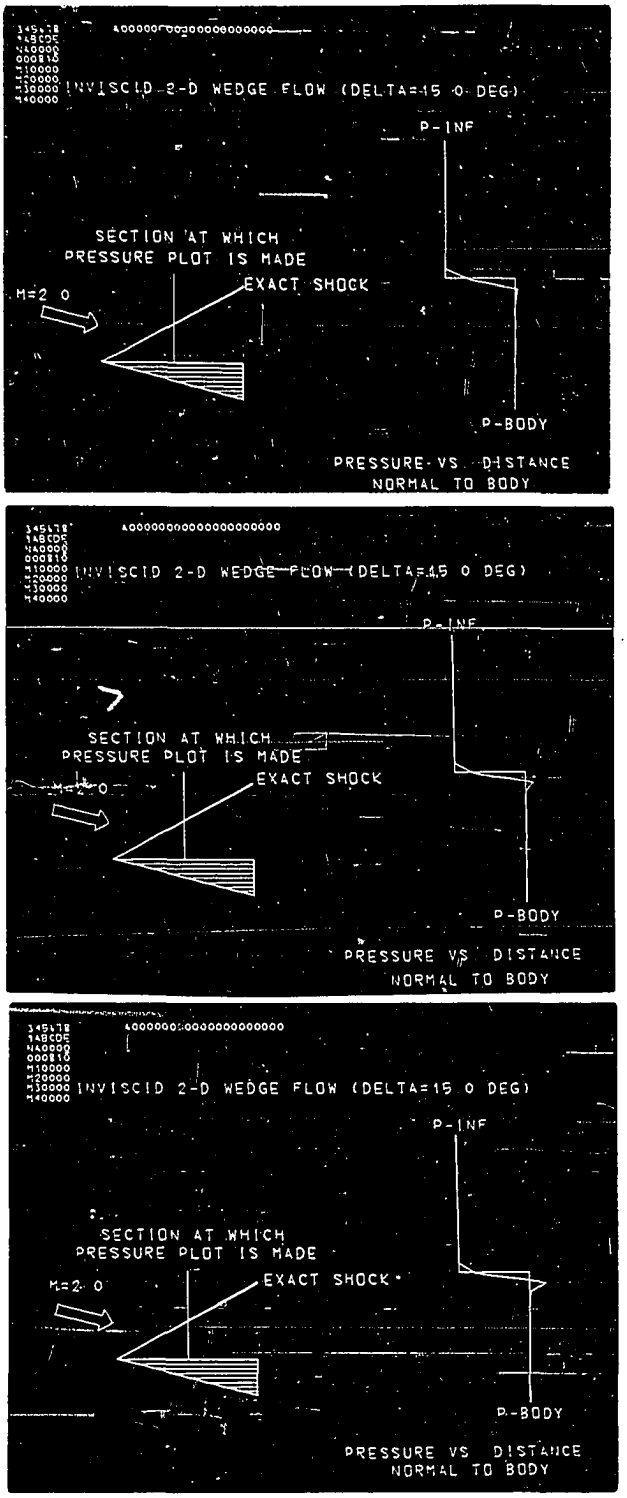

Figure 20. Lax-Wendroff's (C), Burstein's, MacCormack's methods ($\Delta x/\Delta y = 1.0$)

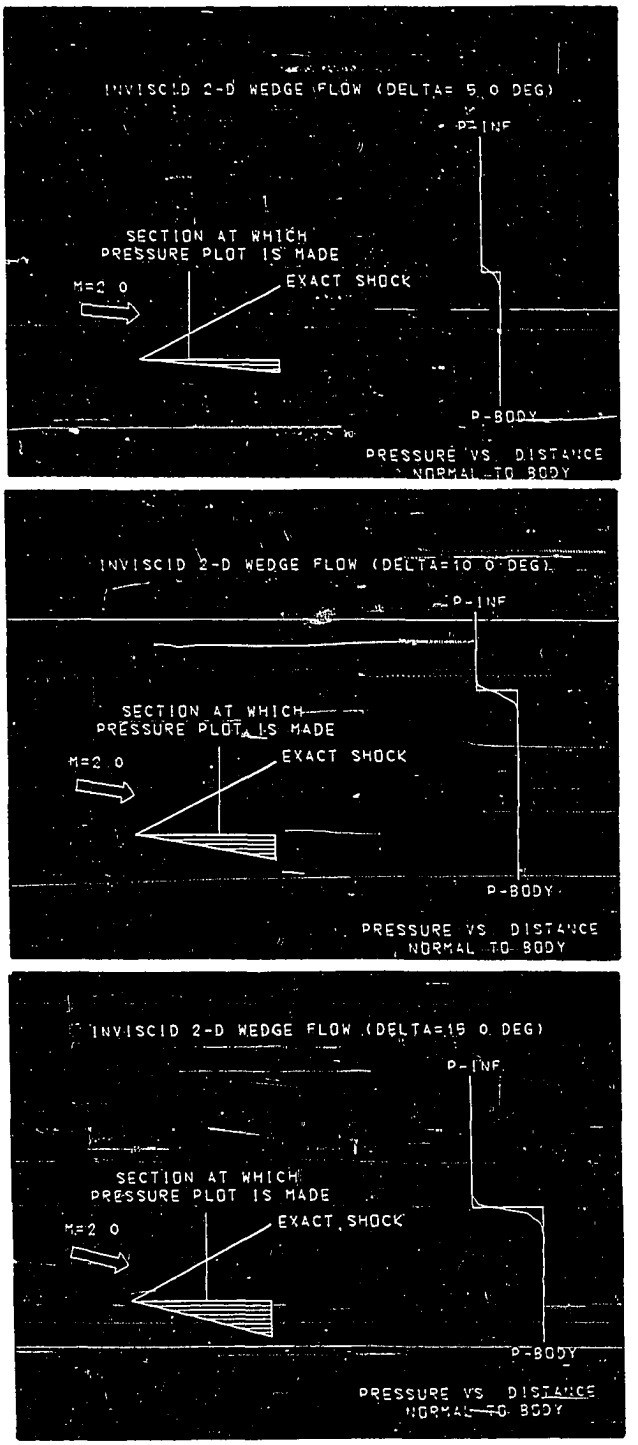

Figure 21. Converged solutions for Mach 2 flow over 5°, 10°, and 15° wedges

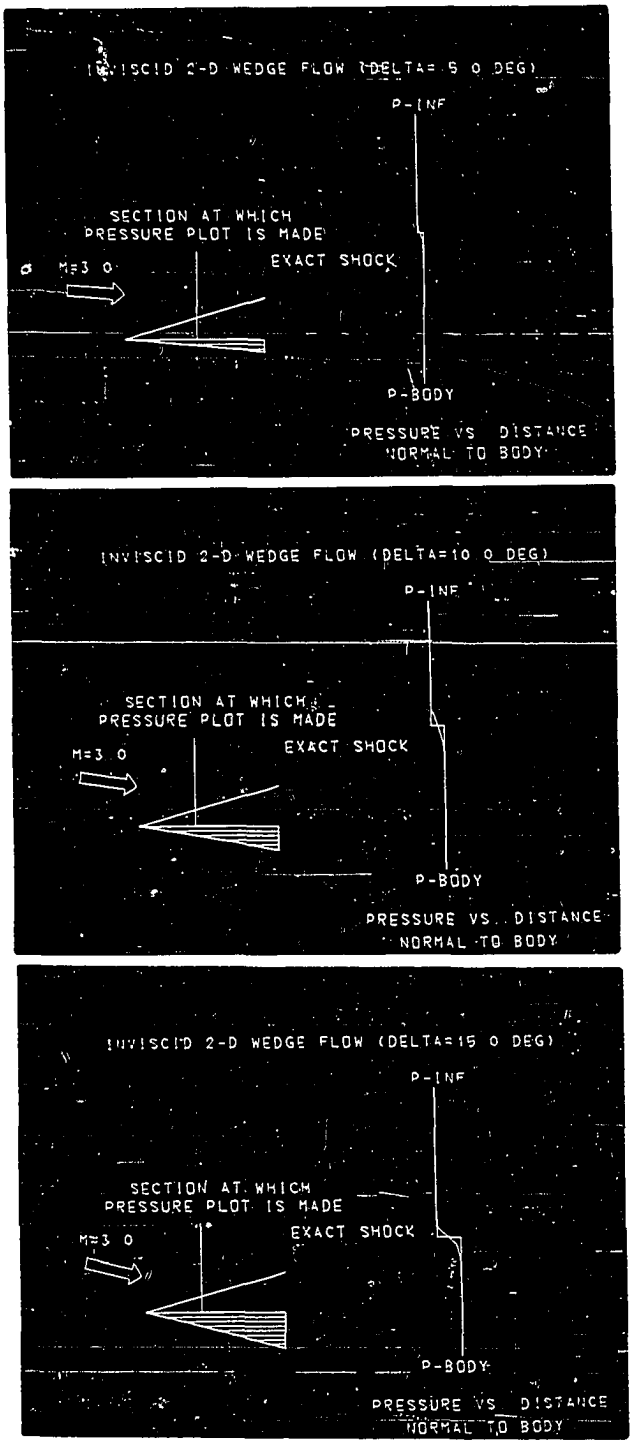

Figure 22. Converged solutions for Mach 3 flow over 5°, 10°, and 15° wedges

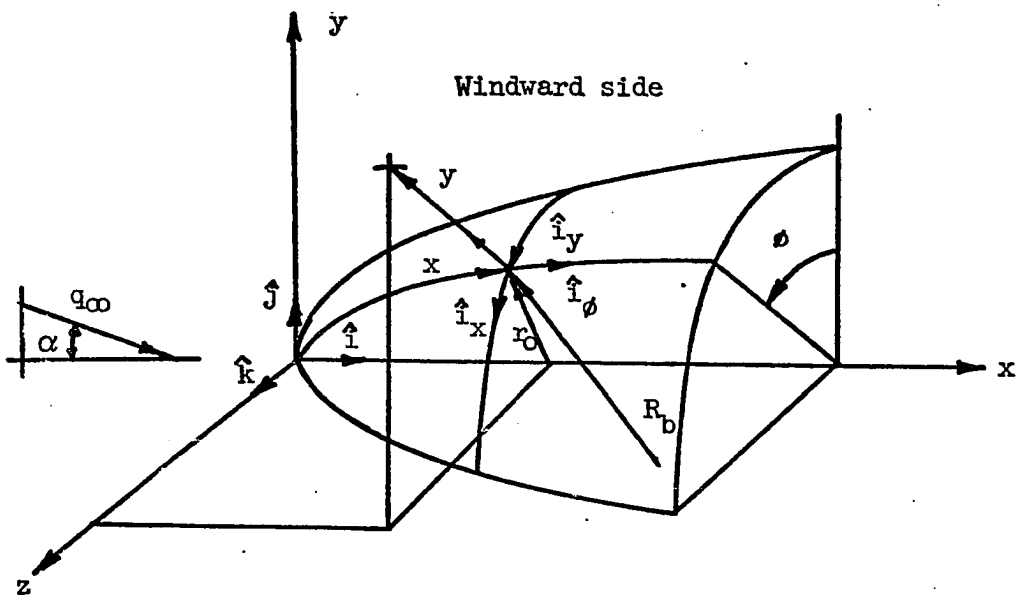

Figure 23. Body oriented coordinate system

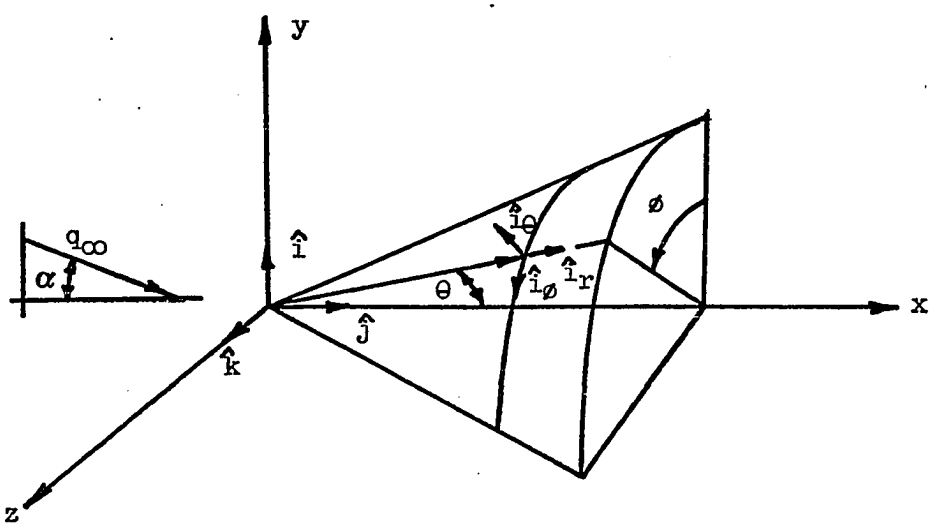

Figure 24. Spherical coordinate system

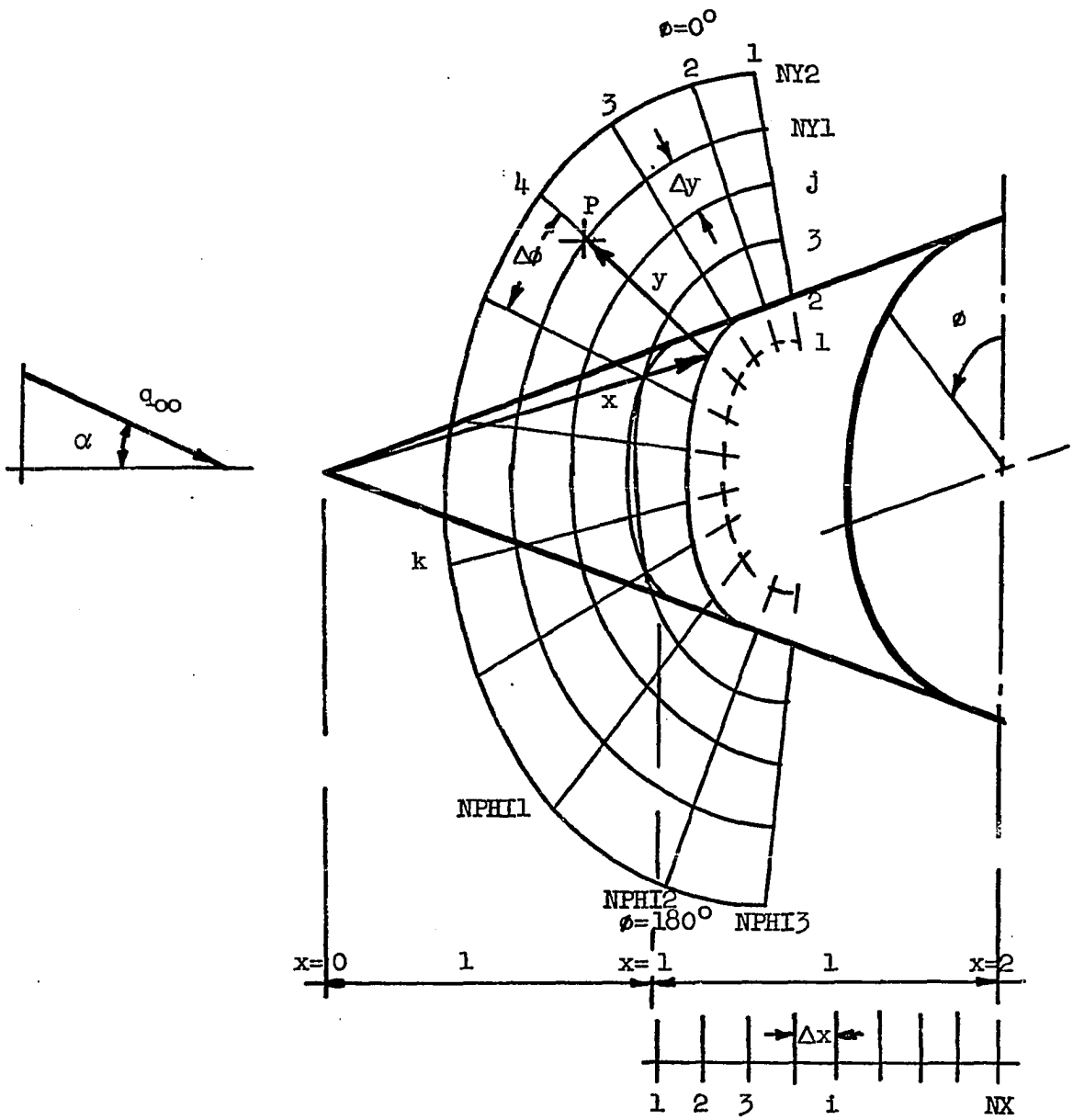

Figure 25. Mesh description for cone

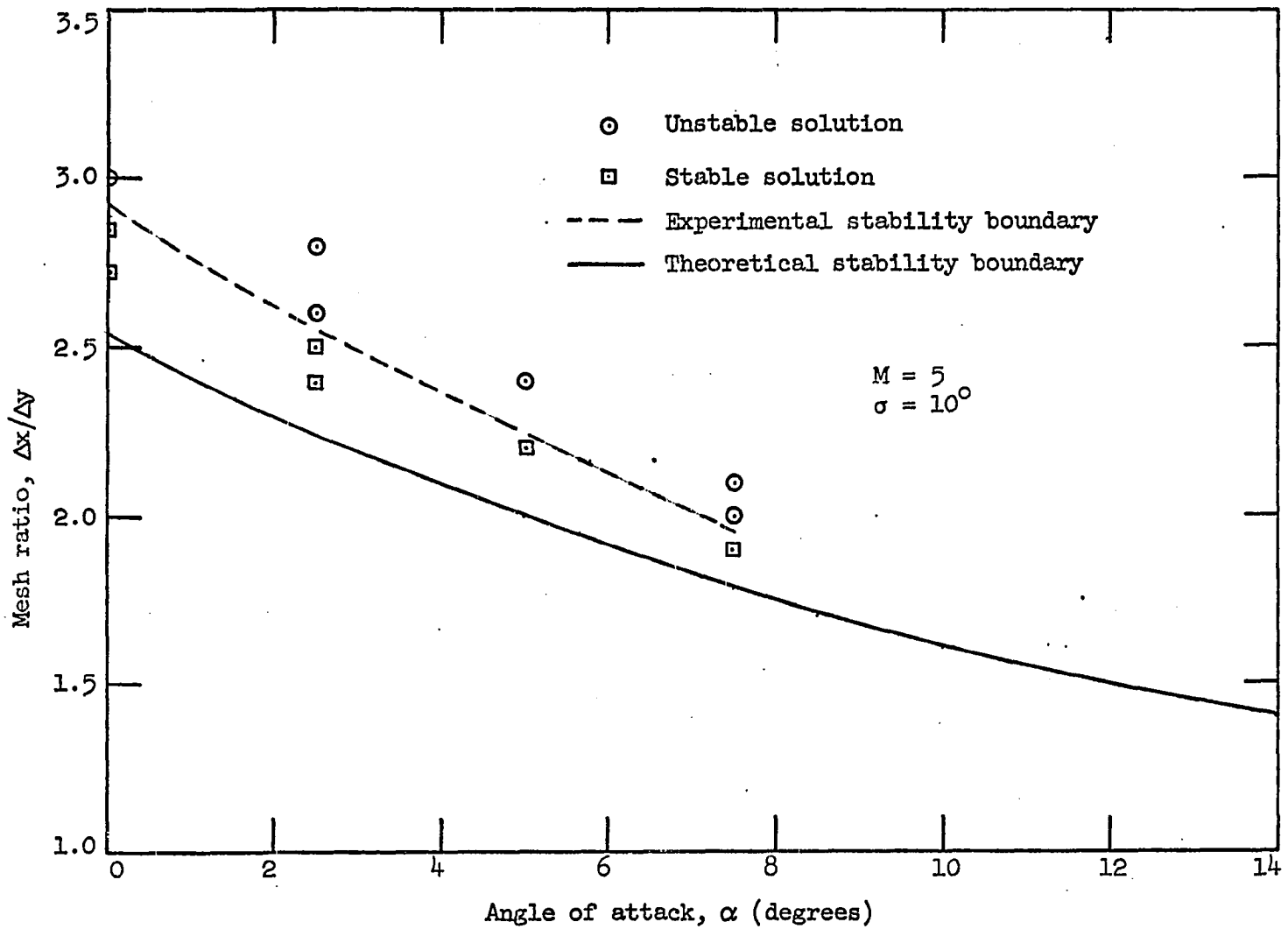

Figure 26. Comparison of theoretical and experimental stability bounds

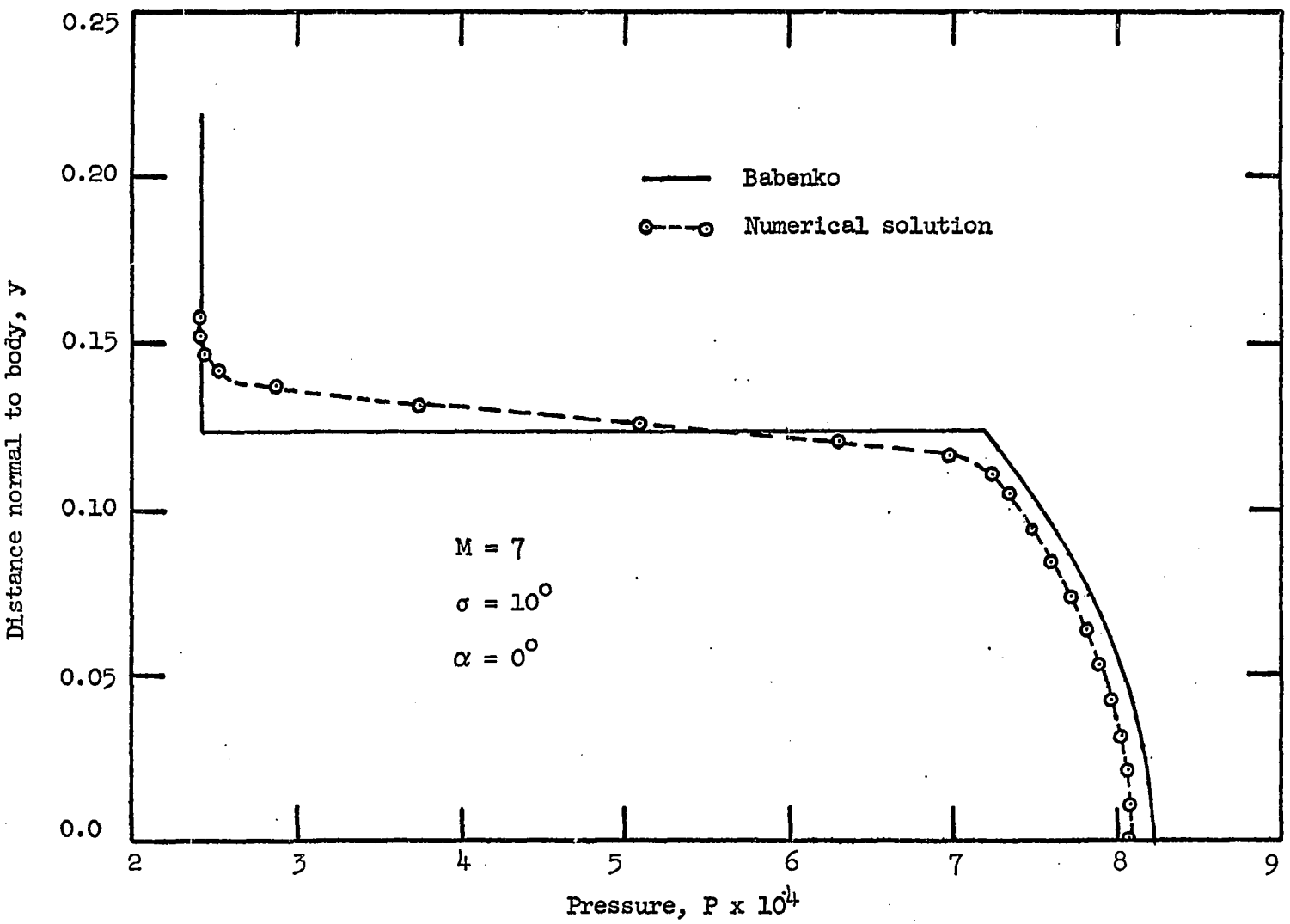

Figure 27. Pressure distribution normal to body using Lax's method in body coordinates

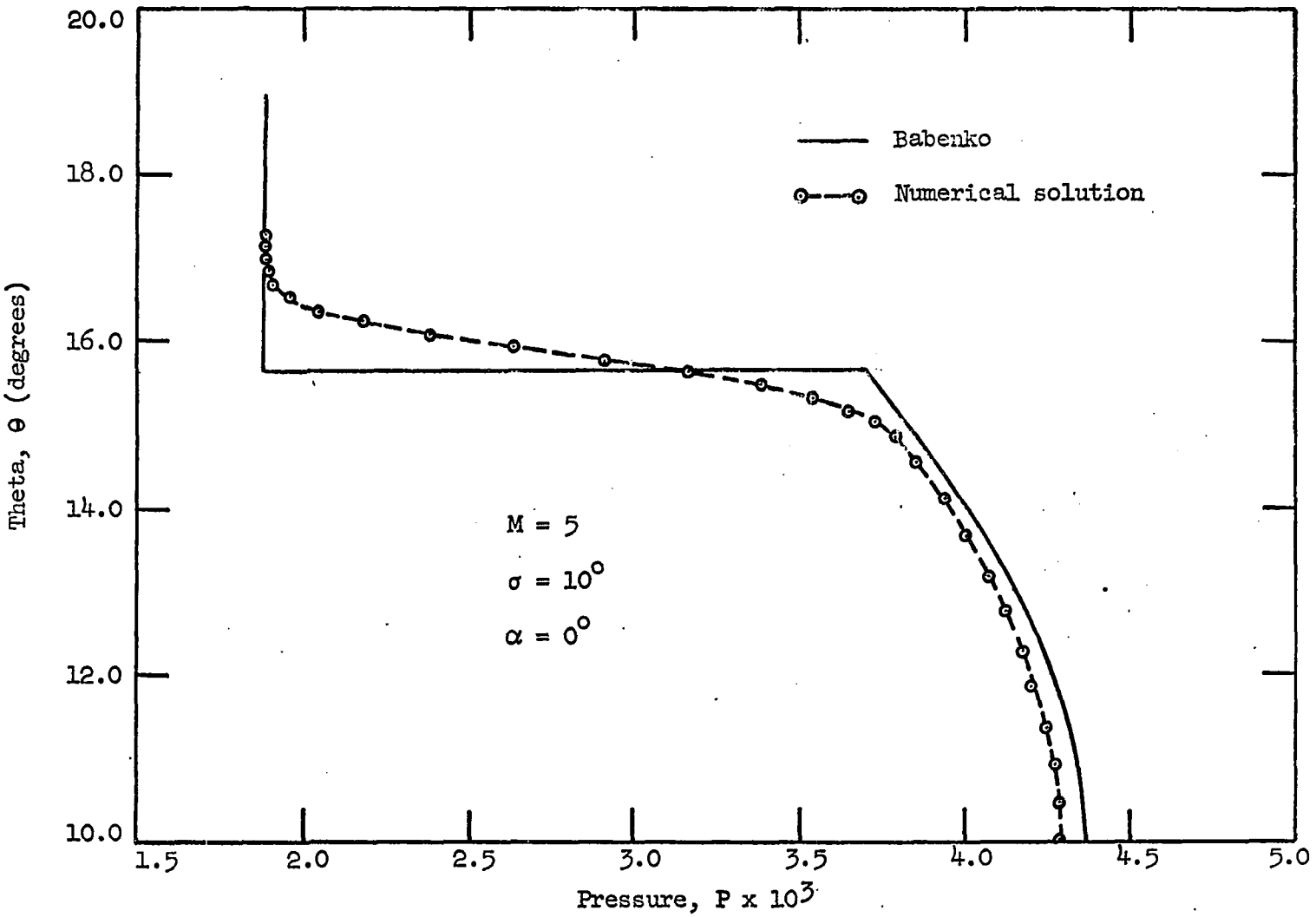

Figure 28. Pressure distribution normal to body using Lax's method in spherical coordinates

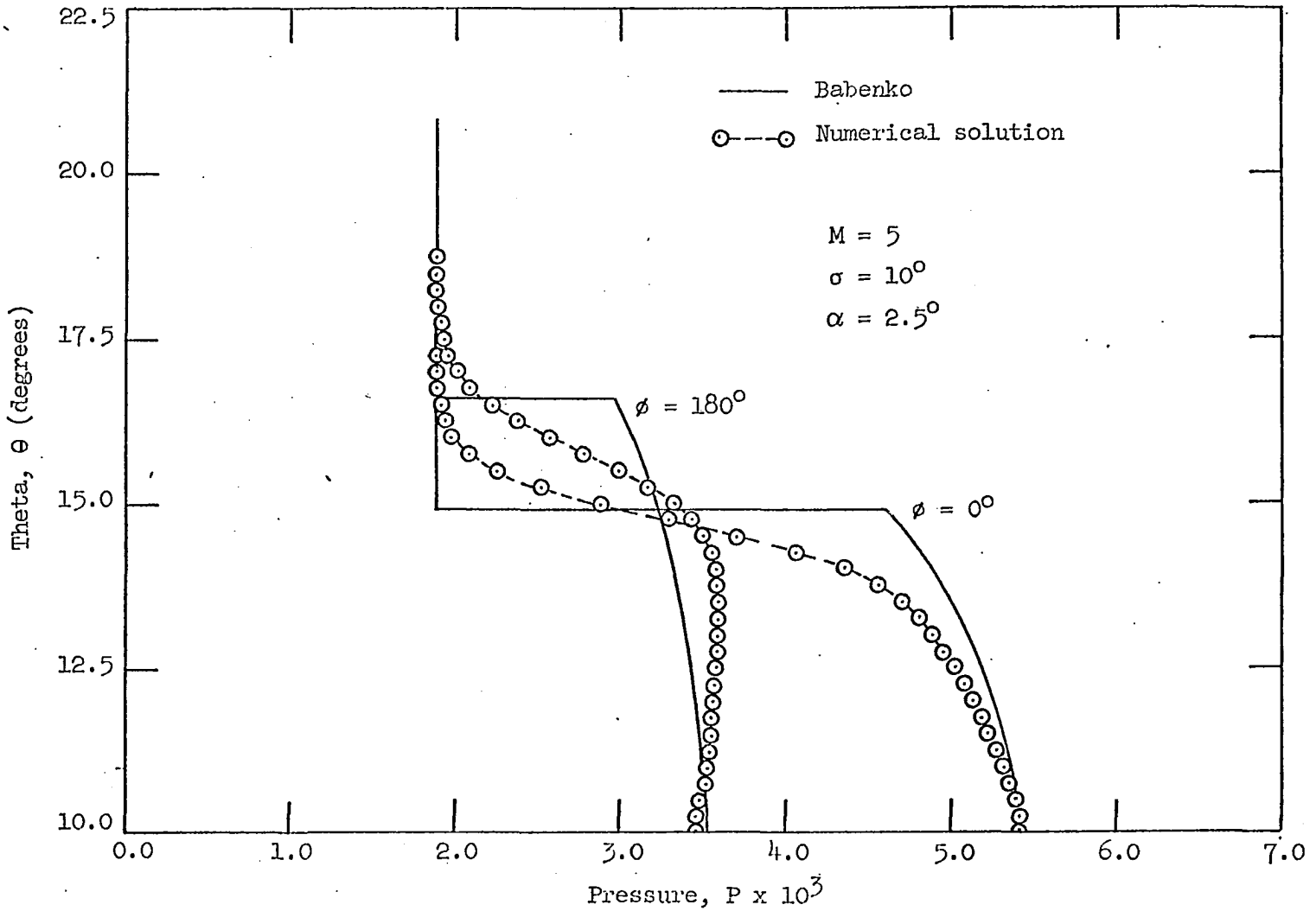

Figure 29. Pressure distribution in shock layer using Lax's method in spherical coordinates (parameter-meridional angle)

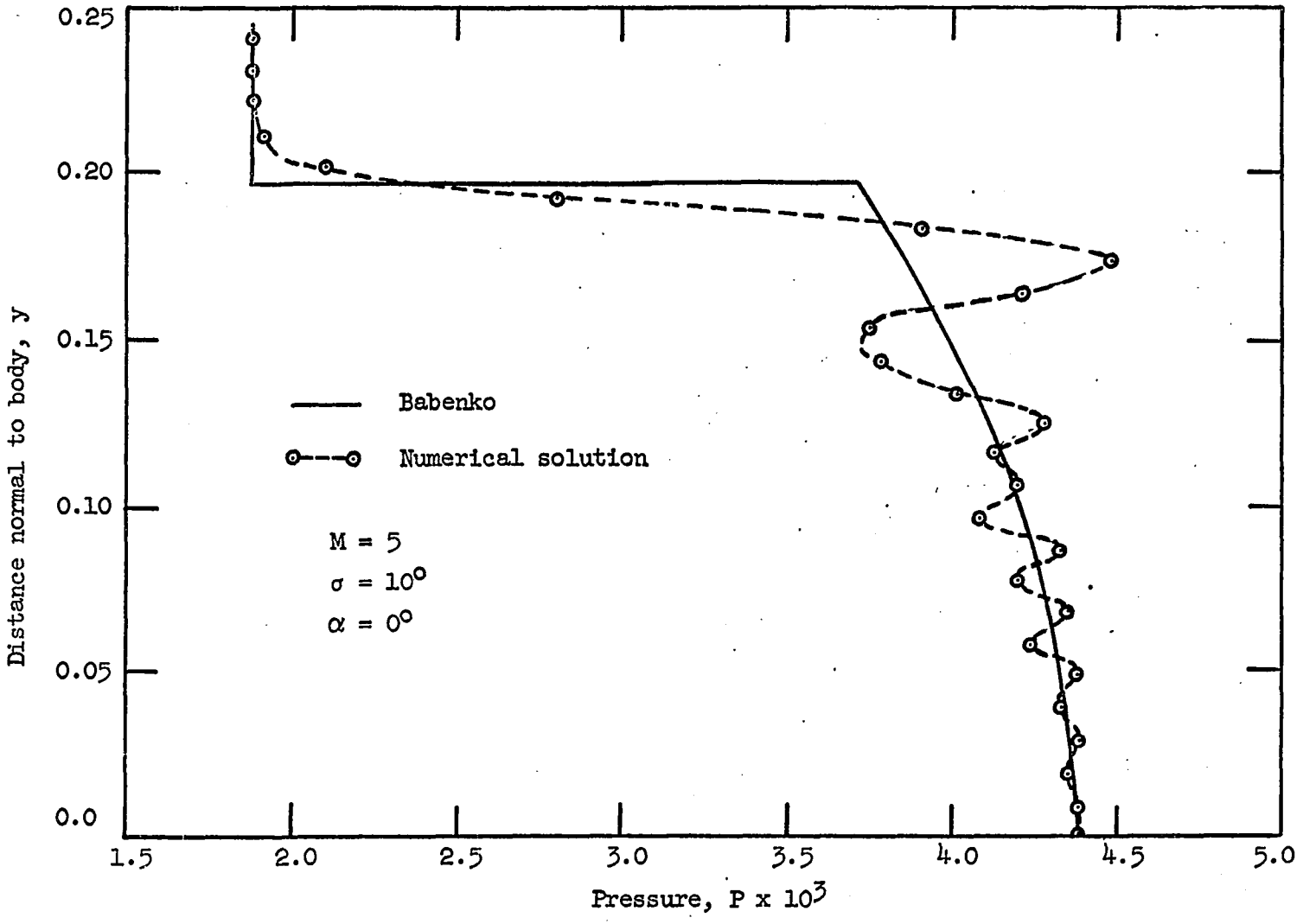

Figure 30. Pressure distribution normal to body using Richtmyer's method in body coordinates

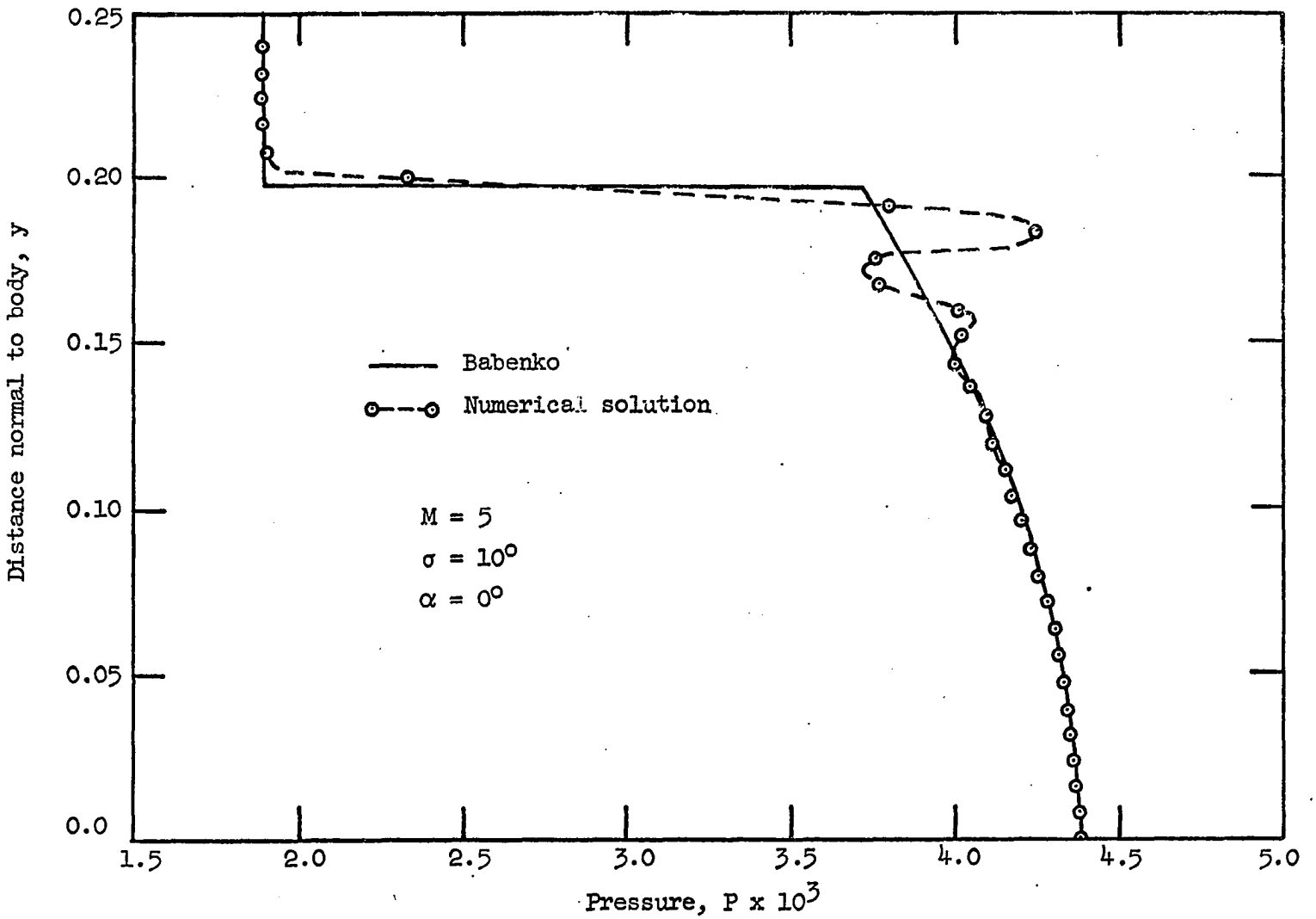

Figure 31. Pressure distribution normal to body using MacCormack's method in body coordinates

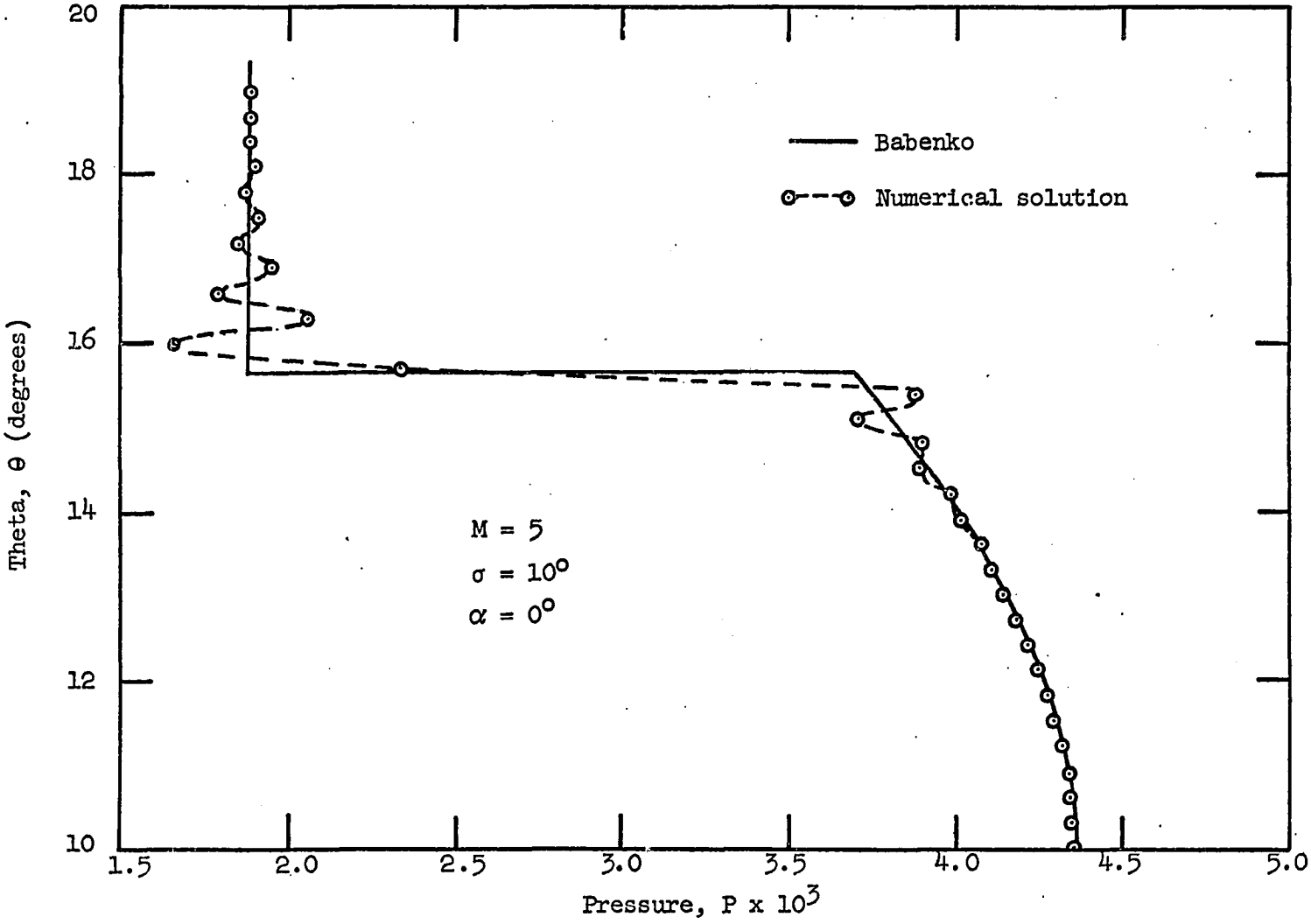

Figure 32. Pressure distribution in shock layer using MacCormack's method in spherical coordinates

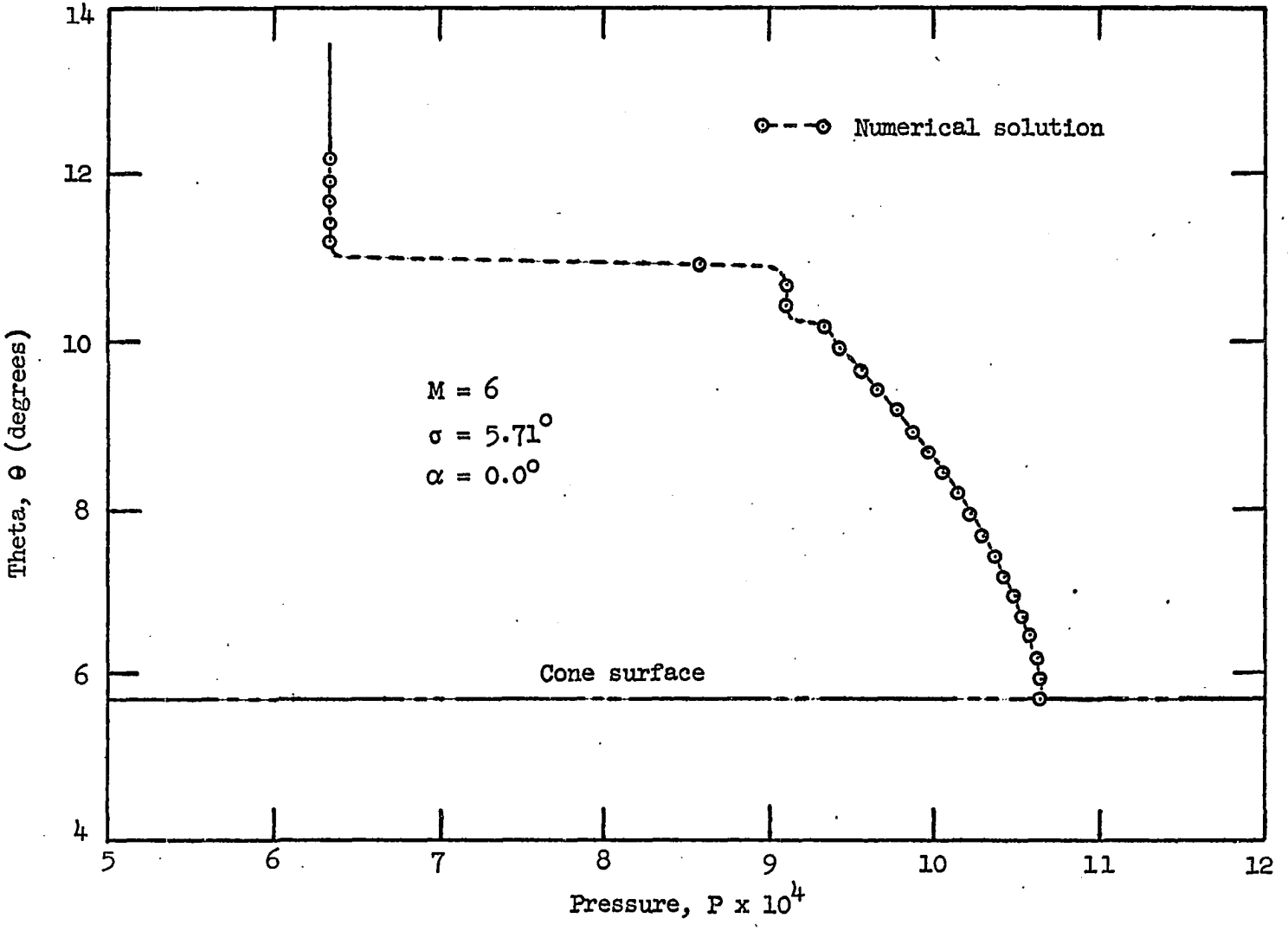

Figure 33. Pressure distribution in shock layer (spherical coordinates)

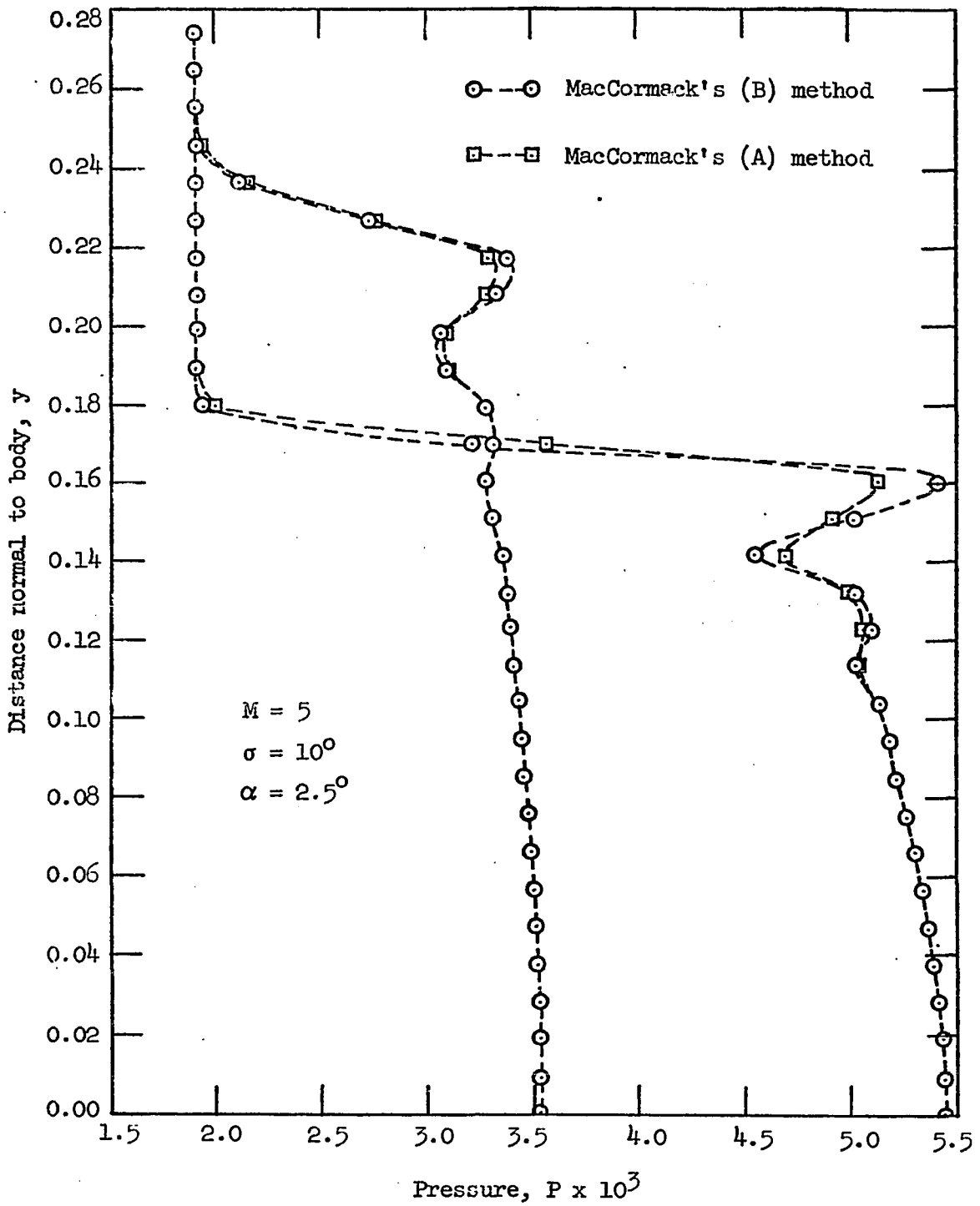

Figure 34. Comparison of variations in MacCormack's method for cone at angle of attack

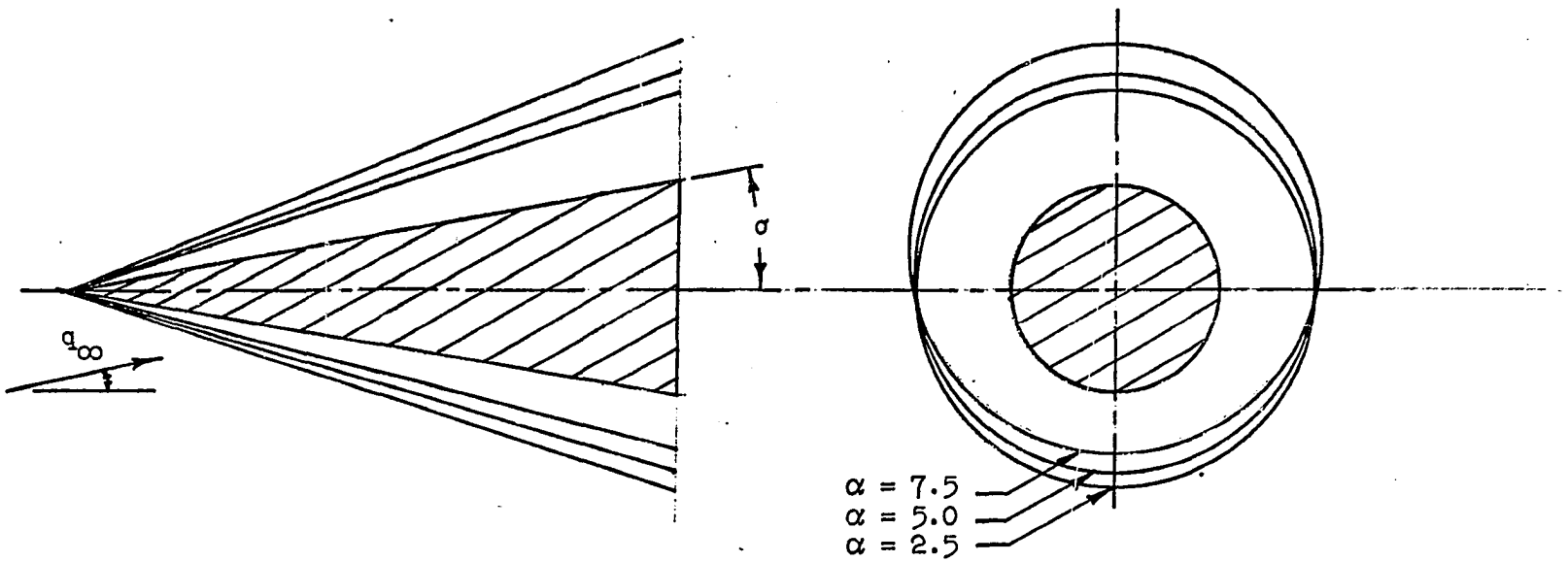

Figure 35. Sketch of shock shapes for Mach 5 flow over a 10° cone at various angles of attack

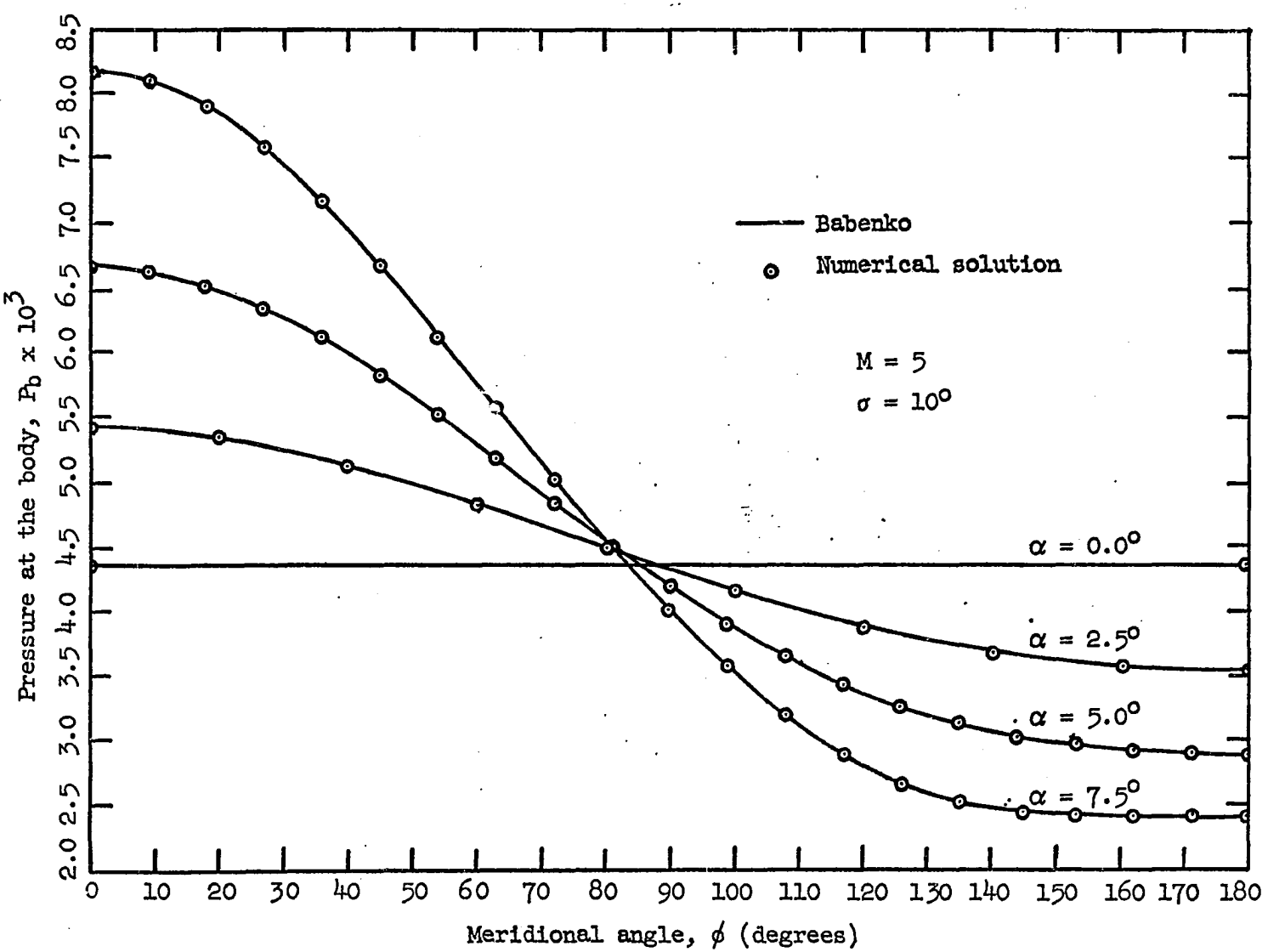

Figure 36. Pressure distribution around body (parameter-angle of attack)

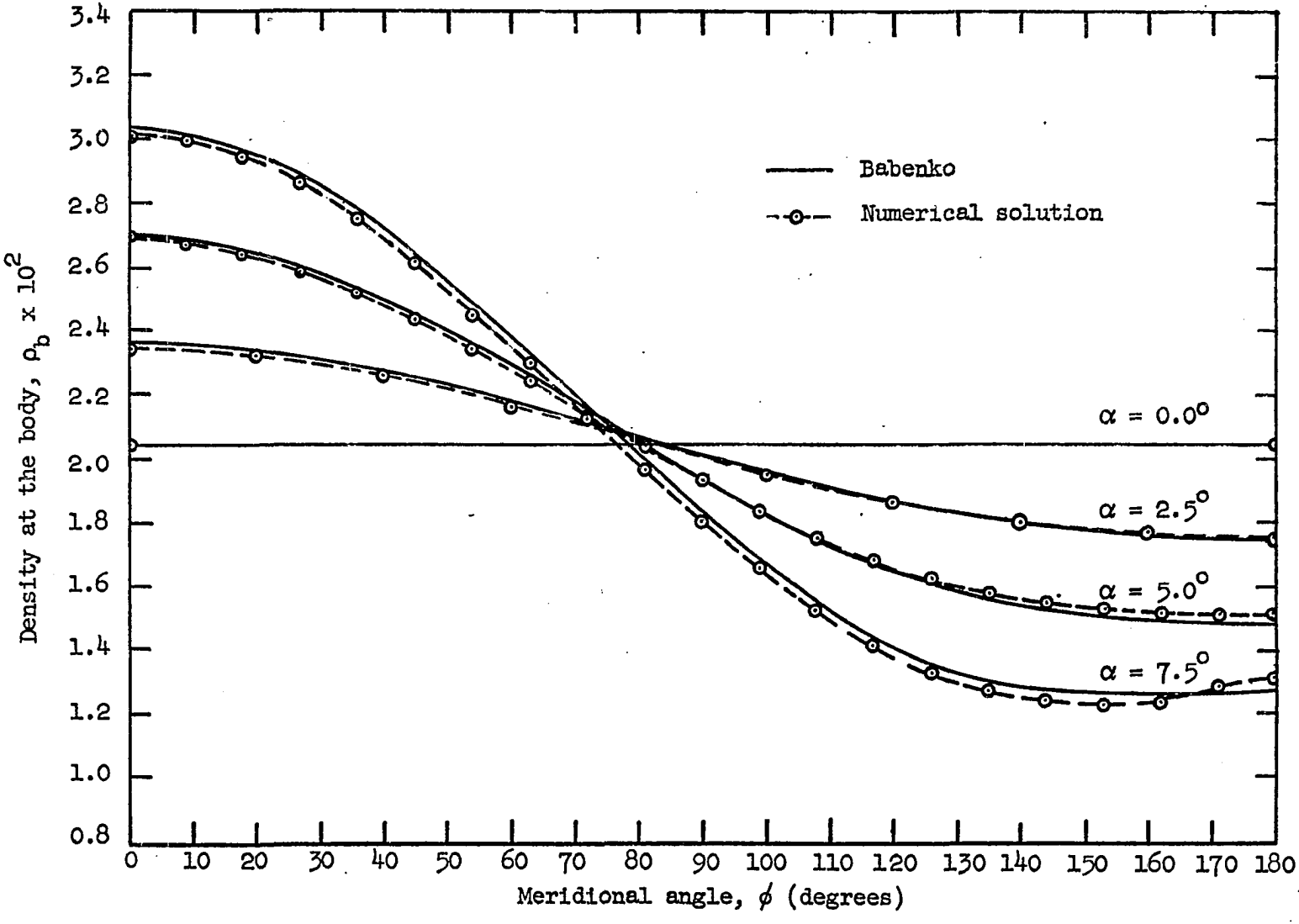

Figure 37. Density distribution around body (parameter-angle of attack)

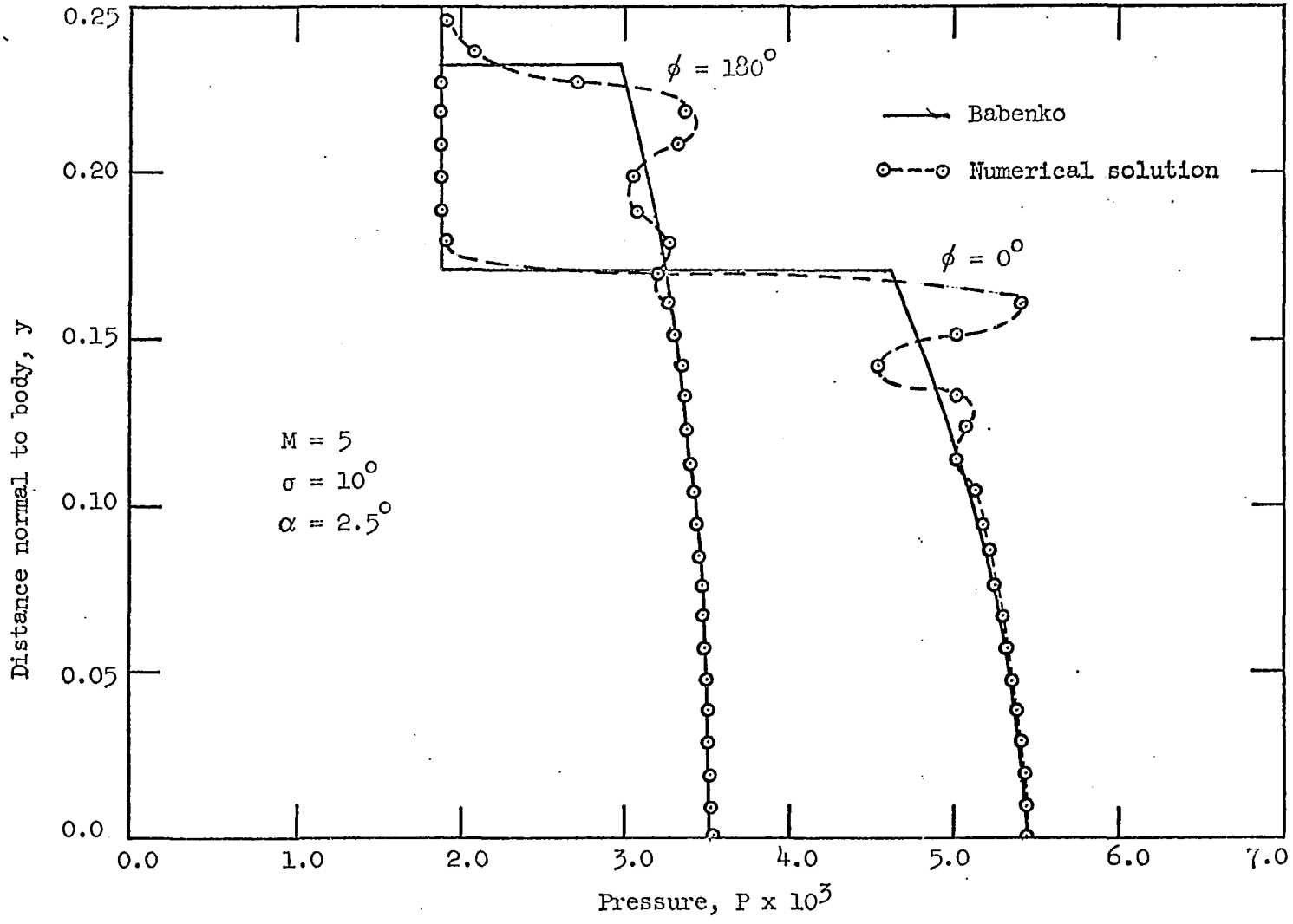

Figure 38. Pressure distribution normal to body (parameter-meridional angle)

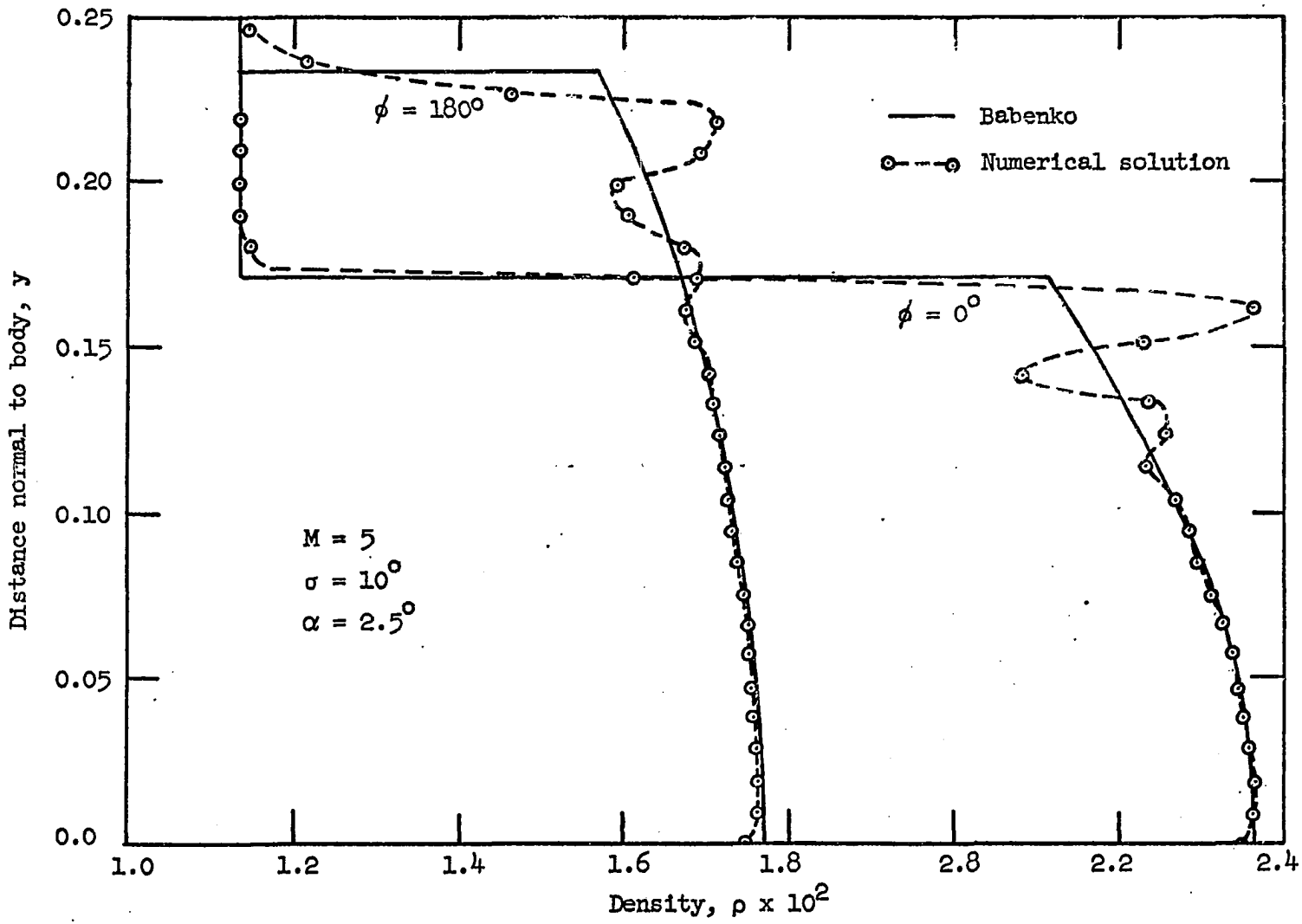

Figure 39. Density distribution normal to body (parameter-meridional angle)

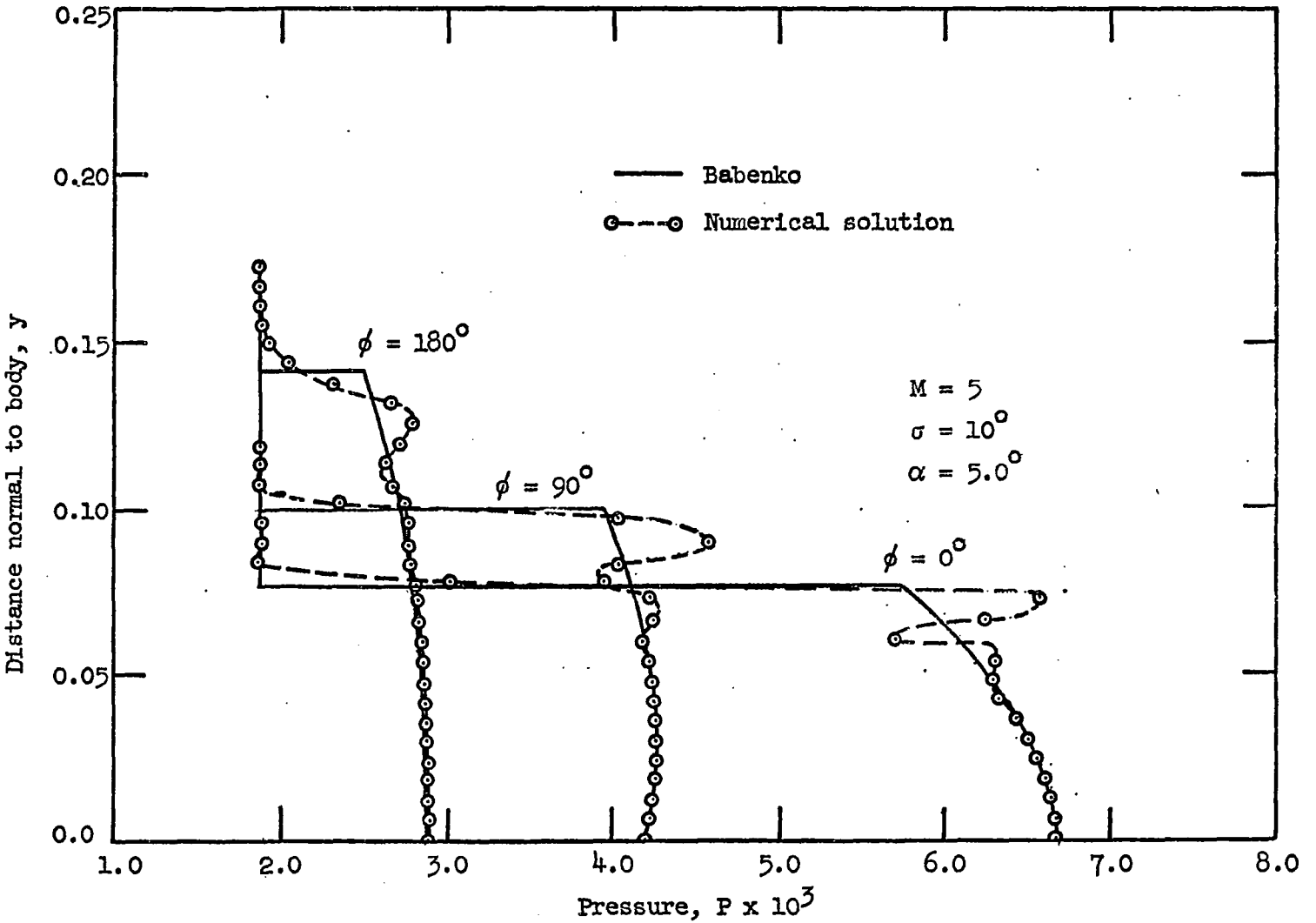

Figure 40. Pressure distribution normal to body (parameter-meridional angle)

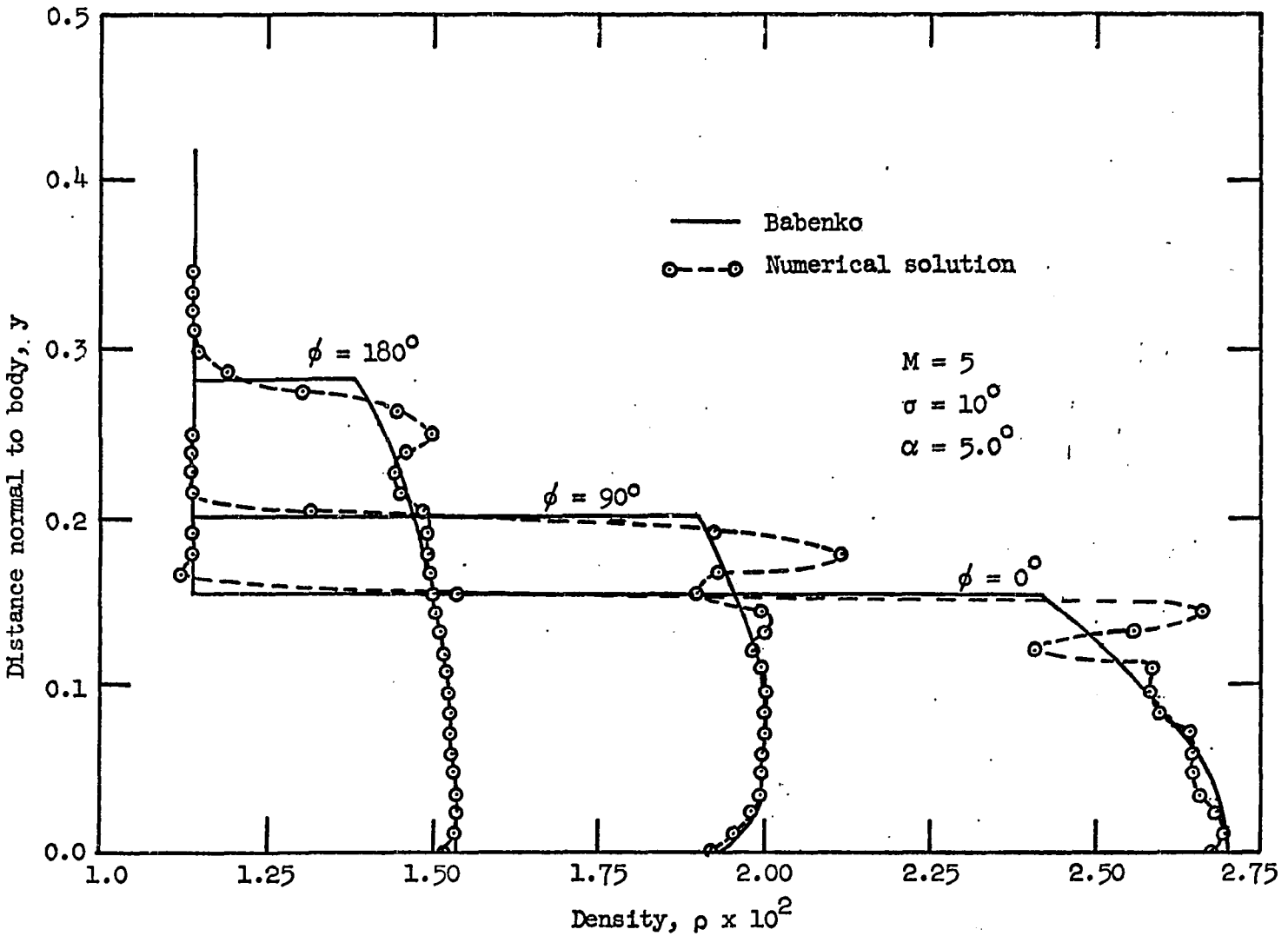

Figure 41. Density distribution normal to body (parameter-meridional angle)

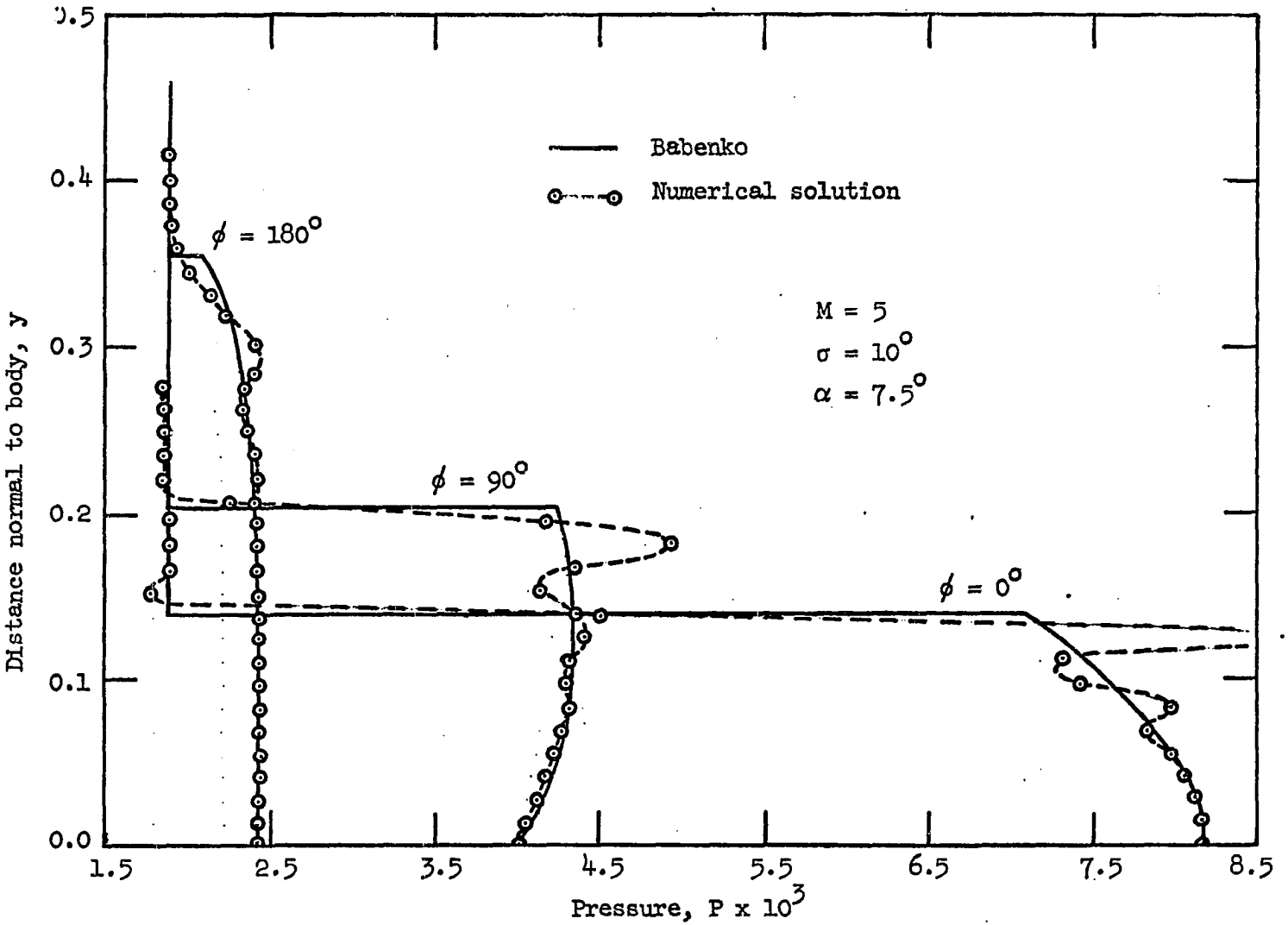

Figure 42. Pressure distribution normal to body (parameter-meridional angle)

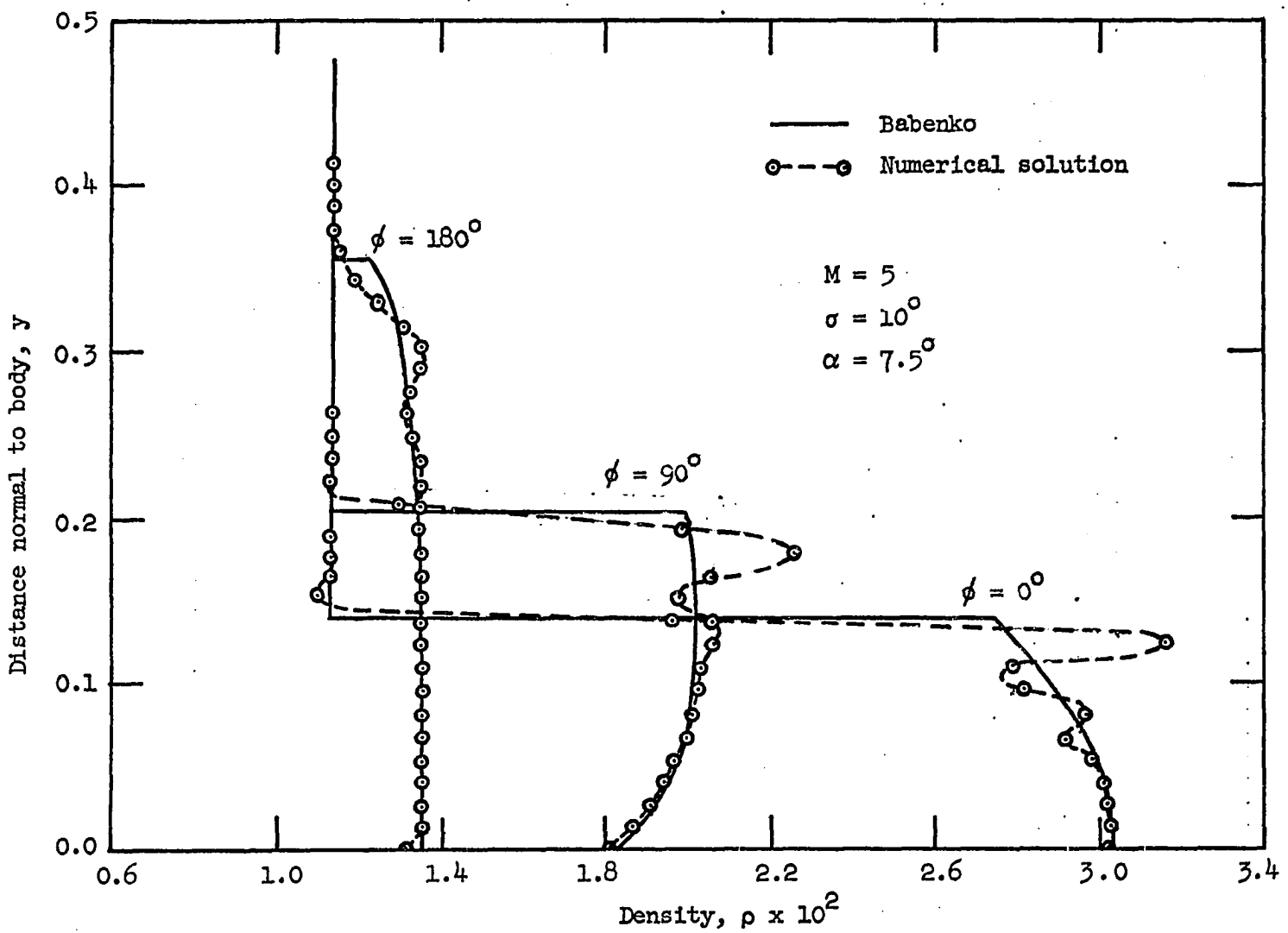

Figure 43. Density distribution normal to body (parameter-meridional angle)

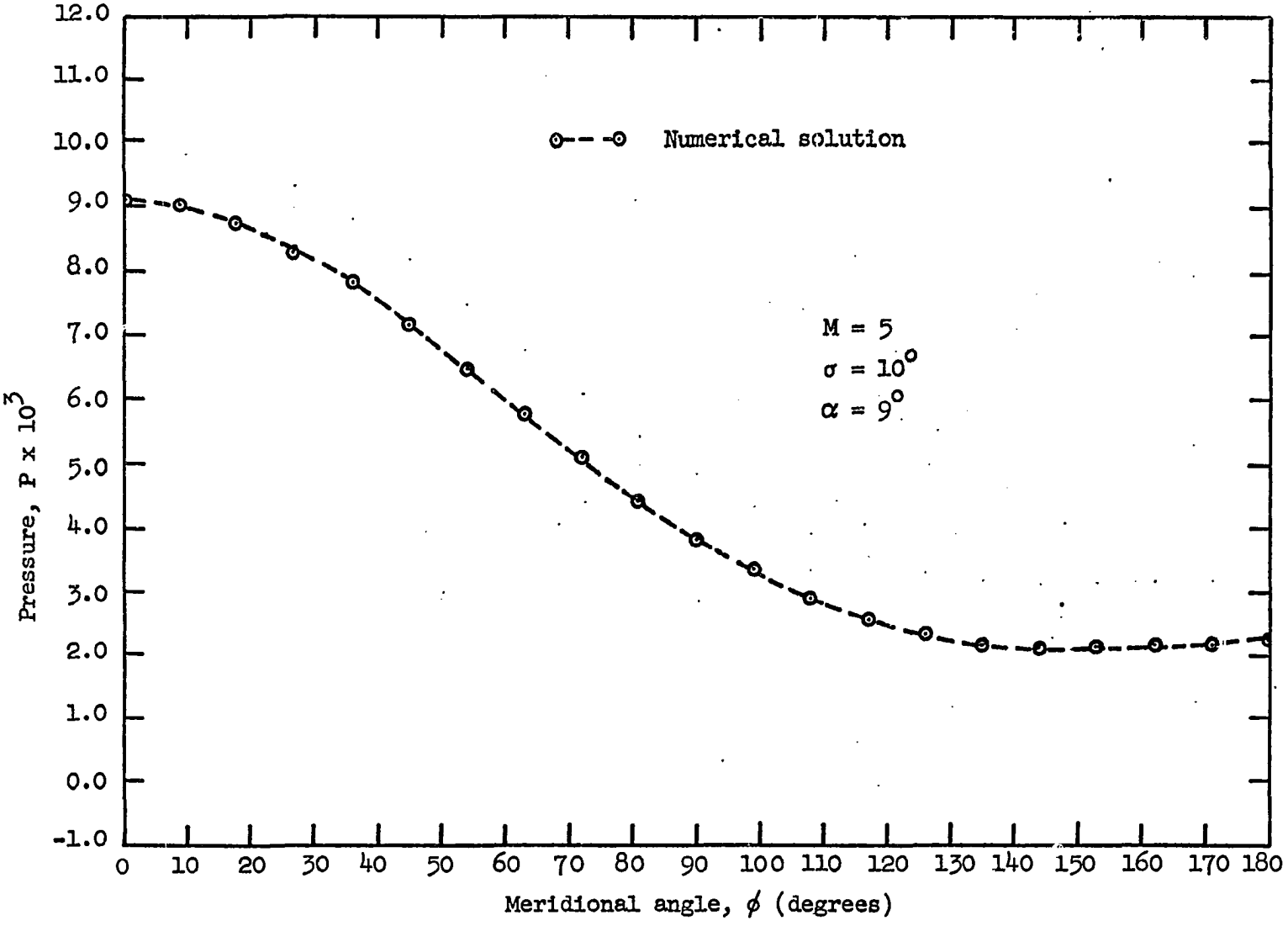

Figure 44. Pressure distribution around body

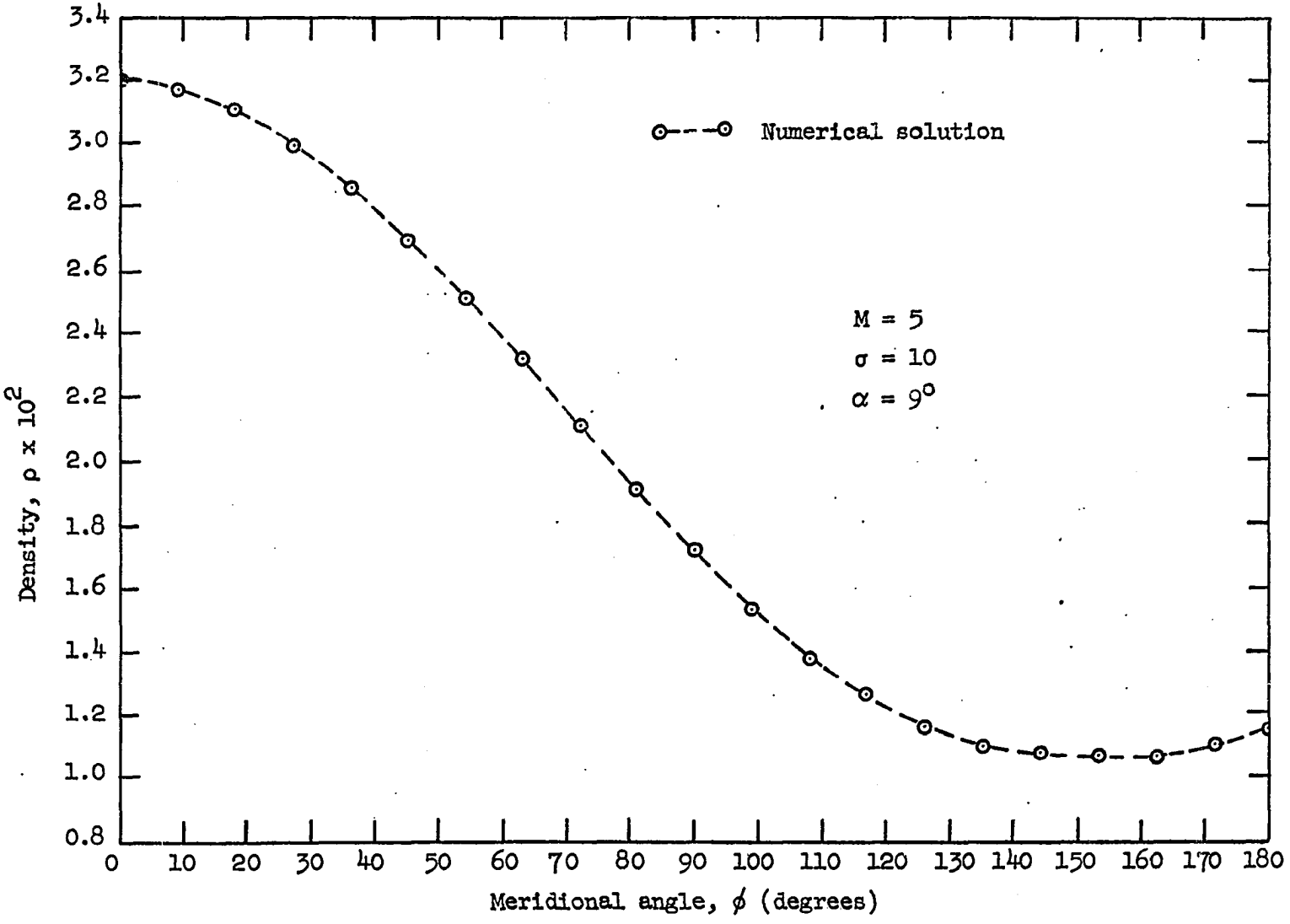

Figure 45. Density distribution around body

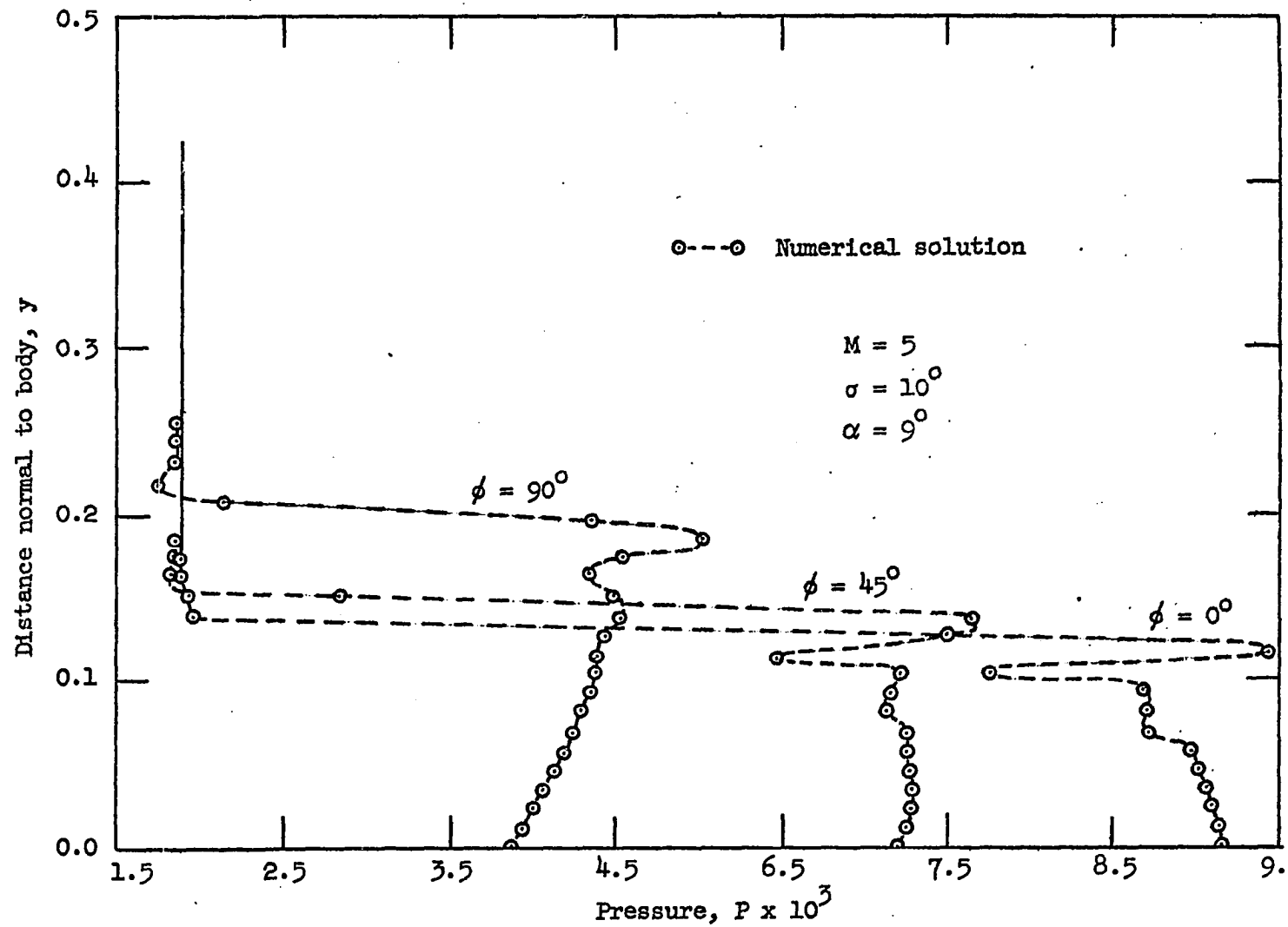

Figure 46. Pressure distribution normal to body (parameter-meridional angle)

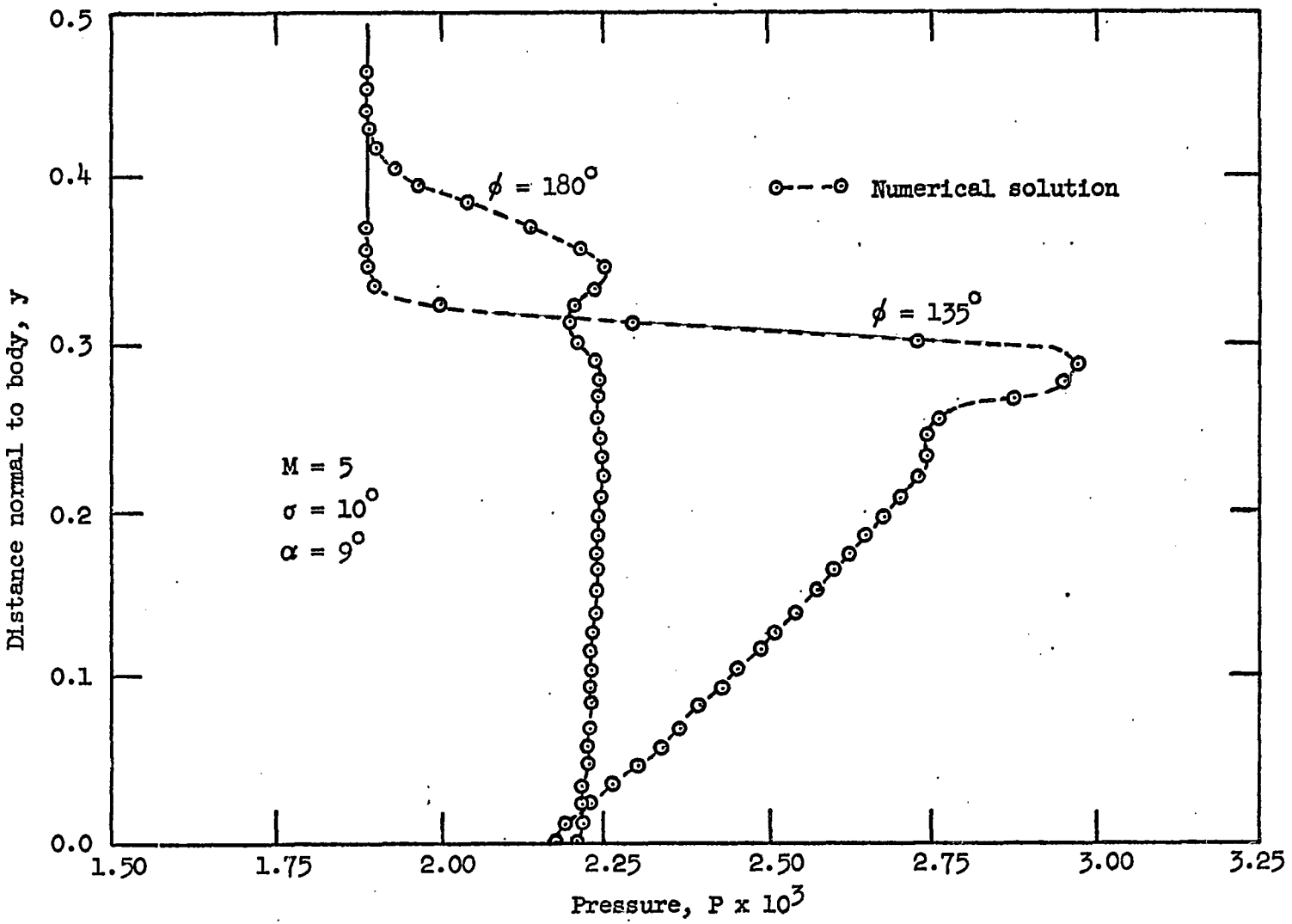

Figure 47. Pressure distribution normal to body (parameter-meridional angle)

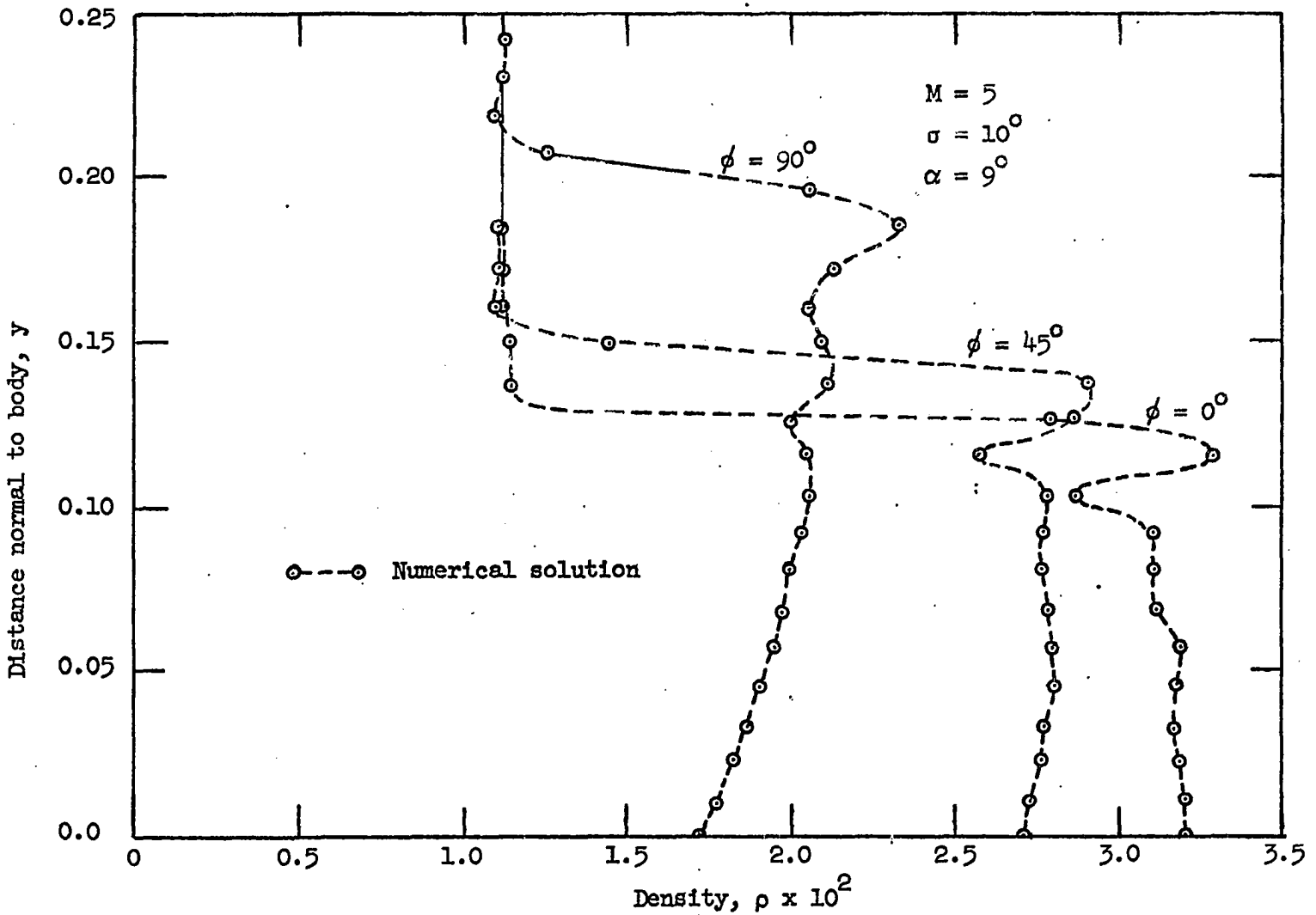

Figure 48. Density distribution normal to body (parameter-meridional angle)

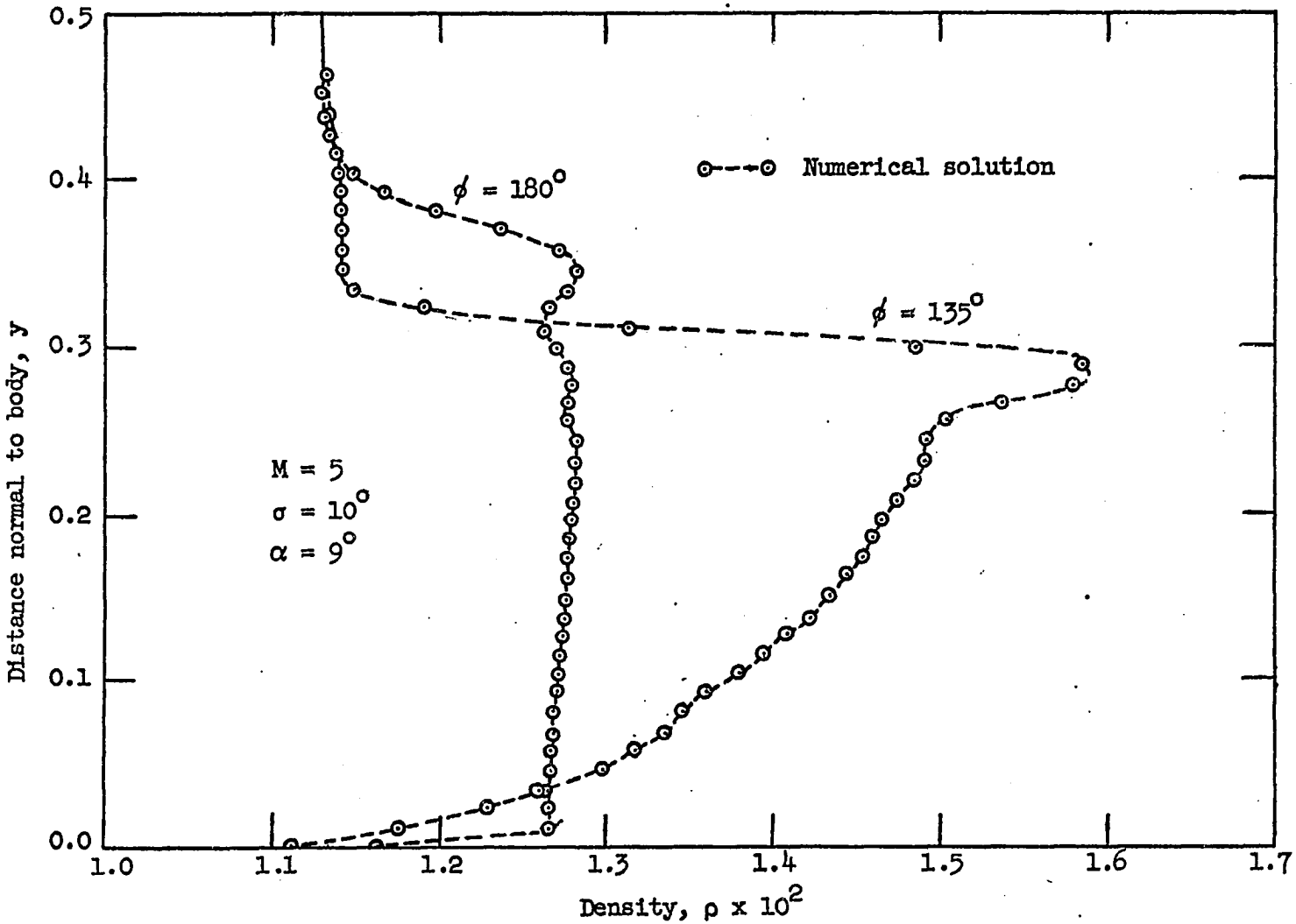

Figure 49. Density distribution normal to body (parameter-meridional angle)

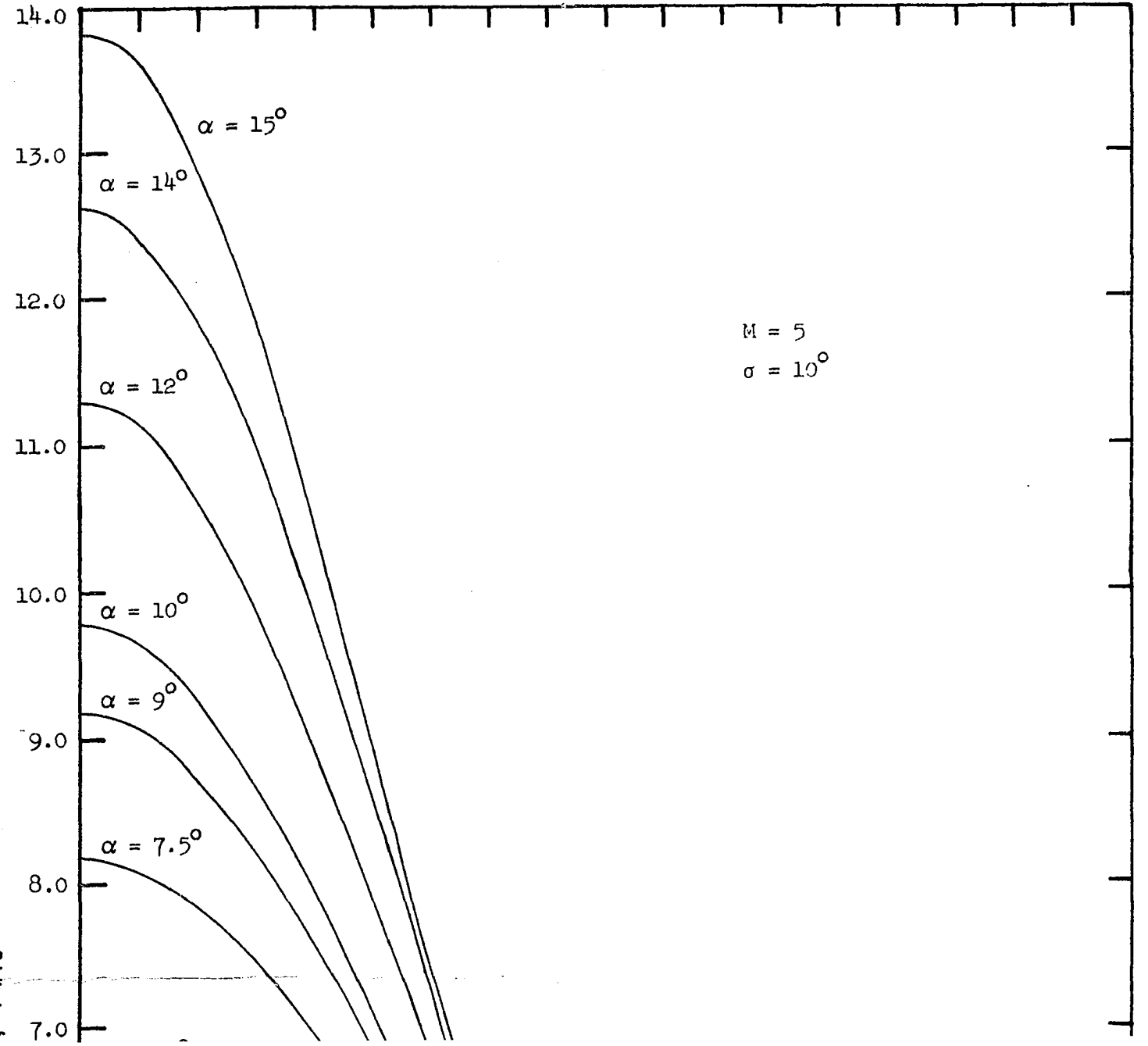
14.0
13.0
12.0
11.0
10.0
9.0
8.0
7.0
P x 10³
α = 15°
α = 14°
α = 12°
α = 10°
α = 9°
α = 7.5°
M = 5
σ = 10°

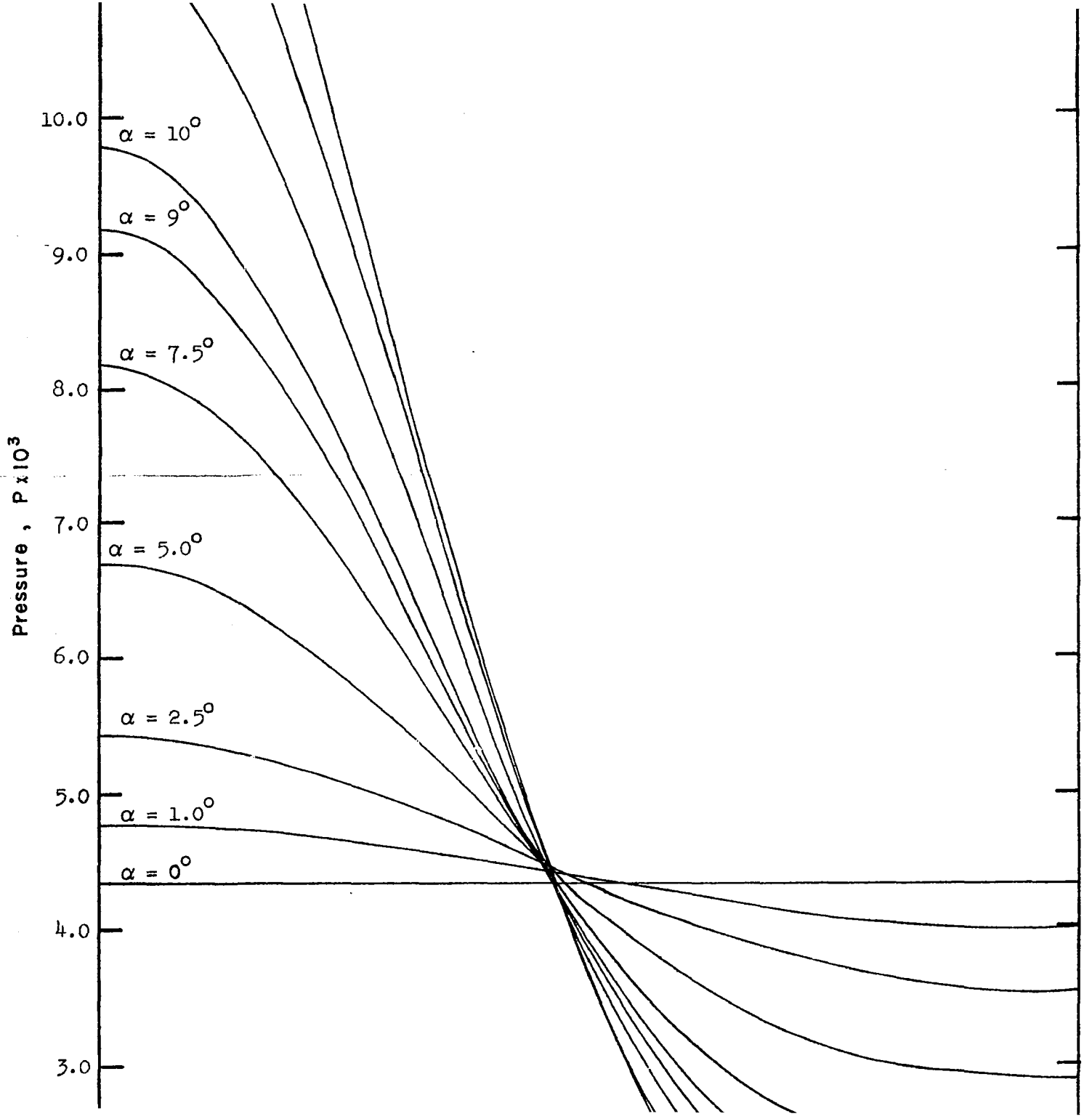
Pressure , P x 10³
10.0
9.0
8.0
7.0
6.0
5.0
4.0
3.0
α = 10°
α = 9°
α = 7.5°
α = 5.0°
α = 2.5°
α = 1.0°
α = 0°

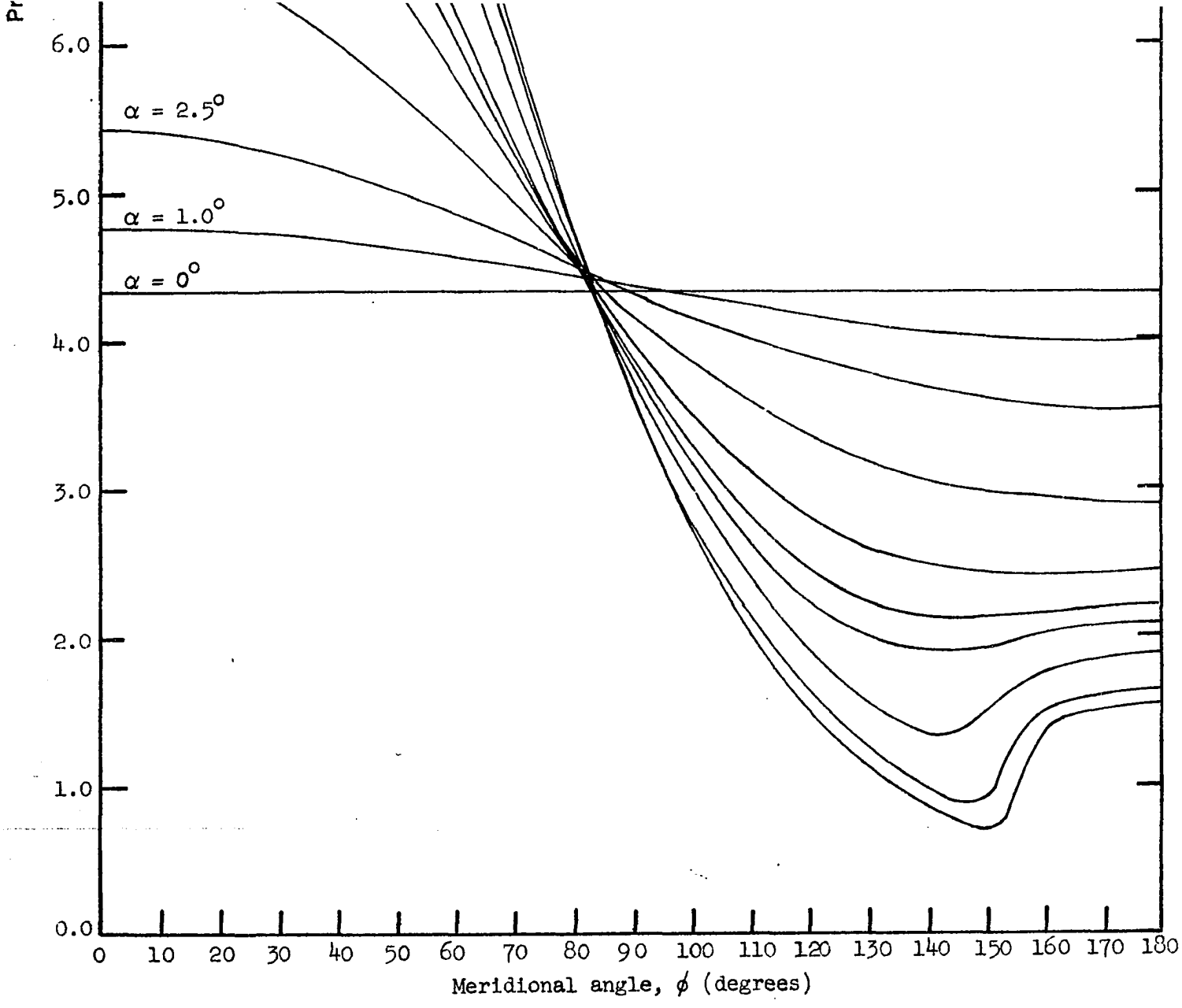

Figure 50. Pressure distribution around body (parameter-angle of attack)

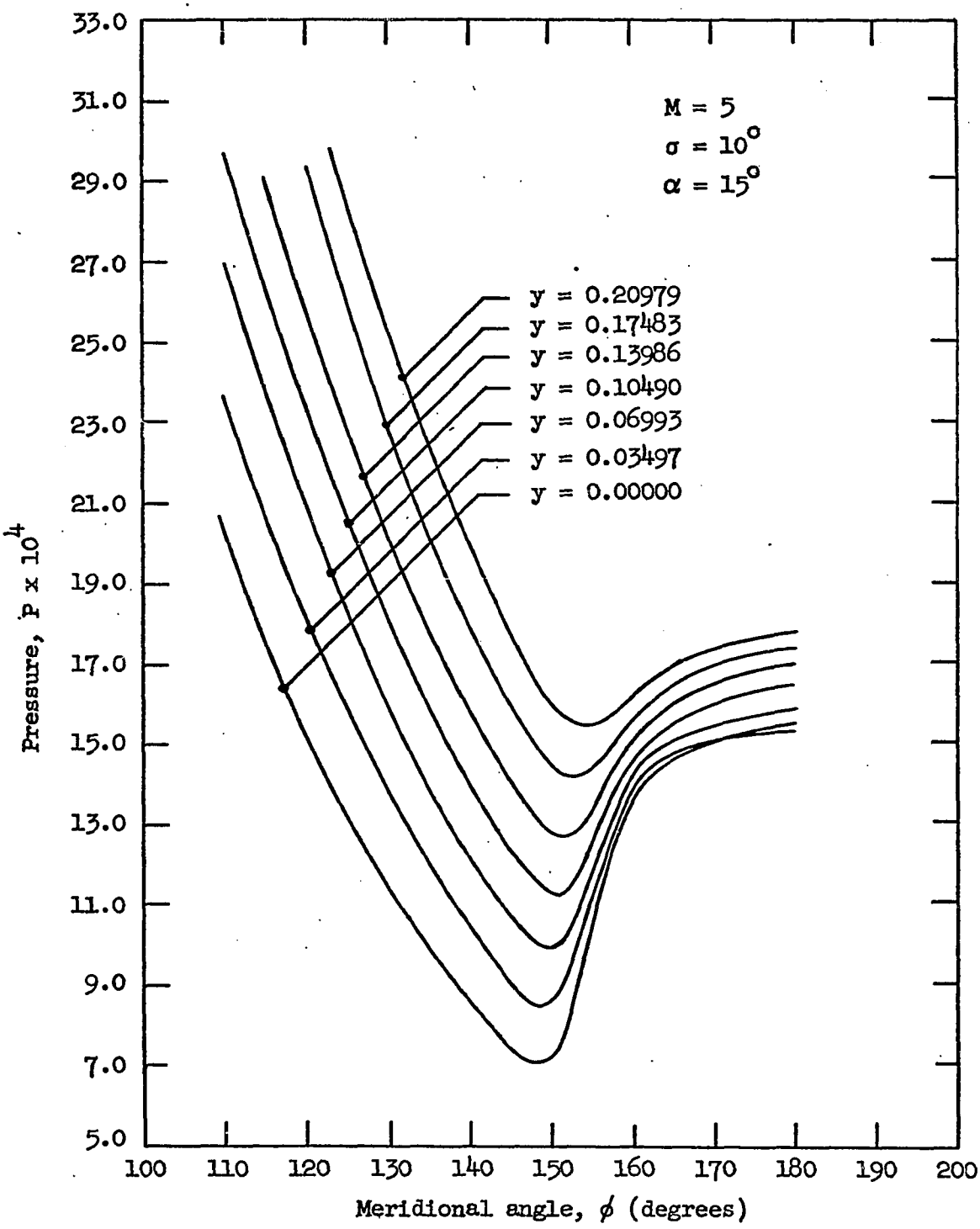

Figure 51. Pressure distribution surrounding embedded shock region (parameter-distance normal to body)

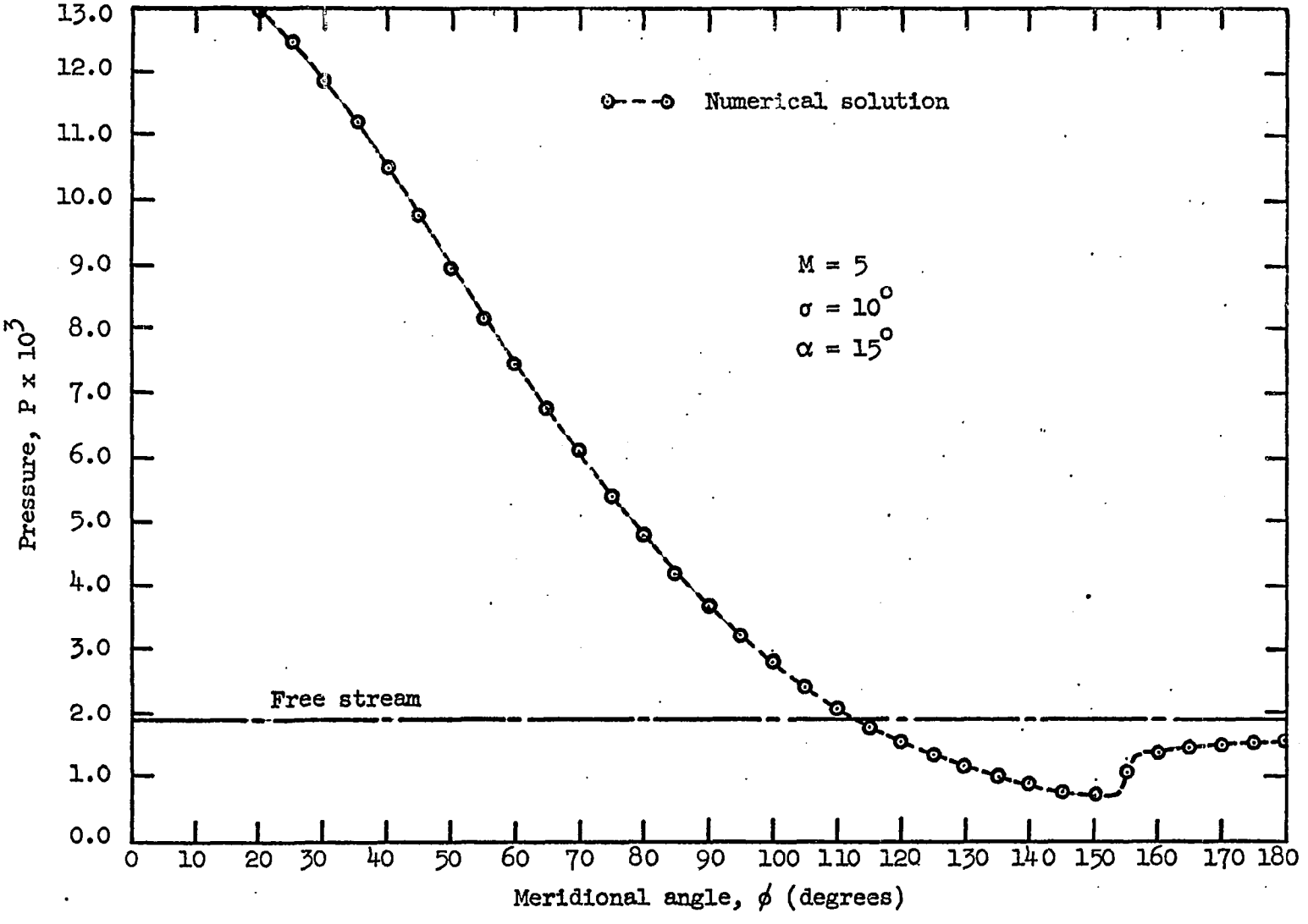

Figure 52. Pressure distribution around body

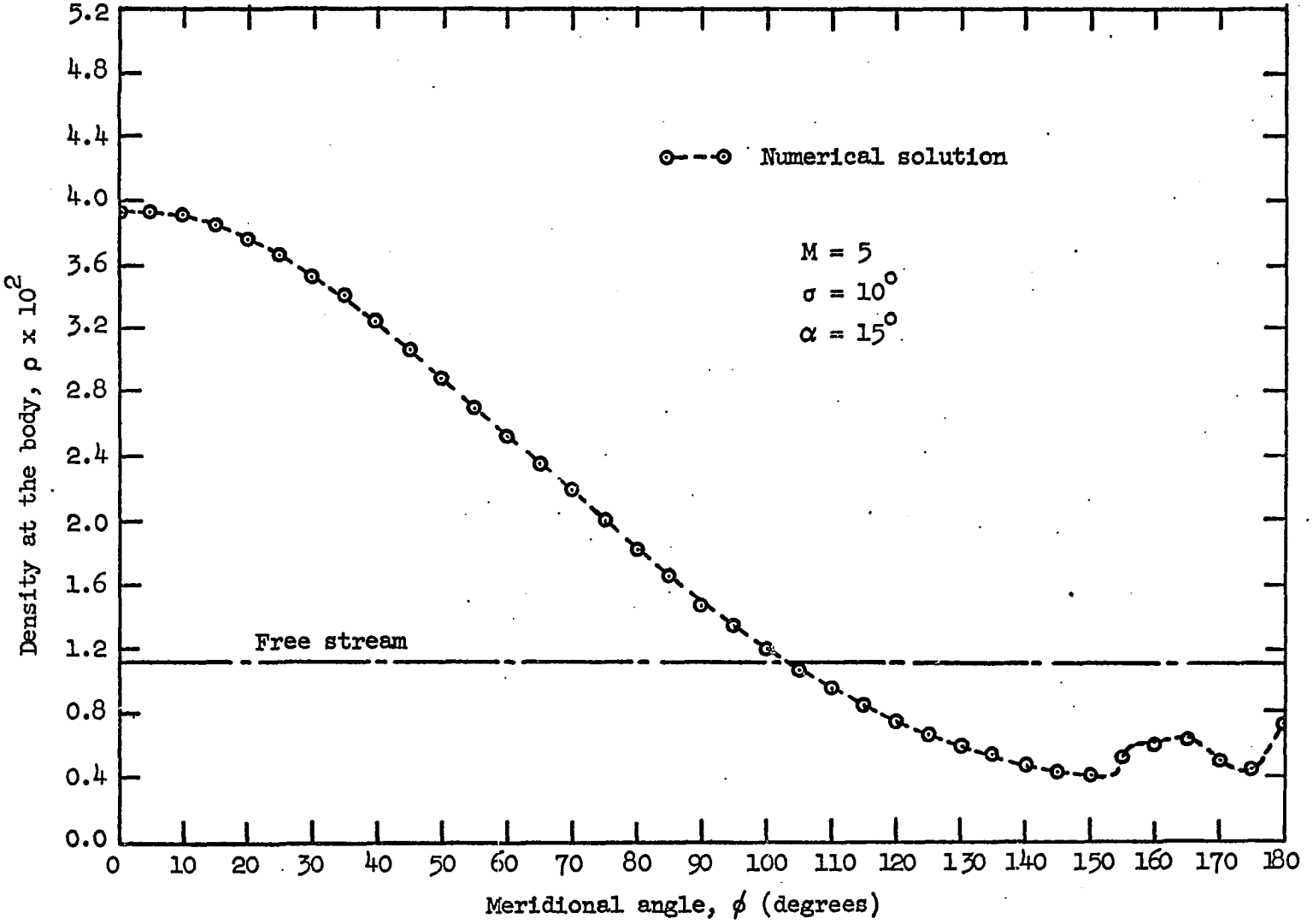

Figure 53. Density distribution around the body

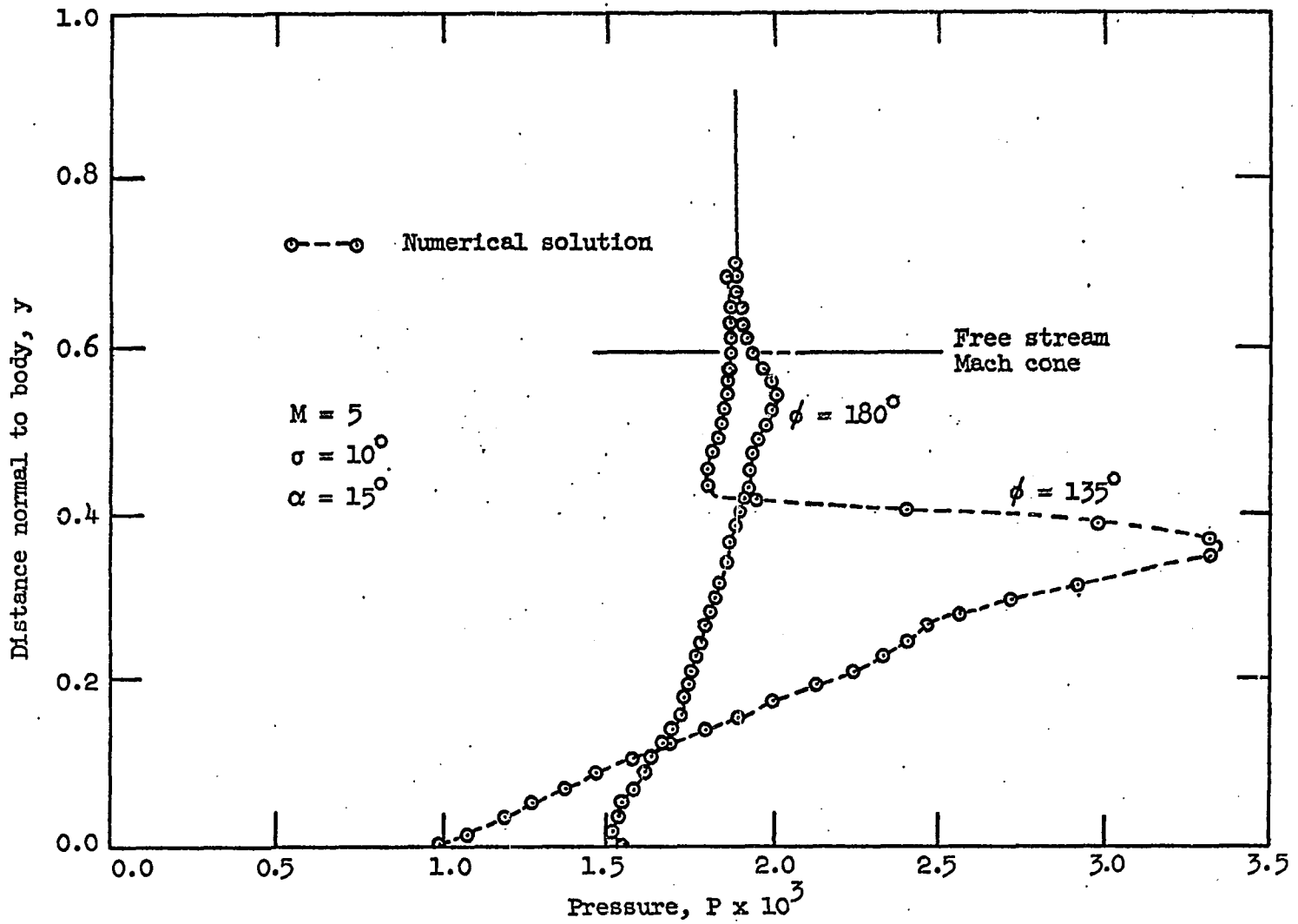

Figure 54. Pressure distribution normal to body (parameter-meridional angle)

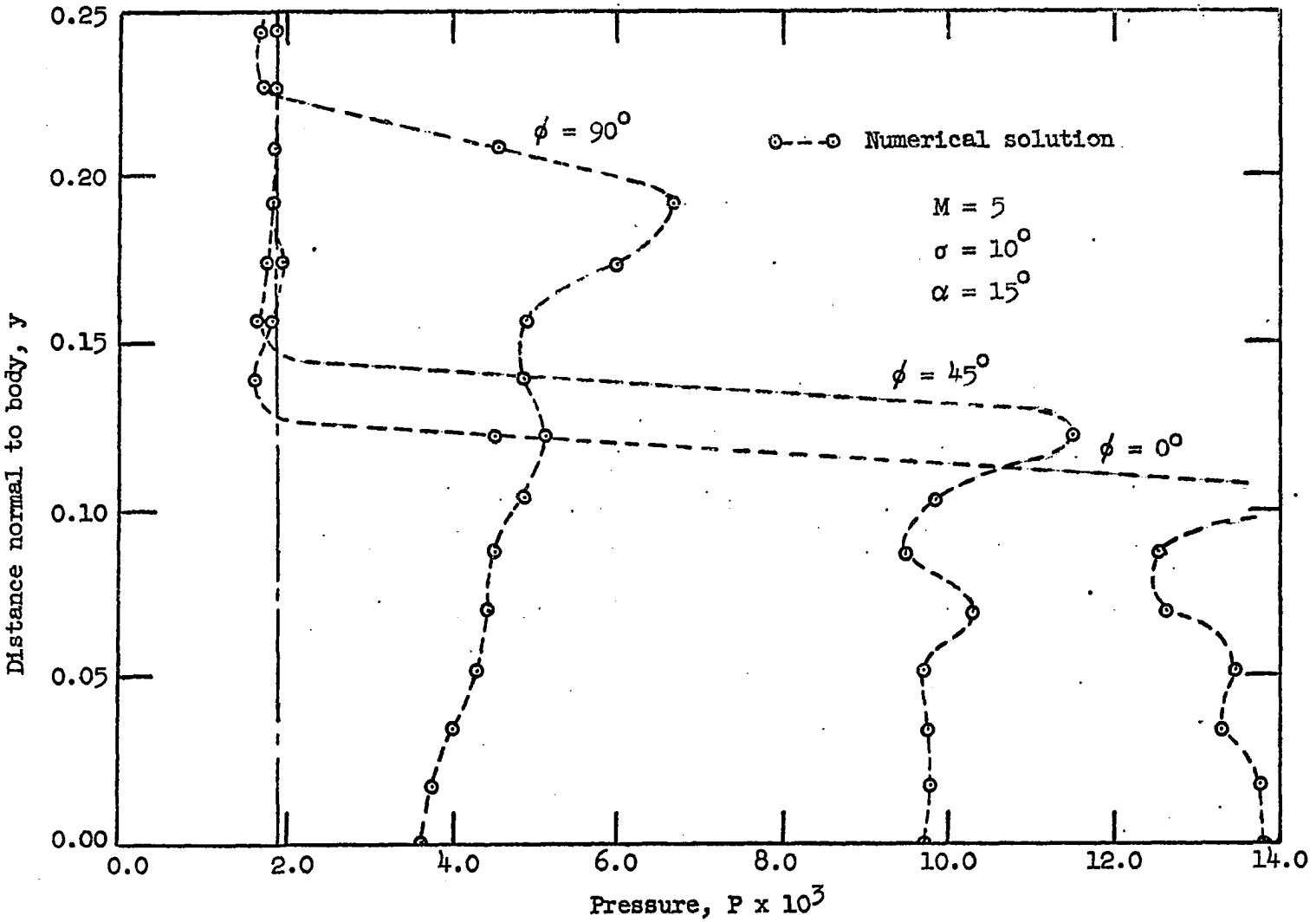

Figure 55. Pressure distribution normal to body (parameter-meridional angle)

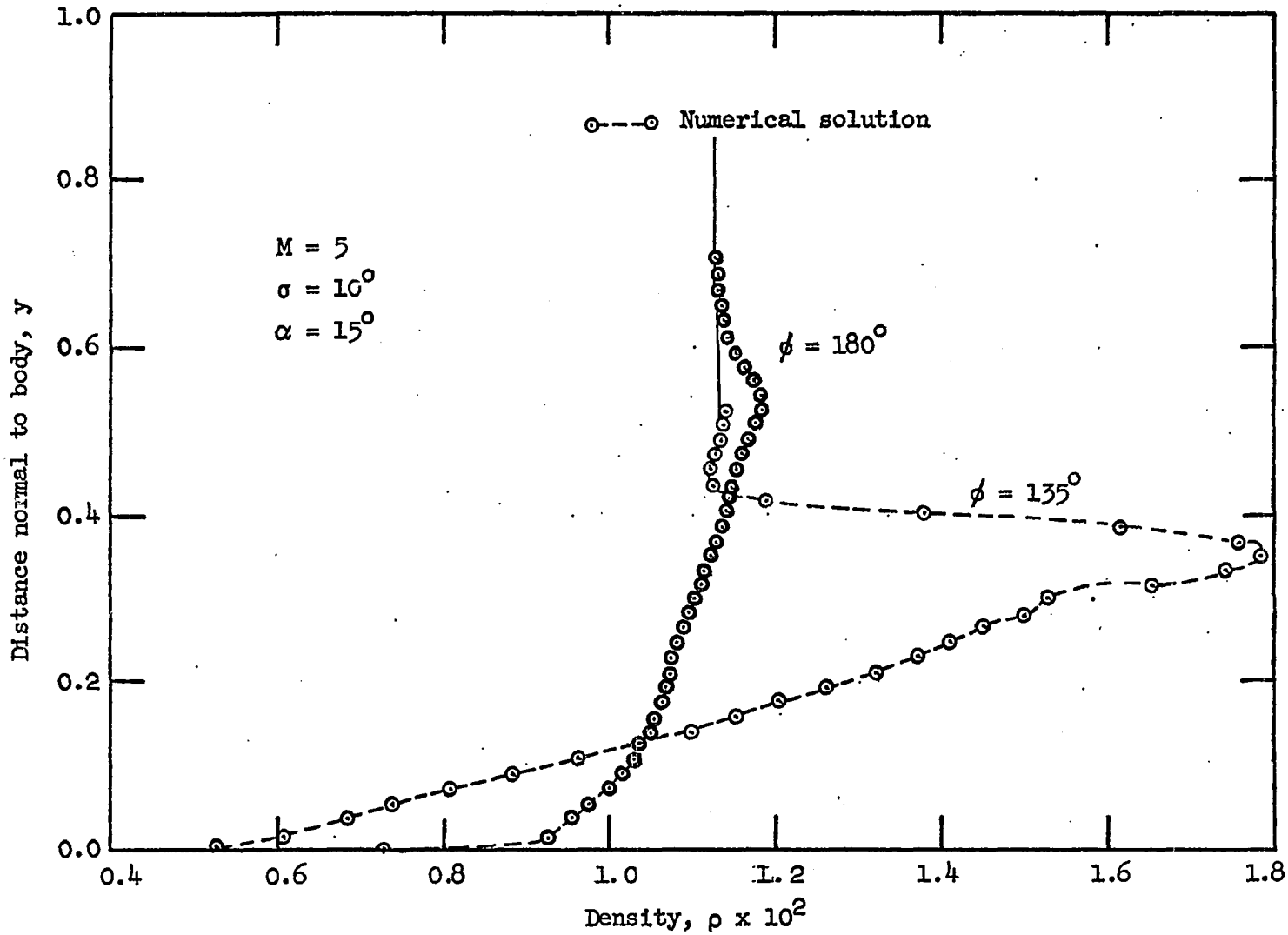

Figure 56. Density distribution normal to body (parameter-meridional angle)

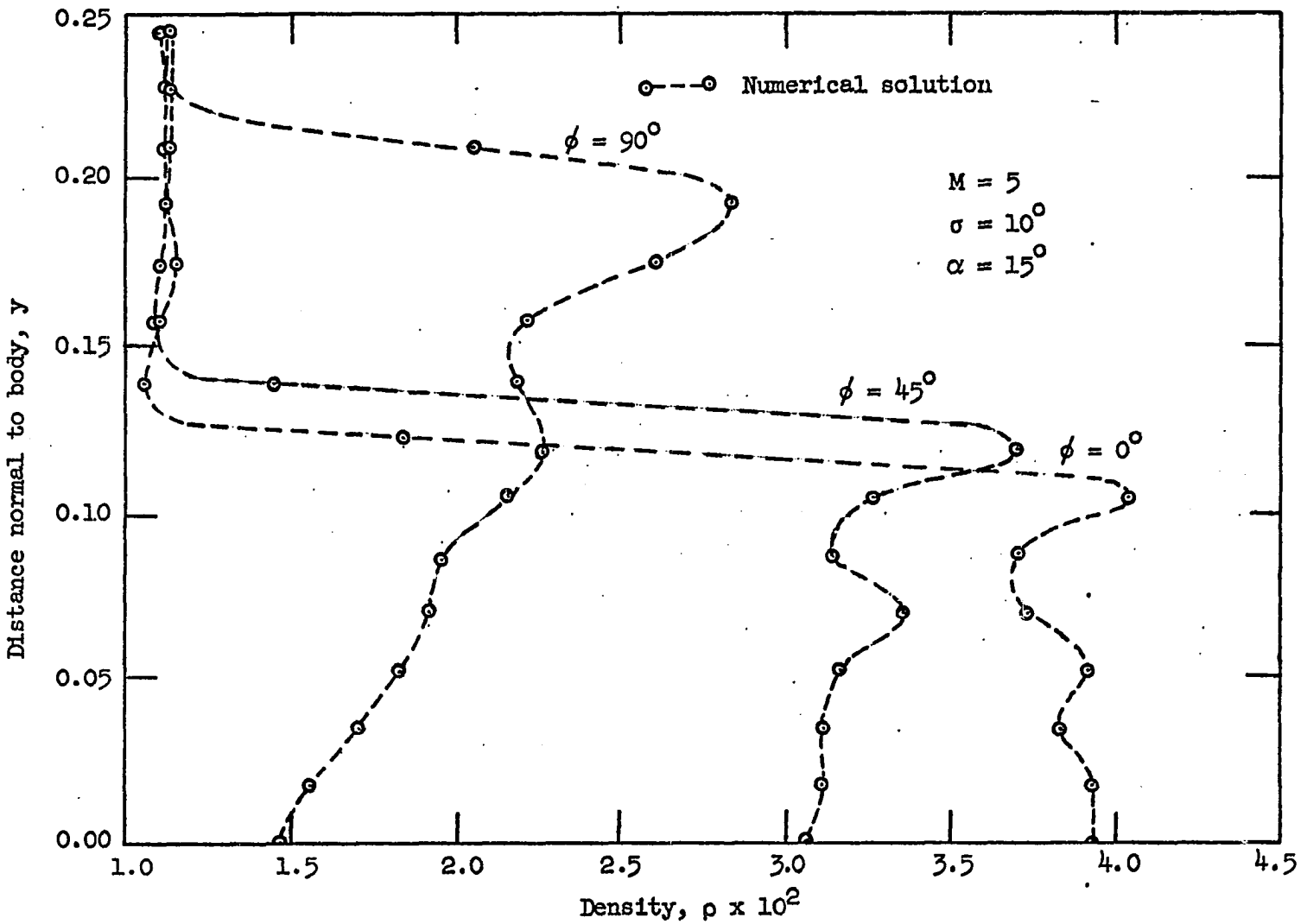

Figure 57. Density distribution normal to body (parameter-meridional angle)

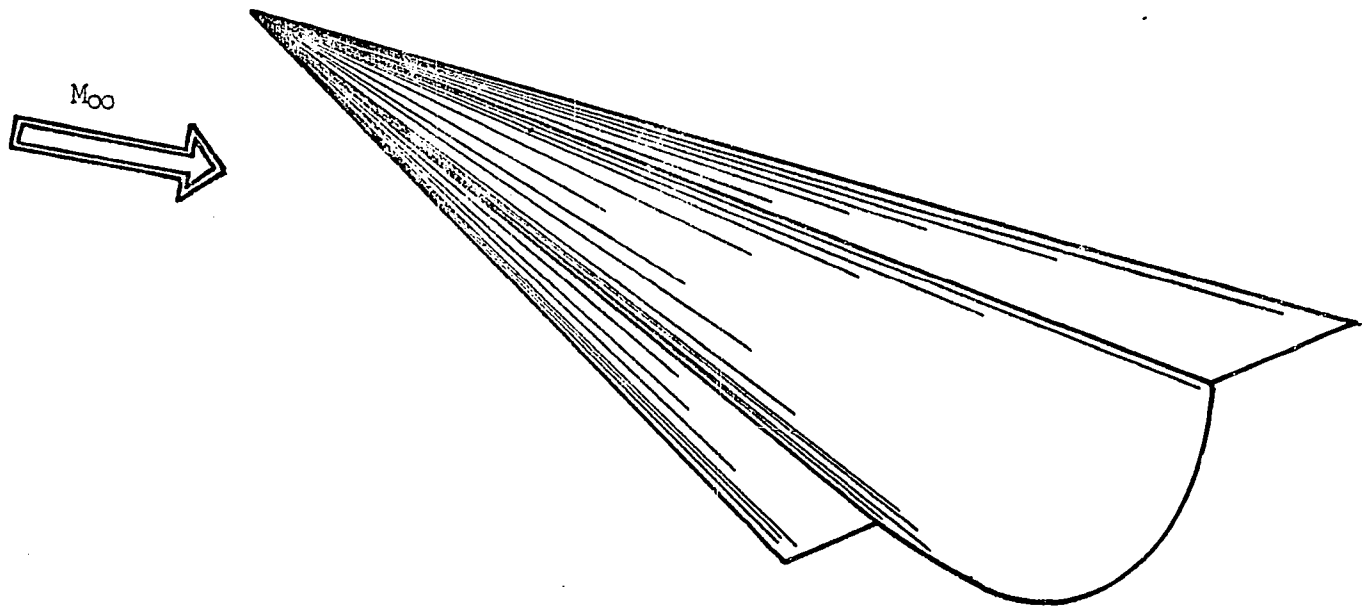

Figure 58. Flat-top or conical wing-body combination

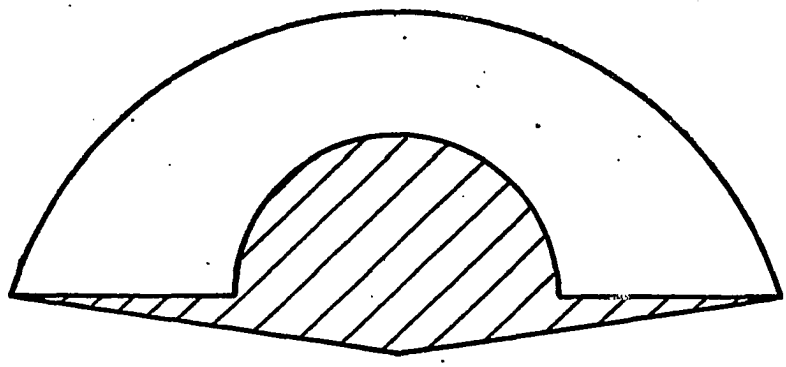

Figure 59. Single shock pattern for conical wing-body combination

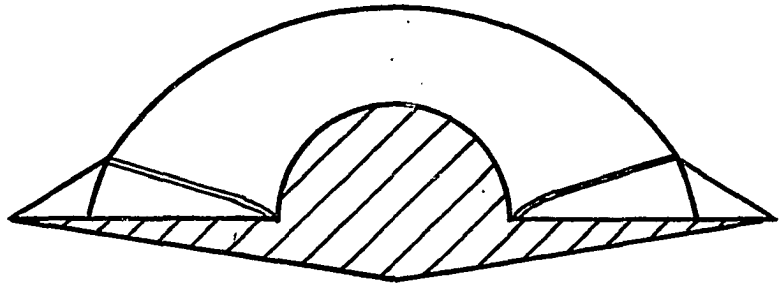

Figure 60. Double shock pattern for conical wing-body combination

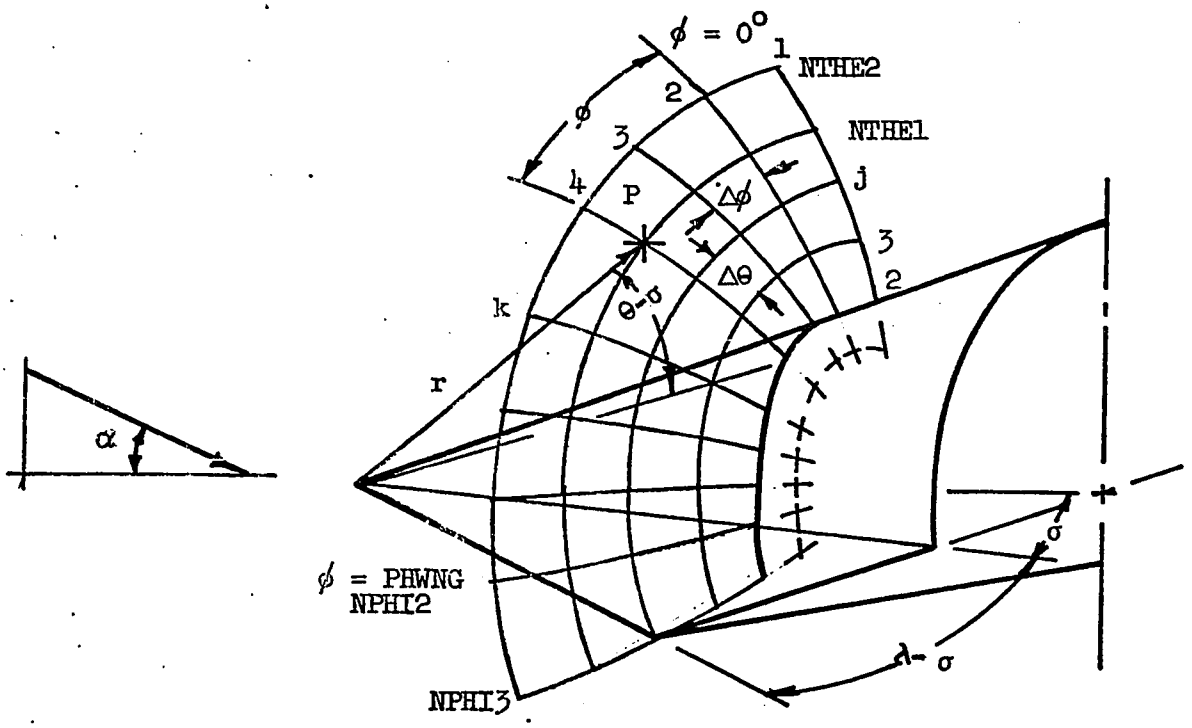

Figure 61. Mesh description for conical wing-body combination

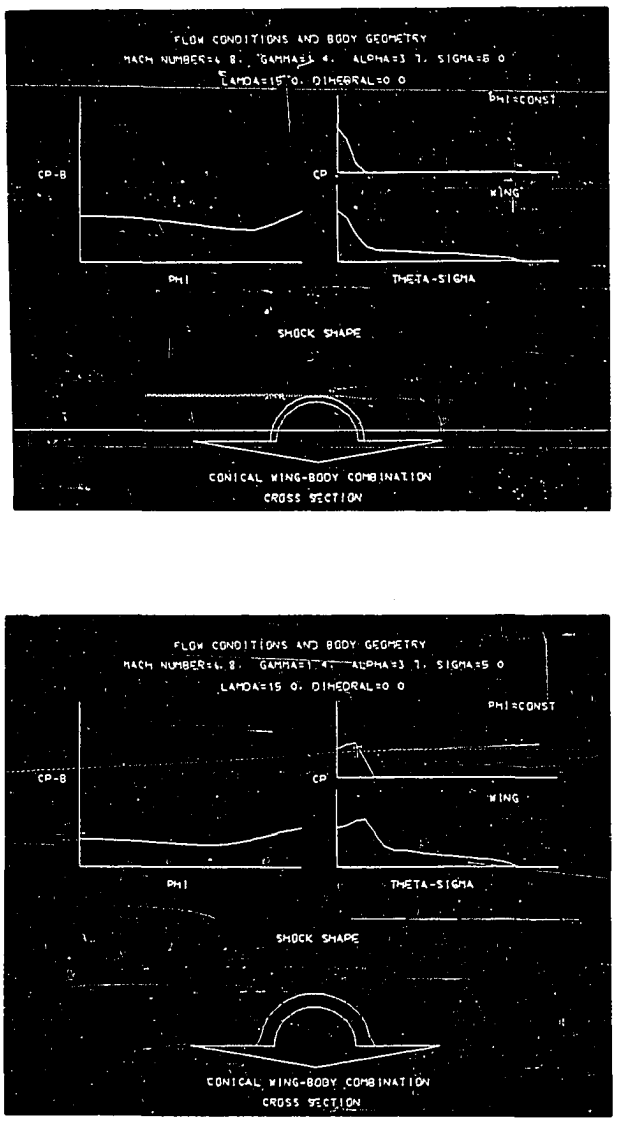

Figure 62. Development of flow field about a conical wing-body combination

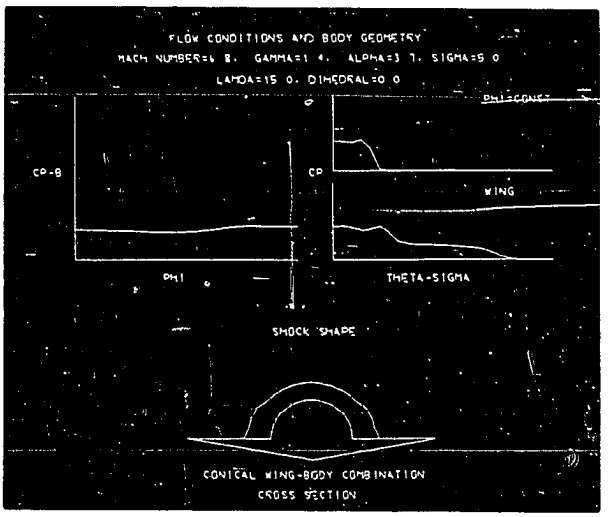

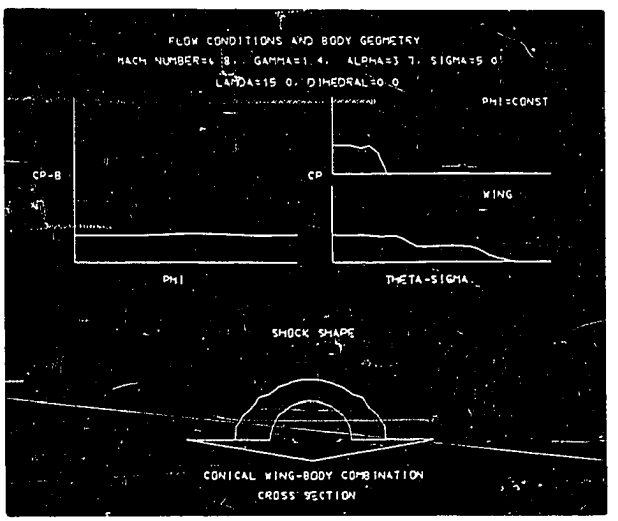

Figure 62. Continued

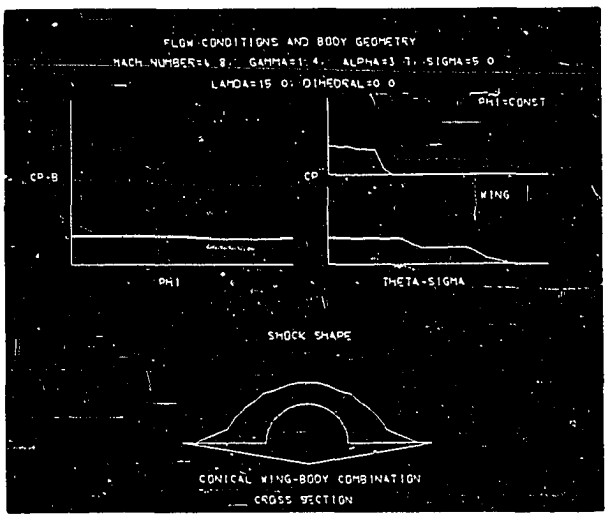

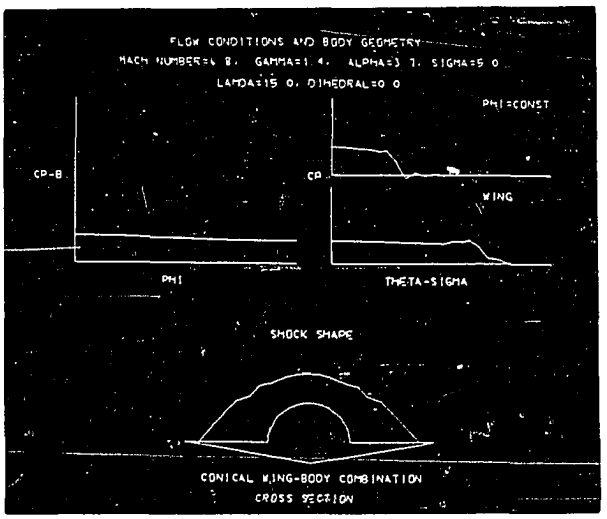

Figure 62. Concluded

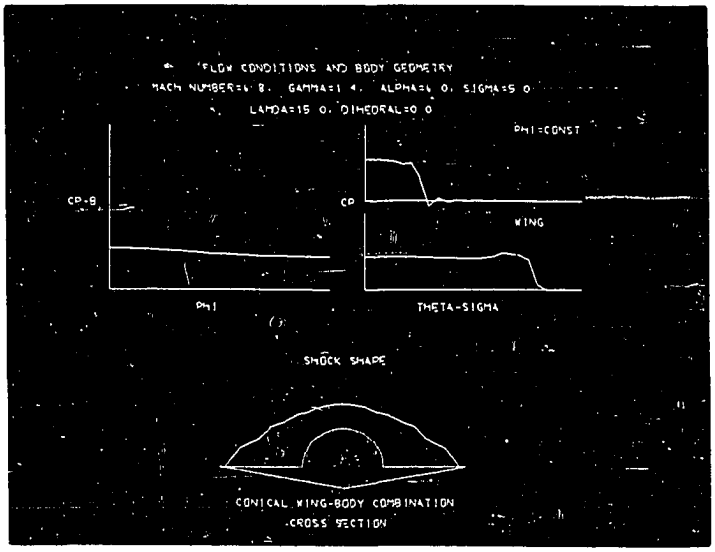

Figure 63. Converged solution of flow field over conical wing-body combination

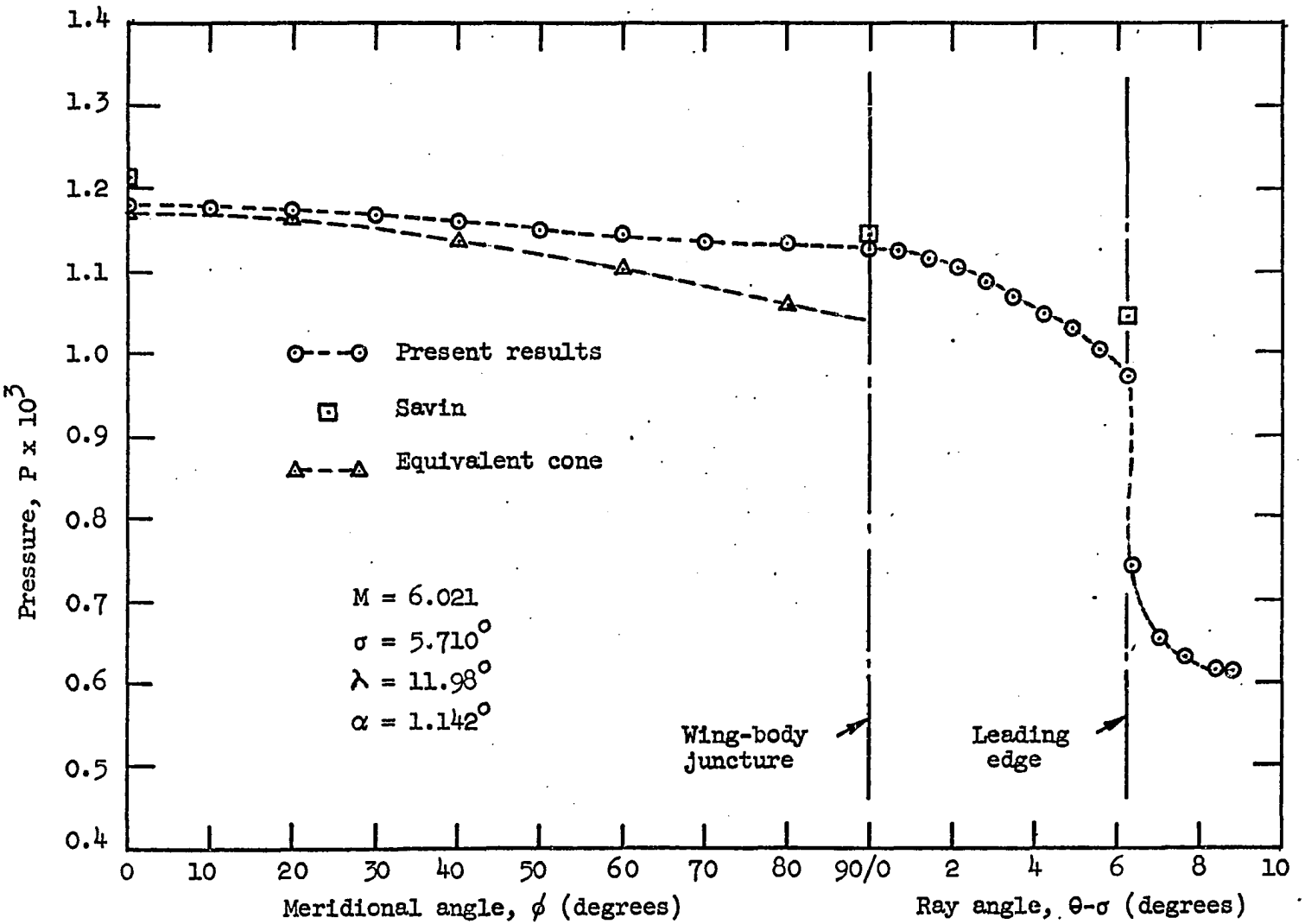

Figure 64. Surface pressure distribution for conical wing-body combination.

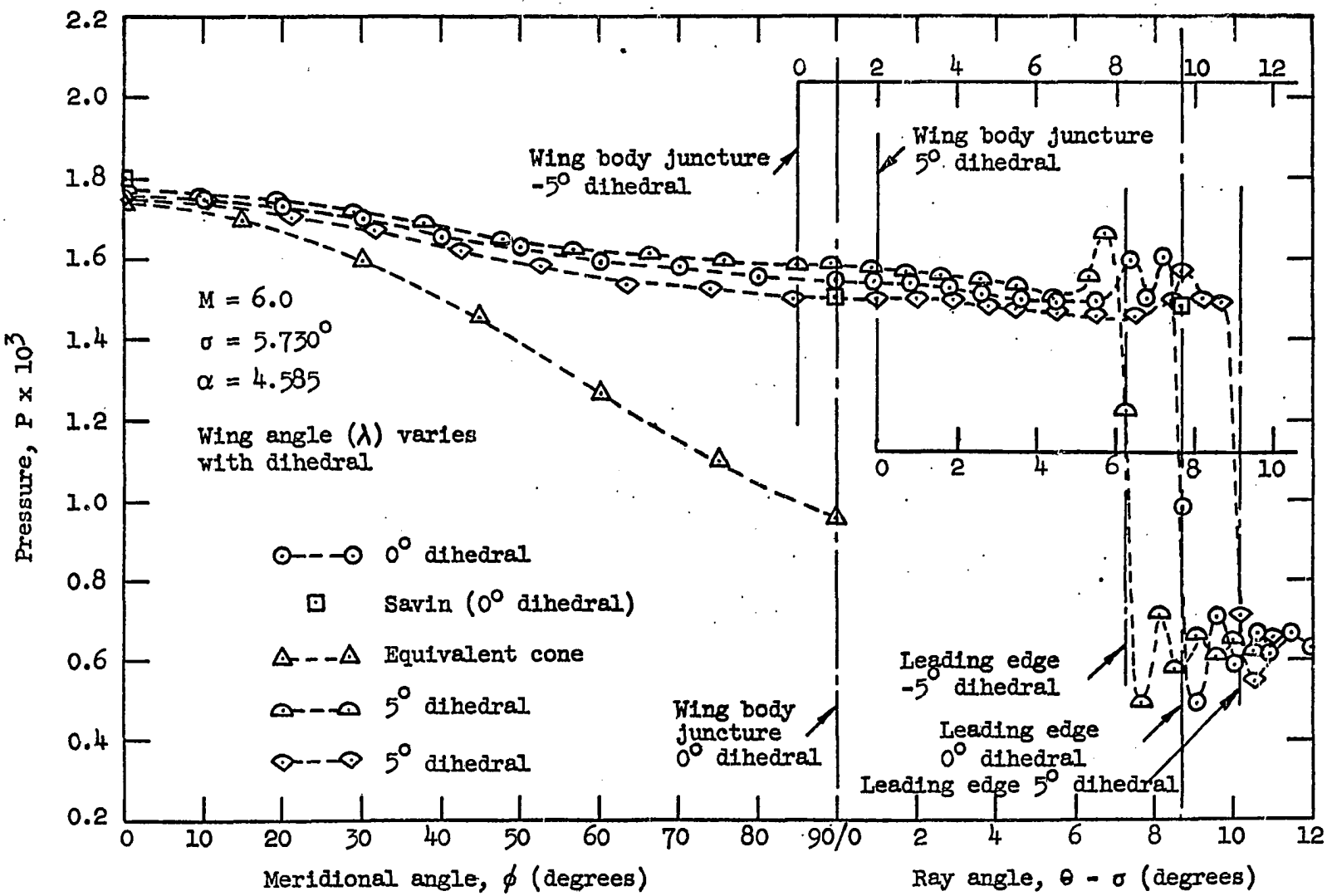

Figure 65. Surface pressure distribution for conical wing-body combination

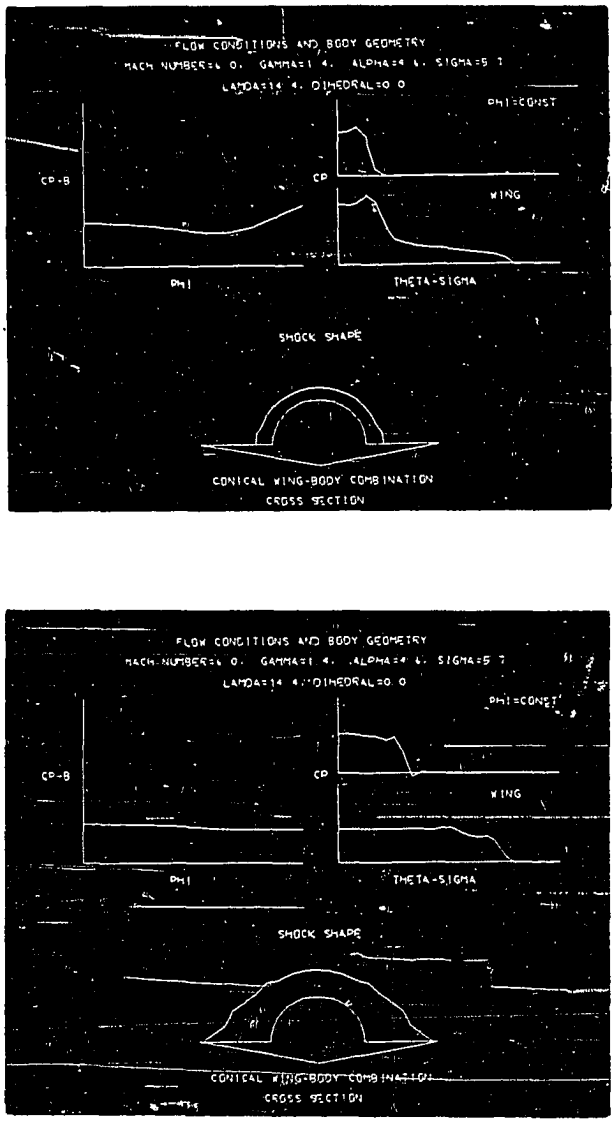

Figure 66. Development of flow field about a conical wing-body combination

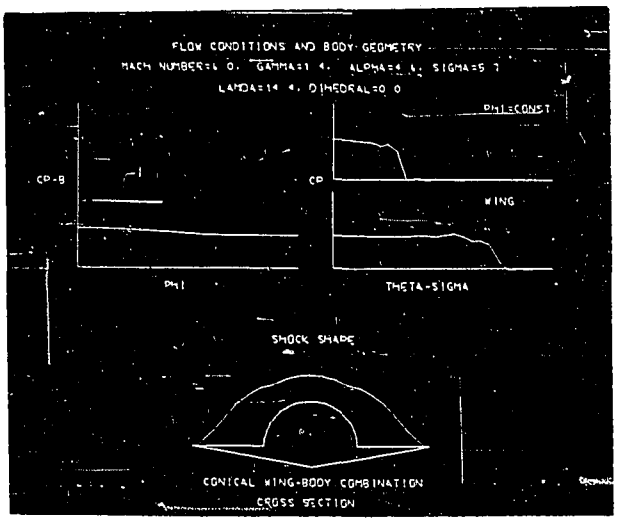

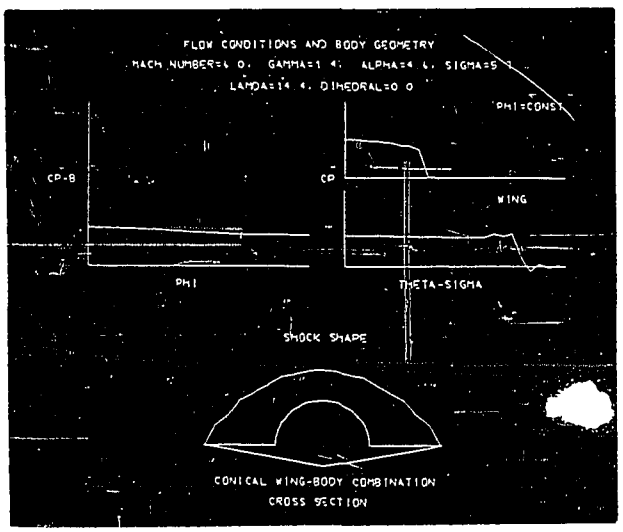

Figure 66. Concluded

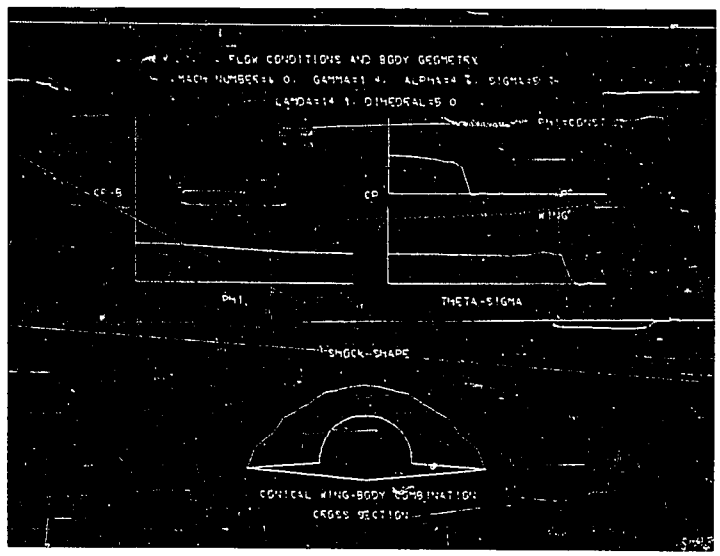

Figure 67. Converged solution of flow field over conical wing-body combination

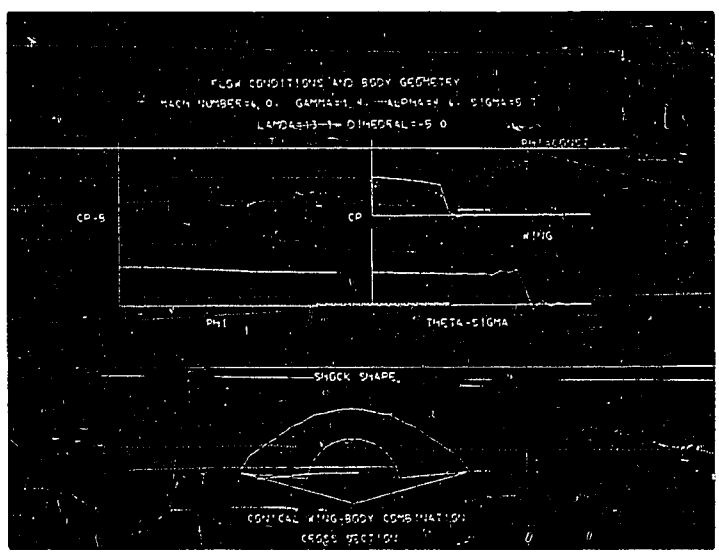

Figure 68. Converged solution of flow field over conical wing-body combination

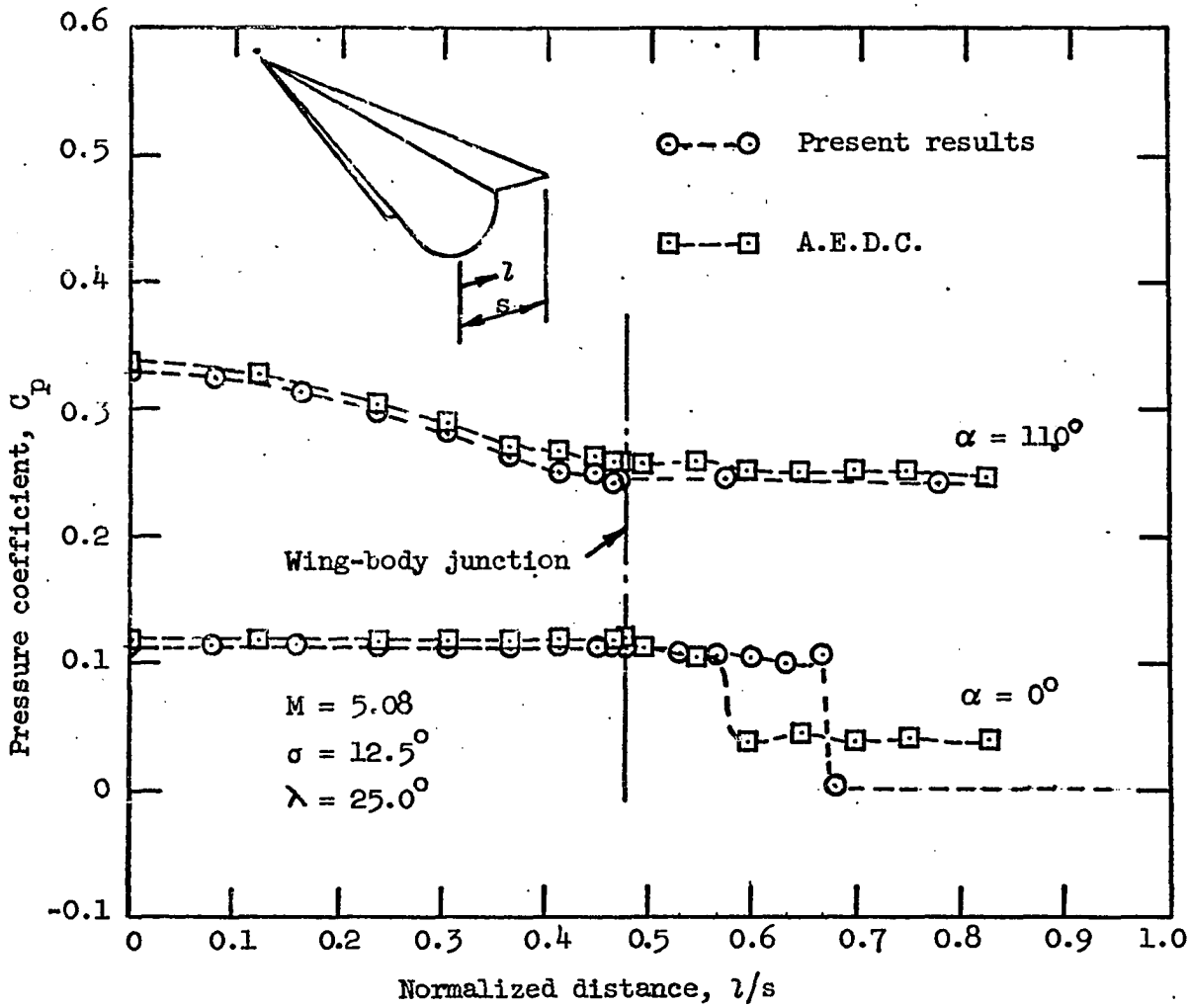

Figure 69. Surface pressure distributions for conical wing-body combination

APPENDIX A

Matrix of Coefficients for Various Difference Schemes

Listed below are the coefficient matrices which describe the numerical differencing schemes used in the solution of the modified Berger's equation and the flow field about a supersonic wedge.

Lax; $q = 1$

$$a_{l,m} = \frac{1}{100}\begin{vmatrix} 50 & 0 & 50 \\ -50 & 0 & 50 \\ 0 & 0 & 0 \\ 0 & 0 & 0 \\ 0 & 0 & 0 \\ 0 & 0 & 0 \end{vmatrix}$$

Burstein; $q = \frac{1}{2}$

$$a_{l,m} = \frac{1}{100}\begin{vmatrix} 0 & 50 & 50 \\ 0 & -100 & 100 \\ 0 & 100 & 0 \\ 0 & 0 & 0 \\ -50 & 50 & 0 \\ -25 & 0 & 25 \end{vmatrix}$$

Richtmyer $(t + \Delta t)$; $q = \frac{1}{2}$

$$a_{l,m} = \frac{1}{100}\begin{vmatrix} 0 & 0 & 0 \\ 0 & -50 & 50 \\ 0 & 100 & 0 \\ 0 & 0 & 0 \\ -100 & 100 & 0 \\ 0 & 0 & 0 \end{vmatrix}$$

Richtmyer $(t + 2\Delta t)$; $q = 1$

$$a_{l,m} = \frac{1}{100}\begin{vmatrix} 50 & 0 & 50 \\ -50 & 0 & 50 \\ 0 & 100 & 0 \\ 0 & 0 & 0 \\ -100 & 0 & 100 \\ 0 & 0 & 0 \end{vmatrix}$$

MacCormack (A); q = 1

$$a_{l,m} = \frac{1}{100}\begin{vmatrix} 0 & 100 & 0 \\ 0 & -100 & 100 \\ 0 & 50 & 0 \\ 0 & 50 & 0 \\ -50 & 50 & 0 \\ 0 & 0 & 0 \end{vmatrix}$$

MacCormack (B); q = 1

$$a_{l,m} = \frac{1}{100}\begin{vmatrix} 0 & 100 & 0 \\ -100 & 100 & 0 \\ 0 & 50 & 0 \\ 0 & 50 & 0 \\ 0 & -50 & 50 \\ 0 & 0 & 0 \end{vmatrix}$$

Lax-Wendroff (A); q = 1

$$a_{l,m} = \frac{1}{100}\begin{vmatrix} 0 & 100 & 0 \\ 0 & -100 & 100 \\ 0 & 100 & 0 \\ 0 & 0 & 0 \\ -50 & 50 & 0 \\ 0 & -50 & 50 \end{vmatrix}$$

Lax-Wendroff (B); q = 1

$$a_{l,m} = \frac{1}{100}\begin{vmatrix} 0 & 100 & 0 \\ -100 & 100 & 0 \\ 0 & 100 & 0 \\ 0 & 0 & 0 \\ 0 & -50 & 50 \\ -50 & 50 & 0 \end{vmatrix}$$

Lax-Wendroff (C); q = 1

$$a_{l,m} = \frac{1}{100}\begin{vmatrix} 0 & 100 & 0 \\ 0 & 50 & -50 \\ 0 & 100 & 0 \\ 0 & 0 & 0 \\ 100 & -100 & 0 \\ -150 & 100 & 50 \end{vmatrix}$$

Lax-Wendroff (D); q = 1

$$a_{l,m} = \frac{1}{100}\begin{vmatrix} 0 & 0 & 0 \\ 50 & -50 & 0 \\ 0 & 100 & 0 \\ 0 & 0 & 0 \\ 0 & 100 & -100 \\ -50 & -100 & 150 \end{vmatrix}$$

Fromm (B); q = 1

$$a_{1,m} = \frac{1}{100} \begin{vmatrix} 25 & 50 & 25 \\ 25 & 0 & -25 \\ 0 & 100 & 0 \\ 0 & 0 & 0 \\ 100 & -100 & 0 \\ -150 & 100 & 50 \end{vmatrix}$$

APPENDIX B

Supersonic Wedge Flow Computer Program

The computer program used in the solution of the supersonic wedge flow problem consisted of a main program and three supporting subroutines. In order to display pertinent results on the IBM 2250 display tube numerous system subroutines are used. These are not described herein.

Table 8 below lists the main program and its subroutines and describes each of their functions in the solution of this problem.

Table 8. Resume of computer program

Name of Subroutine	Function
Main Program	Allows for input of all constants governing numerical solution of problem through alphanumeric keyboard on IBM 2250; calls INITA; prints input data and initial values of the flow variables at each mesh point; calls BNDRY; calls IOCON; integrates generalized difference equation from x = 1 to x = 2 and then performs stepback procedure; displays numerical solution of the pressure distribution and approximate location of shock wave; trips motion picture camera if this option is desired; prints converged values of flow variables at all mesh points.
INITA	Initializes values of the flow variables for each mesh point; determines direction and plots arrow indicating free-stream velocity vector; plots body shape with cross-hatching; determines and plots exact pressure distribution and shock shape.
IOCON(N)	N = 0 - solves for flow variables from conservative variables; N = 1 - arranged flow variables in conservative form.

Table 8 (Continued)

Name of Subroutine	Function
BNDRY(N)	N = 0 - sets values of flow variables at body equal to the values and mesh point above body; N = 1 - sets the normal component of velocity at the body equal to zero.

APPENDIX C

Determination of Eigenvalues

When using the stability analysis based on amplification matrix theory, it is necessary to determine the eigenvalues of the coefficient matrices of the gas-dynamic equations. These eigenvalues are not dependent upon the choice of coordinate system. Therefore, for a general coordinate system (ξ,η,ζ) the steady flow equations can be written in the following form

$$A\frac{\partial U}{\partial \xi} + B\frac{\partial U}{\partial \eta} + C\frac{\partial U}{\partial \zeta} + D = 0 \tag{C1}$$

where A, B, and C are square matrices

$$A = c_1 \begin{vmatrix} u & 0 & 0 & 1/\rho & 0 \\ 0 & u & 0 & 0 & 0 \\ 0 & 0 & u & 0 & 0 \\ \rho c^2 & 0 & 0 & u & 0 \\ \rho & 0 & 0 & 0 & u \end{vmatrix} \tag{C2}$$

$$B = c_2 \begin{vmatrix} v & 0 & 0 & 0 & 0 \\ 0 & v & 0 & 1/\rho & 0 \\ 0 & 0 & v & 0 & 0 \\ 0 & \rho c^2 & 0 & v & 0 \\ 0 & \rho & 0 & 0 & v \end{vmatrix} \tag{C3}$$

$$C = c_3 \begin{vmatrix} w & 0 & 0 & 0 & 0 \\ 0 & w & 0 & 0 & 0 \\ 0 & 0 & w & 1/\rho & 0 \\ 0 & 0 & \rho c^2 & w & 0 \\ 0 & 0 & \rho & 0 & w \end{vmatrix} \tag{C4}$$

where c_1, c_2, and c_3 are constants and where U and D are column matrices - D being a direct result of the non-Cartesian coordinate system

$$U = \begin{vmatrix} u \\ v \\ w \\ p \\ \rho \end{vmatrix} \tag{C5}$$

In the above system of equations the energy equation is used in the form:

$$\bar{q} \cdot (\nabla P - c^2 \nabla \rho) = 0 \tag{C6}$$

where

$$c^2 = \left(\frac{\partial P}{\partial \rho}\right)_s \tag{C7}$$

The speed of sound, c, can be expressed as a function of the enthalpy by the following procedure. It is well known that

$$Tds = dh - dP/\rho \tag{C8}$$

Assuming enthalpy to be a function of P and ρ or $h = h(P,\rho)$, the following can be written:

$$dh = \left.\frac{\partial h}{\partial P}\right)_{\rho} dP + \left.\frac{\partial h}{\partial \rho}\right)_{P} d\rho \tag{C9}$$

Substituting Equation C9 into Equation C8 and dividing through by $d\rho$ yields:

$$T\frac{dS}{d\rho} = \left.\frac{\partial h}{\partial P}\right)_{\rho} \cdot \frac{dP}{\partial \rho} + \left.\frac{\partial h}{\partial \rho}\right)_{P} - \frac{dP}{\rho d\rho} \tag{C10}$$

Evaluating Equation C10 at constant entropy and solving for $\left.\partial P/\partial \rho\right|_s$ yields:

$$\left.\frac{\partial P}{\partial \rho}\right)_{s} = \frac{\rho \left.\frac{\partial h}{\partial \rho}\right)_{P}}{1 - \rho \left.\frac{\partial h}{\partial P}\right)_{\rho}} \tag{C11}$$

Therefore,

$$c^2 = \frac{\rho \left.\frac{\partial h}{\partial \rho}\right)_{P}}{1 - \rho \left.\frac{\partial h}{\partial P}\right)_{\rho}} \tag{C12}$$

Equation C1 is now multiplied by the matrix A - inverse (A^{-1}) so that the coefficient of $\partial U/\sigma z$ is unity. This results in the following equation:

$$\frac{\partial U}{\partial \xi} + A^{-1}B\frac{\partial U}{\partial \eta} + A^{-1}C\frac{\partial U}{\partial \zeta} + A^{-1}D = 0 \tag{C13}$$

where

$$A^{-1} = \begin{vmatrix} \frac{-u}{c^2-u^2} & 0 & 0 & \frac{1}{\rho(c^2-u^2)} & 0 \\ 0 & 1/u & 0 & 0 & 0 \\ 0 & 0 & 1/u & 0 & 0 \\ \frac{\rho c^2}{c^2-u^2} & 0 & 0 & \frac{-u}{c^2-u^2} & 0 \\ \frac{\rho}{c^2-u^2} & 0 & 0 & \frac{-1}{u(c^2-u^2)} & 1/u \end{vmatrix} \tag{C14}$$

It is now desirous to determine the eigenvalues of the matrices $A^{-1}B$ and $A^{-1}C$. These are the eigenvalues necessary for the stability analysis.

The matrix $A^{-1}B$ is:

$$A^{-1}B = \begin{vmatrix} \frac{-vu}{c^2-u^2} & \frac{c^2}{c^2-u^2} & 0 & \frac{v}{\rho(c^2-u^2)} & 0 \\ 0 & v/u & 0 & \frac{1}{\rho u} & 0 \\ 0 & 0 & v/u & 0 & 0 \\ \frac{\rho v c^2}{c^2-u^2} & -\frac{\rho u c^2}{c^2-u^2} & 0 & \frac{uv}{c^2-u^2} & 0 \\ \frac{\rho v}{c^2-u^2} & -\frac{\rho u}{c^2-u^2} & 0 & \frac{v}{u(c^2-u^2)} & v/u \end{vmatrix} \qquad (C15)$$

By inspection two eigenvalues can be readily found, they being the only nonzero elements in either a column or row. They are identical and equal to v/u. This, therefore, reduces the five-by-five square matrix, $A^{-1}B$, to the following three-by-three matrix:

$$E = \begin{vmatrix} \frac{uv}{u^2-c^2} & \frac{-c^2}{u^2-c^2} & \frac{-v}{(\rho u^2-c^2)} \\ 0 & v/u & 1/\rho u \\ \frac{-\rho v c^2}{u^2-c^2} & \frac{\rho u c^2}{u^2-c^2} & \frac{uv}{u^2-c^2} \end{vmatrix} \qquad (C16)$$

Solving for the eigenvalues of this matrix results in the following cubic equation:

$$-\sigma^3 + \sigma^2\left(\frac{v}{u} + \frac{2uv}{c^2-u^2}\right) + \sigma\left(\frac{3v^2-c^2}{c^2-u^2}\right) + \frac{v}{u(u^2-c^2)^2}\left[(u^2-c^2)\,v^2 + c^4 - u^2c^2\right] = 0 \qquad (C17)$$

where σ representes an eigenvalue. By substituting the quantity v/u for σ in Equation C17 it can be shown that it is an eigenvalue of the matrix E in Equation C16. This reduced Equation C17 to the following quadratic:

$$\sigma^2 + \frac{2uv}{u^2-c^2}\,\sigma + \frac{v^2-c^2}{u^2-c^2} = 0 \tag{C18}$$

This can be solved using the quadratic formula yielding the following two eigenvalues:

$$\sigma_{1,2} = \frac{-uv \pm c\sqrt{u^2+v^2-c^2}}{u^2-c^2} \tag{C19}$$

The matrix $A^{-1}C$ is:

$$A^{-1}C = \begin{vmatrix} \frac{-uw}{c^2-u^2} & 0 & \frac{c^2}{c^2-u^2} & \frac{w}{\rho(c^2-u^2)} & 0 \\ 0 & \frac{w}{u} & 0 & 0 & 0 \\ 0 & 0 & \frac{w}{u} & \frac{1}{\rho u} & 0 \\ \frac{\rho w c^2}{c^2-u^2} & 0 & \frac{-\rho c^2 u}{c^2-u^2} & \frac{-wu}{c^2-u^2} & 0 \\ \frac{\rho w}{c^2-u^2} & 0 & \frac{-\rho u}{c^2-c^2} & \frac{-w}{u(c^2-u^2)} & \frac{w}{u} \end{vmatrix} \tag{C20}$$

Again two of the eigenvalues can be found by inspection. They are again identical and equal to w/u. The matrix $A^{-1}C$, therefore, reduces to:

$$F = \begin{vmatrix} \frac{uw}{c^2-u^2} & \frac{-c^2}{u^2-c^2} & \frac{-w}{\rho(u^2-c^2)} \\ 0 & \frac{w}{u} & \frac{1}{\rho u} \\ \frac{-\rho w c^2}{u^2-c^2} & \frac{\rho u c^2}{u^2-c^2} & \frac{uw}{u^2-c^2} \end{vmatrix} \tag{C21}$$

This is identical to the matrix E of Equation C16 with v replaced by w.

Therefore, the eigenvalues of F are:

$$\sigma_{1,2,3} = \frac{-uw \pm c\sqrt{u^2+w^2-c^2}}{u^2-c^2}, \frac{w}{u} \qquad (C22)$$

From looking at the eigenvalues of the two matrices $A^{-1}B$ and $A^{-1}C$ one observes that for $u > c$ the eigenvalues are real and the governing system of equation is hyperbolic.

APPENDIX D

Derivation of Exact Boundary Conditions

The numerical boundary conditions that are applied at the surface of a cone at angle of attack in a supersonic flow field are based on the assumption that certain flow variables can be represented as either even or odd functions with respect to the distance normal to the body. For the case of a cone at zero angle of attack the boundary conditions based on this assumption are exact and can be demonstrated as follows.

The flow field between the shock and body is irrotational and at a constant entropy. For zero angle of attack at the cone's surface the v and w velocity components are zero and the remaining flow variables are independent of x.

The irrotational assumption states that:

$$\nabla \times \bar{q} = 0 \tag{D1}$$

In scalar form for the body coordinate system used in this study Equation D1 becomes:

$$x \sin \sigma \frac{\partial w}{\partial y} = \frac{\partial v}{\partial \phi} - w \cos \sigma \tag{D2}$$

$$x \sin \sigma \frac{\partial w}{\partial x} = \frac{\partial u}{\partial \phi} - w \sin \sigma \tag{D3}$$

$$\frac{\partial v}{\partial x} = \frac{\partial u}{\partial y} \tag{D4}$$

Under the above assumptions Equation D4 reduces to

$$\left.\frac{\partial u}{\partial y}\right|_b = 0 \tag{D5}$$

which implies that u behaves locally as an even function with respect to y at the cone's surface.

The y-momentum equation for the aforementioned assumptions reduces to the following at the body:

$$\left.\frac{\partial P}{\partial y}\right|_b = 0 \qquad (D6)$$

Substituting Equations D5 and D6 into the adiabatic energy equation yields:

$$\left.\frac{\partial \rho}{\partial y}\right|_b = 0 \qquad (D7)$$

Equations D6 and D7 imply that both the pressure and density can be considered as even functions at the body with respect to the distance normal to the cone's surface.

Since v is zero at the body and possesses a finite derivative with respect to y there it can be considered as an odd function with respect to the distance normal to the body.

APPENDIX E

Correction Factors

The correction factors which must be added to the differenced equations in order to keep the initially uniform free stream flow variables constant throughout the integration are given below for each of the gas-dynamic equations.

The correction factors in the body coordinate system for difference schemes which use Lax's method as the predictor or for Lax's method itself contain terms which correct for the error introduced by the differenced derivative expressions in addition to the usual correction factors. The correction factors are accurate to the order of $(\Delta\theta)^4$ and $(\Delta\phi)^4$ and are as follows:

Continuity;

$$C1 = -\rho q \sin\alpha \cos\phi\left[\frac{\sin\alpha}{2}\left(\frac{\Delta\phi^2}{2!} - \frac{\Delta\phi^4}{4!}\right) + \frac{\Delta x}{r}\left(\frac{\Delta\phi^2}{3!} - \frac{\Delta\phi^4}{5!}\right)\right], \quad (E1)$$

Momentum in the x direction;

$$C2 = \rho q^2\left\{\frac{1}{2}\sin 2\alpha \cos\sigma \cos\phi\left[\sin\sigma\left(-\frac{\Delta\phi^2}{2!} + \frac{\Delta\phi^4}{4!}\right) - \frac{\Delta x}{r}\left(\frac{\Delta\phi^2}{3!} - \frac{\Delta\phi^4}{5!}\right)\right] + \sin^2\alpha \sin\sigma \cos 2\phi\left[\sin\sigma\left(\frac{\Delta\phi^2}{2!} - 4\frac{\Delta\phi^4}{4!}\right) + \frac{\Delta x}{r}\left(\frac{4\Delta\phi^2}{3!} - \frac{16\Delta\phi^4}{5!}\right)\right]\right\}, \quad (E2)$$

Momentum in the y direction;

$$C3 = \rho q^2\left\{\frac{1}{2}\sin 2\alpha \cos\phi\left[-\frac{1}{2}\cos 2\sigma\left(\frac{\Delta\phi^2}{2!} - \frac{\Delta\phi^4}{4!}\right) + \sin\sigma\frac{\Delta x}{r}\left(\frac{\Delta\phi^2}{3!} - \frac{\Delta\phi^4}{5!}\right)\right] + \sin^2\alpha \cos\sigma \cos 2\phi\left[\sin\sigma\left(\frac{\Delta\phi^2}{2} - 4\frac{\Delta\phi^4}{4!}\right) + \frac{\Delta x}{r}\left(\frac{4\Delta\phi^2}{3!} - \frac{16\Delta\phi^4}{5!}\right)\right]\right\}. \quad (E3)$$

Momentum in the ϕ direction;

$$C4 = \rho q^2\left[\frac{1}{4}\sin 2\alpha \cos\sigma \sin\phi\left(\frac{\Delta\phi^2}{2!} - \frac{\Delta\phi^4}{4!}\right) - \sin^2\alpha \sin\sigma \sin 2\phi\left(\frac{\Delta\phi^2}{2!} - \frac{4\Delta\phi^4}{4!}\right) - \frac{\Delta x}{r}\sin 2\phi \sin^2\alpha\left(\frac{4\Delta\phi^2}{3!} - \frac{16\Delta\phi^4}{5!}\right)\right] \quad (E4)$$

Equations E1 through E4 are evaluated at the point being integrated and then added to the respective equation.

In spherical coordinates correction factors were only used to correct the error introduced by the term averaged in the Lax predictor. These correction factors for their respective equations are listed below.

Continuity;

$$C1 = \frac{1}{2}\left[\rho u\left(\frac{\Delta\theta^2}{2!} - \frac{\Delta\theta^4}{4!}\right) - \rho q \sin\alpha \sin\theta \cos\phi\left(\frac{\Delta\phi^2}{2!} - \frac{\Delta\phi^4}{4!}\right)\right], \quad (E5)$$

Momentum in the r direction;

$$C2 = \frac{1}{2}\rho\left\{A(u^2 - r^2) + q^2\left[\sin^2\alpha \sin^2\theta\, B\,(\cos^2\phi - \sin^2\phi) - 2(\cos\alpha \cos\theta \sin\alpha \sin\theta \cos\phi\right]\right\}, \quad (E6)$$

where

$$A = \Delta\theta^2 - \Delta\theta^4/3$$
$$B = \Delta\phi^2 - \Delta\phi^4/3$$
$$C = \Delta\phi^2/2 - \Delta\phi^4/24$$

Momentum in the θ direction,

$$C3 = -\frac{1}{4}\rho q^2\left[(-AG - BH)\,\Delta\theta^2 + (AG + BH)\frac{\Delta\theta^4}{3} + (AK - 2CJ + GD)\frac{\Delta\phi^2}{2} + (-AK - 8CJ + 6IK - GD)\frac{\Delta\phi^4}{4!}\right], \quad (E7)$$

where

$$A = \cos\alpha \cos\theta - \sin\alpha \sin\theta \cos\phi$$

$$B = \cos\alpha \sin\theta + \sin\alpha \cos\theta \cos\phi$$

$$C = \sin\alpha \sin\theta \sin\phi$$

$$D = \sin\alpha \sin\theta \cos\phi$$

$$G = -\cos\alpha \sin\theta - \sin\alpha \cos\theta \cos\phi$$

$$H = -\cos\alpha \cos\theta + \sin\alpha \sin\theta \cos\phi$$

$$J = \sin\alpha \cos\theta \sin\phi$$

$$K = \sin\alpha \cos\theta \cos\phi$$

Momentum in the ϕ direction;

$$C4 = \frac{1}{2}\left\{\rho u w \left(\frac{\Delta\theta^2}{2!} - \frac{\Delta\theta^4}{4!}\right) + \rho q^2 \left[\sin\alpha \cos\alpha \cos\theta \sin\phi \left(\frac{\Delta\phi^2}{2!} - \frac{\Delta\phi^4}{4!}\right) - \sin^2\alpha \sin\theta \sin\phi \cos\phi \times \left(\frac{4\Delta\phi^2}{2!} - \frac{16\Delta\phi^4}{4!}\right)\right]\right\} \qquad (E8)$$

Equations E5 through E8 are evaluated at the point being integrated and then added to the respective equation.

APPENDIX F

Cone at Angle of Attack Computer Program

The computer program used in the solution of the cone at incidence problem consists of a main program plus three subroutines. The programs which are used for both the IBM 1800 and 7094 computer systems vary only in the storage space allotted, the restart tape option which is not available on the 1800 and the programming necessary to display results on the C.R.T.

Table 9 below lists the main program and its subroutines and describes each of their functions in the solution of this problem.

Table 9. Resume of computer program for a cone at incidence

Name of Subroutine	Function
Main Program	Allows for input of all constants governing numerical solution of problem through data cards; calls INITA; prints input and initial values of the flow variables at each mesh point; calls BNDRY; calls IOCON; integrates differential equations according to difference scheme selected; writes restart tape after step-back procedure occurs (7094 only); displays pertinent results on C.R.T. and trips motion picture camera (1800 only); prints values of all flow variables at each mesh point succeeding step back.
INITA	Initializes values of the flow variables at each mesh point when restart tape is not used or reads restart tape for this information; determines certain constants used in program such as $\Delta\phi$, Δx, Δy, and $\Delta x/\Delta\phi$; plots known information on C.R.T. (1800 only).
IOCON(N)	N = 0 - solves for flow variables from conservative variables; N = 1 - arranges flow variables in conservative form; calculates correction factors for Lax's and Richtmyer's methods.

Table 9 (Continued)

Name of Subroutine	Function
BNDRY(N)	N = 0 - applies symmetry boundary conditions at the 0 and 180 degree planes, and applies reflection principle boundary conditions at the body; N = 1 - sets the normal component of velocity at the body and the cross flow velocity component at the 0 and 180 degree planes equal to zero.

APPENDIX G

Conical Wing-Body at Angle of Attack

Computer Program

The computer program used in the solution for the flow field about a conical wing-body combination at angle of attack consists of a main program plus three supporting subroutines. The computer program is used on either the IBM 1800 or 7094 computer systems.

Table 10 below lists the main program and its subroutines and describes each of their functions in the solution of this problem.

Table 10. Resume of computer program for conical wing-body combination

Name of Subroutine	Function
Main Program	Allows for input of all constants governing numerical solution of problem through data cards; calls INITA; prints input and initial values of the flow variables at each mesh point; calls BNDRY; calls IOCON; integrates differenced equations according to MacCormack's method; writes restart tape (7094 only); displays pertinent results on C.R.T. and trips motion picture camera (1800 only); prints values of all flow variables at each mesh point.
INITA	Initializes values of the flow variables at each mesh point when restart tape is not used or reads restart tape for this information; determines constants required by the program; plots initial data on C.R.T. (1800 only).
IOCON(N)	N = 0 - solves for flow variables from conservative variables; N = 1 - arranges flow variables in conservative form .
BNDRY(N)	N = 0 - applies symmetry boundary conditions at $\phi = 0^{o}$ plane, and applies reflection principle boundary conditions at body and wing; N = 1 - sets the normal component of velocity at the body and the cross-flow velocity component at the wing and $\phi = 0^{o}$ plane equal to zero.